Miguel Antonio Fernández Sampedro

Characterization of amino acid changes in visual pigment evolution and interaction with associated proteins

Doctoral thesis

GBMI

UNIVERSITAT POLITECNICA DE CATALUNYA BARCELONATECH

UNIVERSITAT POLITÈCNICA
DE CATALUNYA
BARCELONATECH

Characterization of amino acid changes in visual pigment evolution and interaction with associated proteins

By

Miguel Antonio Fernández Sampedro

Under the direction of

Prof. Dr. Pere Garriga Solé

At

Molecular and Industrial Biotechnology group (GBMI)

Department of Chemical Engineering.

*Thesis submitted to the Agri-food Technology and Biotechnology doctoral program at the "**Universitat Politècnica de Catalunya**" in partial fulfilment of the requirements for the degree of Doctor of Philosophy*

Terrassa 2018

UNIVERSITAT POLITÈCNICA DE CATALUNYA
BARCELONATECH
Escola de Doctorat

Curs acadèmic: 2017/2018

Acta de qualificació de tesi doctoral

Nom i cognoms

Miguel Antonio Fernández Sampedro

Programa de doctorat

Tecnologia agroalimentària i biotecnologia

Unitat estructural responsable del programa

Enginyeria química

Resolució del Tribunal

Reunit el Tribunal designat a l'efecte, el doctorand / la doctoranda exposa el tema de la seva tesi doctoral titulada “Characterization of amino acid changes in visual pigment evolution and interaction with associated proteins”.

Acabada la lectura i després de donar resposta a les qüestions formulades pels membres titulars del tribunal, aquest atorga la qualificació:

☐ NO APTE ☐ APROVAT ☐ NOTABLE ☐ EXCEL·LENT

(Nom, cognoms i signatura) President/a	(Nom, cognoms i signatura) Secretari/ària	
(Nom, cognoms i signatura) Vocal	(Nom, cognoms i signatura) Vocal	(Nom, cognoms i signatura) Vocal

_____, _____ d'/de _____ de _____

El resultat de l’escrutini dels vots emesos pels membres titulars del tribunal, efectuat per l’Escola de Doctorat, a instància de la Comissió de Doctorat de la UPC, atorga la MENCIÓ CUM LAUDE:

☐ SÍ ☐ NO

(Nom, cognoms i signatura) President de la Comissió Permanent de l’Escola de Doctorat	(Nom, cognoms i signatura) Secretari de la Comissió Permanent de l’Escola de Doctorat

Barcelona, _____ d'/de _____ de _____

A mis padres y a mi familia, con un recuerdo especial a mi abuela Esperanza quien despertó en mí el interés por la naturaleza y la ciencia.

"When you make the finding yourself – even if you're the last person on Earth to see the light – you'll never forget it" - Carl Sagan

Abstract

Visual opsins are G protein-coupled receptors that function as light photoreceptors in the vertebrate retina. Rhodopsin is the visual pigment located in the rod photoreceptor cells specialized in scotopic vision.

Bovine and mouse rhodopsins have been thoroughly used as *in vitro* and *in vivo* models for physiological and biochemical characterization. In the last years, different lines of evidence point to significant functional differences among rhodopsins of different species. In this thesis bovine, murine and human rhodopsins were immunopurified and biochemically characterized, revealing differences in their thermal stabilities and retinal release rates. Besides, the Y102H RP-like rhodopsin mutation was introduced in the human and bovine backgrounds to bring up potential phenotypic differences. Therefore, keeping in mind that a large body of studies on human genetic retinal degenerative diseases related with opsins (e.g. retinitis pigmentosa) have used these models, our results suggest that using human rhodopsin for future studies would be advised.

The most important biochemical differences were observed between the diurnal (human and bovine) versus nocturnal (mouse) species, especially in their retinal release rates. In addition, we also found a novel relevant amino acid position that appears to be significantly correlated with rhodopsin molecular adaptation to the nocturnal (L290) and the diurnal (I290) niches throughout terrestrial therian mammals. Previous studies suggested that L290 is present in the inferred therian ancestor rhodopsin in agreement with mammalian "nocturnal bottleneck" theories. Thus, the L290I substitution could have an important role in mammal rhodopsin molecular evolution and adaptation as it is likely to be the result of independent analogous changes,

a fact that can be well-appreciated in the primate and rodent orders. This hypothesis was experimentally confirmed by the L290I mutation in murine rhodopsin that resulted in a Meta II decay rate similar to that of bovine rhodopsin.

These results provide support for a role of the Meta II decay rate in rhodopsin evolution, beyond the well-studied λ_{max} spectral shift used by animal species to adapt to different light environments. Moreover, a novel mechanism is proposed involving a compromise between improving rod protection under bright light in nocturnal species by means of a stabilized Meta II conformation, and a faster dark adaption that occurs under dim-light conditions in diurnal species by means of a faster retinal release

Our statistical analysis found three new candidate positions for positive selection in the mammal therian branch. The reverse mutations (F13M, Q225R and A346S) were introduced into bovine rhodopsin and the expressed proteins were immunopurified to functionally and biochemically characterize the consequences of these ancestral changes. Position 225 appears to be important for the function of the protein affecting the G-protein activation process, and position 346 would also regulate functionality of the receptor by enhancing G-protein activation and presumably affecting protein phosphorylation by rhodopsin kinase. Position 13 was shown to be very important for the proper folding and glycosylation of rhodopsin as only in the engineered thermally stable double Cys mutant (N2C/N282C) background was able to be regenerated with 11-*cis*-retinal. Similarly a double Cys mutation (W90C/A169C) previously proposed for the green cone opsin was biochemically analyzed confirming the formation (at least partially) of this bond.

Finally, a recently detected interaction between the membrane protein peripherin-2 and rhodopsin was functionally studied, showing reduced G-protein activation, by rhodopsin, in presence of peripherin-2 when the two proteins were in a partially solubilised system. These results could have physiological implications in the desensitization process involving rhodopsin on the rim of discs of photoreceptor cells.

Keywords: G protein-coupled receptors, visual opsins, rhodopsin, peripherin-2, immunopurification, molecular evolution, scotopic vision, protein stability, functionality.

Table of contents

Lists of figures

Lists of tables

List of abbreviations

1D4	---	Protein tag corresponding to TETSQVAPA
^{35S}GTPγS	---	Guanidine 5'-O-(3-thio)-triphosphate
9 –mer peptide	---	Oligopeptide corresponding to TETSQVAPA
A_{max}	---	Maximum absorbance
CNG ion channel	---	Cyclic nucleotide–gated ion channel
DM	---	n-Dodecyl-D-maltoside
DMEM	---	Dulbecco's Modified Eagle's Medium
DNA	---	Deoxyribonucleic acid
DTNB	---	Ellman reagent, 5, 5'-dithio-bis-(2-nitrobenzoic acid)
ECL	---	Extra cellular loop (Intradiscal side on opsins)
FBS	---	Foetal bovine serum
GDP	---	Guanosine diphosphate
GPCR	---	G Protein couple receptor
Gt	---	G protein transducin
GTP	---	Guanosine triphosphate
ICL	---	Intracellular loops (Cytoplasm side on opsins)
kDa	---	Kilo Daltons
L.B.	---	Lysogeny broth
LWS	---	Long wave-sensitive (Red opsin)
Meta I, II and III	---	Metarhodopsin I, II and III
MWS	---	Medium wave-sensitive (Green opsin)
PBS	---	phosphate buffered saline
PEI	---	Polyethylenimine
Prph2	---	Periphrin-2 or peripherin/RDS
RDH	---	Retinal dehydrogenases

RH1 and RH2	---	Rhodopsin and green opsin genes respectively
Rho	---	Rhodopsin
ROS	---	Rod outer segments
RP	---	Retinitis Pigmentosa
RPE	---	Retinal pigment epithelium
RPE65	---	Retinal pigment epithelium-specific 65 kDa protein
S.E.	---	Standard error
SDS-Page	---	Sodium dodecyl sulphate polyacrylamide gel electrophoresis
SWS1 and SWS2	---	Short wave-sensitive, blue and UV opsin genes
$t_{1/2}$	---	Half time
TBS	---	Tris buffered saline
TM	---	Transmembrane
TNB	---	2-nitro-5-thiobenzoic acid
TTBS	---	Tween tris buffered saline
UV-Vis	---	Ultraviolet-Visible
WT	---	Wild type
λ_{max}	---	Wavelength of maximum peak absorbance

List of amino acids:

A	---	Ala	---	Alanine
C	---	Cys	---	Cysteine
D	---	Asp	---	Aspartic acid
E	---	Glu	---	Glutamic acid
F	---	Phe	---	Phenylalanine
G	---	Gly	---	Glycine
H	---	His	---	Histidine
I	---	Ile	---	Isoleucine
K	---	Lys	---	Lysine
L	---	Leu	---	Leucine
M	---	Met	---	Methionine
N	---	Asn	---	Asparagine
P	---	Pro	---	Proline
Q	---	Gln	---	Glutamine
R	---	Arg	---	Arginine
S	---	Ser	---	Serine
T	---	Thr	---	Threonine
V	---	Val	---	Valine
W	---	Trp	---	Tryptophan
Y	---	Tyr	---	Tyrosine

1 Introduction

1.1 G protein-coupled receptors

The G protein-coupled receptors (GPCRs) superfamily consists of a wide variety of membrane protein receptors that are found in most eukaryote organisms, pointing to an ancient origin (Fredriksson & Schio, 2005). This protein superfamily is one of the largest and more diverse in mammals, and in the case of humans it is composed by approximately 800 different receptors (Fig 1.1) (Flock et al., 2017). These protein receptors connect the extracellular environment to the cell interior through a seven transmembrane (TM) domain. The environmental signals, like physiologic hormones, neurotransmitters, odorants, tastants and light are perceived by these accurate sensors, that are targets of approximately 30 % of known drugs (as for example β-blockers and antihistamines) making them highly prominent in pharmacology developments (Hofmann et al., 2009; Venkatakrishnan et al., 2013).

Based on different methodologies, several classifications have been developed for GPCRs (Z. Zhang, Wu, Yu, & Xiao, 2012). Some systems have excluded sensory GPCRs (light, odour and taste receptors) and classified them according to their pharmacological properties as that used by the International Union of Basic and Clinical Pharmacology (Venkatakrishnan et al., 2013). Although the most widely used are the A-F system and the GRAFS classification, being the main difference between them the created subdivision of the secretin family in secretin and adhesion families based on the human phylogenetic tree on the GRAFS system (Hu, Mai, & Chen, 2017). In this way the GRAFS system classifies these proteins into 5 distinct classes (A-F system equivalence in brackets):

- **G**lutamate like family (Class C) has a variety of functions in behavioural and mood regulation, as well as in the central and

peripheral nervous systems. Their long N-terminal domain interacts with small molecules (Fredriksson & Schio, 2005). It includes the metabotropic glutamate family, GABA receptors, calcium-sensing receptors, and taste receptors (Hu et al., 2017).

- **R**hodopsin (Rho) like family (Class A), this is the largest and more heterogeneous group of GPCRs, and includes hormones, neurotransmitters, and light receptors, accounting for 80 % of GPCRs. (Hu et al., 2017; Z. Zhang et al., 2012). The family can be further divided into four groups α, β, γ, δ (Katritch, Cherezov, & Stevens, 2013). Some GPCRs, playing physiological roles in visual and smell senses belong to this family, as for example the visual opsins like Rho.
- **A**dhesion like family (Class B2), in the A-F system was considered within the same class than the secretin like receptors. They have a long N terminal domain (Z. Zhang et al., 2012).
- **F**rizzled/ Taste 2 receptors like family (Class F) control the cell fate, proliferation, and polarity that are basic functions within Metazoan development (Fredriksson & Schio, 2005).
- **S**ecretin receptor family (Class B1) Receptors in this family mainly act through hormones and neuropeptides. The N-terminal domain interacts with large peptides, being an hormone-binding domain (Fredriksson & Schio, 2005; Z. Zhang et al., 2012).

The first reported crystal structure of a GPCR was that of bovine Rho in 2000 (Palczewski et al., 2000) and it has been used as model for the structural analysis of GPCRs based on biochemical and biophysical studies. Rho was the only crystal structure elucidated at high resolution solved in the GPCR

field until 2007, when two structures of the β2-adrenergic receptor were determined (Tesmer, 2010). Currently, several other GPCR structures have been solved in class A GPCR, like different members of aminergic GPCRs (β-adrenergic, acetylcholine muscarinic M3 receptor, H1 human histamine receptor and dopamine D3 receptor) and A_{2A} human adenosine receptor (Katritch et al., 2013; Tesmer, 2010). This list is expected to increase in the future because of the continued effort of multiple international research teams.

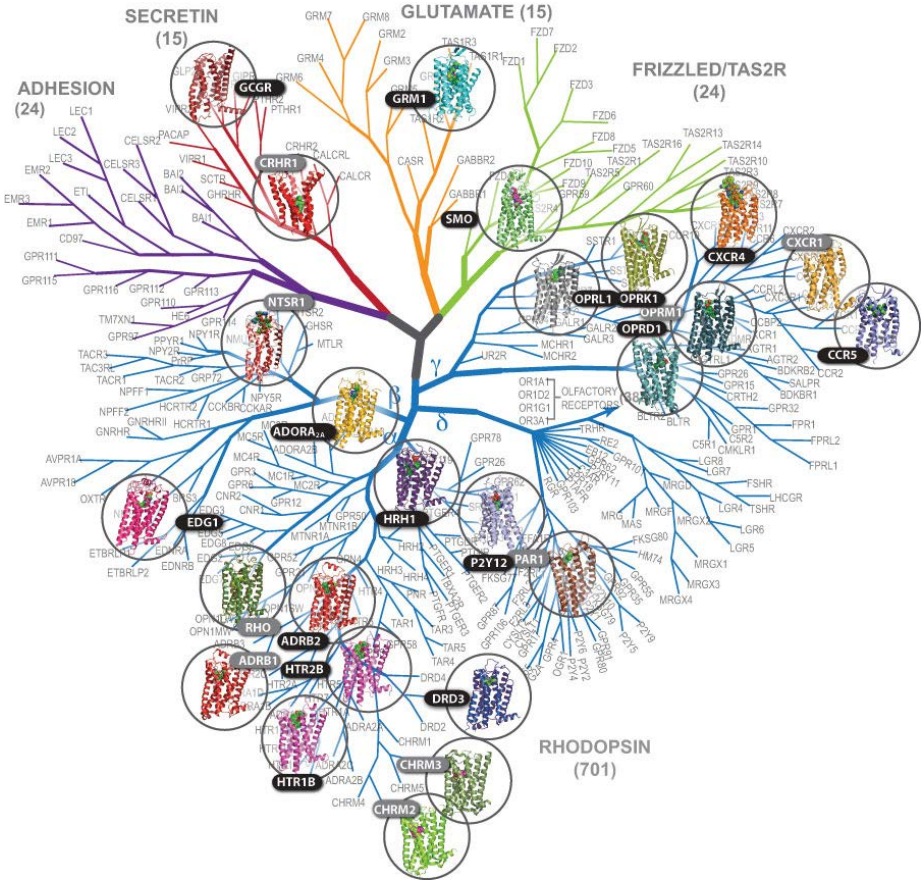

Figure 1.1 Dendogram of human GPCRs based on sequence similarity in the seven TM domain. Structures solved are highlight in circles and the number of members on each class is shown in brackets. The olfactory receptors subfamily is the largest subgroup with more than 300 members (although only 4 receptors are shown here) inside the Rho like family of GPCR. Figure retrieved from (Parmley, 2014).

The common structure of GPCRs is divided into three specific regions: the extracellular domain which contains the N-terminal domain and three extracellular loops (ECL1, ECL2 and ECL3), the TM domain conformed by the 7 α-helices (TM1 to TM7) that provide the core of the protein inserted into the plasma membrane of the cell, and the intracellular domain with three intracellular loops (ICL1, ICL2 and ICL3), an intracellular amphipathic helix (H8) and the C-terminal domain (Fig. 1.2). In general, the extracellular domain modulates the ligand access (some families of GPCRs have long N-terminal domains containing different kinds of functional or ligand binding domains), the TM domain forms the structural part where the ligand binds and translocates the signal to the intracellular domain by means of a conformational change after its activation; and finally the intracellular domain in the cytosolic region interacts with the G-protein starting the visual phototransduction cascade (Fredriksson & Schio, 2005; Venkatakrishnan et al., 2013).

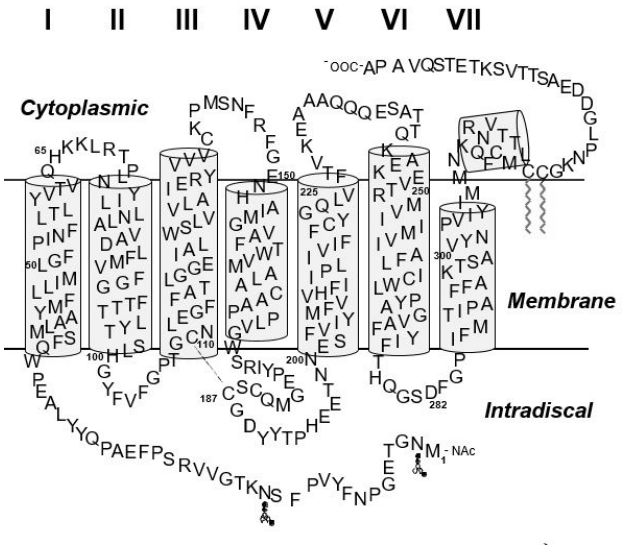

Figure 1.2 Secondary structure model of bovine Rho. A typical model structure for GPCRs. The seven α-helices and the extracellular and intracellular loops can be observed.

1.2 Visual opsins and photoreceptor cells

Vision starts when photons are absorbed by the visual pigments located on the photoreceptor cells in the retina of the eye. In vertebrates there are two types of photoreceptors cells, rod and cone cells, that differ in their dimension and shape of the rod outer segment (ROS) as well as in their physiological response (Fu & Yau, 2007) (Fig. 1.3). Rod and cone cells, have different types of visual opsins.

Rods are responsible for scotopic vision, i.e. when the dim light conditions provide illumination intensities that are under the threshold of cone functionality. On the other side, cone cells are responsible for photopic vision by working under bright daylight conditions, when rod cells are saturated (Imamoto & Shichida, 2014). In agreement with this visual duplicity, the physiological response of rods shows 100 fold more sensitivity than cones, even being able to generate a response from a single photon of light (Kefalov, 2012). In contrast, cones have a faster response and regeneration rate, thus having a faster adaptability to light intensity changes than rods (Fu & Yau, 2007; Imamoto & Shichida, 2014). In that way, this double system is clearly beneficial for human vision by importantly increasing the visual function over a wide range of light environments.

Each rod cell contains a single type of rod visual pigment, visual Rho. Meanwhile, there are different types of cone visual pigments depending on the species analysed. Each visual pigment consists of the seven TM GPCR apoprotein and the 11-*cis*-retinal chromophore, bound to K296 in TM7 by a protonated Schiff base linkage (Fig. 1.3) (Palczewski, 2006), which acts in the dark as a strong inverse agonist. The opsin part is a glycoprotein with a molecular weight of 40 kDa. The Schiff base linkage is located in the highly

conserved residue, in visual pigments (Lys298 in Rho), that is found in TM7 (Fredriksson & Schio, 2005).

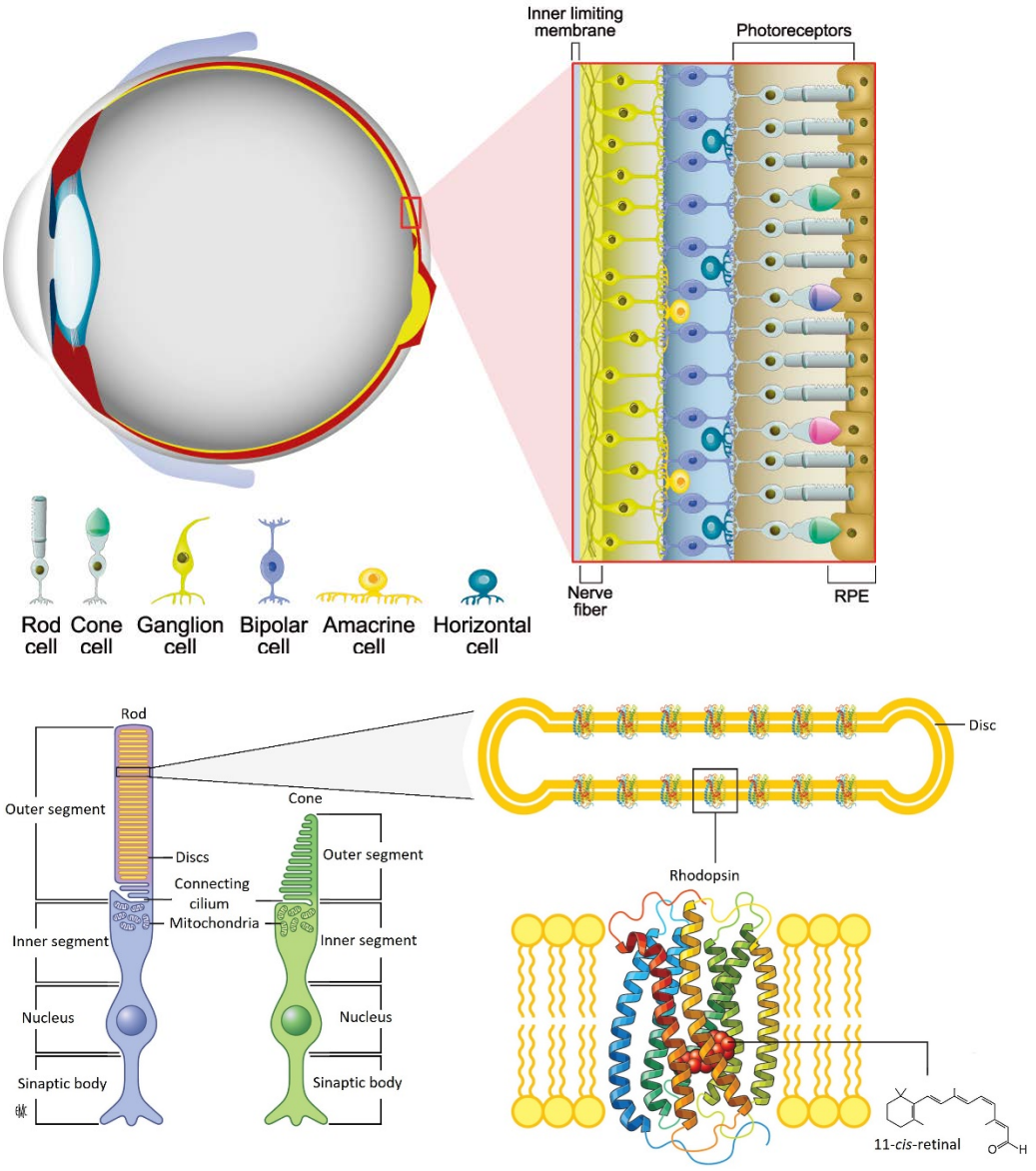

Figure 1.3 Retinal structure and cell composition. Photoreceptor cells scheme and Rho organization in the discs membranes of rod cells. Upper panel: schematic detail of a transversal cut of the retina where the multilayer complex composed by a set of different

visual cell layers can be observed. Bottom panel: Detail of the photoreceptor cells, rods and cones. Mouse ROS is formed by approximately 800 membranous discs (Burns & Pugh, 2010). Adapted from (Salesse, 2017).

1.2.2 Rho

Rho is the visual pigment, belonging to the Rho family (or Class A) of GPCRs, responsible for vision at low light intensities and located in the rod photoreceptor cells where it represents around 85 % of the total membrane proteins content in the disks of ROS (Molday, 1998) (Fig. 1.3 right panel). These pigments have a wavelength maximum (λ_{max}) of their visible absorption band in the vicinity of 500 nm (498 nm in bovine Rho) and allow animals to have monochromatic vision under dim light conditions. Disks are formed from evaginations of the plasma membrane and move up the length of the rod cell as the disks age (Gurevich & Gurevich, 2015).

Bovine Rho has been widely used as a model to study photo transduction due to the high abundance of this pigment in the bovine retina (Fu & Yau, 2007). Moreover, Rho has also been used as a model for GPCRs as it was the first crystal structure solved in the superfamily (Hofmann et al., 2009).

1.2.2 Cone opsins

The different types of cone opsins, having different wavelength visible absorption maxima, allow animals to discriminate colours under bright light conditions (Imamoto & Shichida, 2014). Absorption maxima of cone visual pigments expand from 360 nm to 600 nm in different animal species (Imamoto & Shichida, 2014). In the case of humans, there are 3 different cone opsins that are expressed individually in each cone photoreceptor cell: the red cone opsin or long wave-sensitive (LWS) opsin maximally absorbing at 563 nm, the green cone opsin or medium wave-sensitive (MWS) opsin

absorbing at 532 nm and the blue cone opsin or short wave-sensitive (SWS) opsin absorbing at 424 nm (Imamoto & Shichida, 2014; Lamb, 2013).

1.2.3 Rho photoactivation

The light stimulus of a single photon arriving to the photoreceptors cells in the vertebrate retina is absorbed by the 11-*cis*-retinal covalently bound to Rho. This triggers a fast isomerization of the chromophore to all-*trans*-retinal that involves a change in the protein conformation through a series of intermediates including bathorhodopsin, lumirhodopsin (that have very short lifetimes) and Metarhodopsin I (Meta I) (Palczewski, 2006). Subsequent deprotonation of the Schiff base linkage leads to the active state conformation, Meta II, that has the ability to bind and activate the G protein transducin (Gt) (Tesmer, 2010) which initiates the intracellular cascade. Moreover, Meta II shows a λ_{max} at 380 nm, similar to that of free retinal and contrasting with the λ_{max} of the dark conformation of the pigments. Some authors have suggested that Meta I and Meta II are in a rapid equilibrium so they may be considered as a single photoproduct (Ala-Laurila et al., 2006). Other studies include in this equilibrium also Meta III, and therefore the mixture found upon photoactivation would be mainly composed of Meta II and Meta III states because Meta I is less stable (Fig. 1.4) (Stehle et al., 2014). The formation of Meta III comes by the anti → syn isomerization of the retinal Schiff base (Mahalingam & Vogel, 2006) and can occur spontaneously from the Meta I/Meta II equilibrium or can be also induced from Meta II by blue light (Bartl & Vogel, 2007; Heck et al., 2003; Piechnick, Heck, & Sommer, 2011). Finally, during Meta II/Meta III decay the Schiff base is eventually hydrolysed and retinal is irreversibly released (*in vitro*) from the Rho binding pocket (Salom et al., 2006; Stehle et al., 2014).

Compared with Rho, the cone visual opsins have short-lived photointermediates that allow to accelerate the photoactivation process.

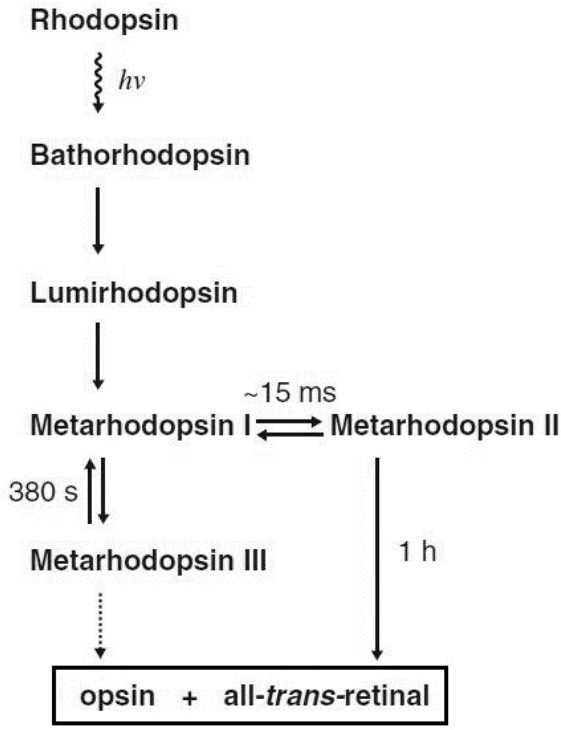

Figure 1.4 Reaction scheme of Rho photoactivation. Different photointermediates upon absorption of a photon from the Rho inactive state. Bathorhodopsin and lumirhodopsin have very short lifetimes. Retrieved from (Imamoto & Shichida, 2014).

1.2.4 Retinoid visual cycle

After photobleaching Rho decays to free opsin that needs to be regenerated with fresh 11-*cis*-retinal to recover rod photosensitivity for proper visual sensitivity. This is possible by the uptake of retinoids from the diet, which are absorbed by the small intestine and are hydrolyzed to retinol that can undergo cellular transport. After different stages and, by means of blood

transport, retinol arrives to the target cells, the retinal pigment epithelium (RPE) cells, that highly express STRA6 (Fig. 1.5) which facilitates retinol uptake into the incorporate it to the visual cycle (Perusek & Maeda, 2013).

Nevertheless, the main contribution of retinal supply comes from recycling the all-*trans*-retinal that is released from photoactivated Rho. This recycling process, called "visual cycle", occurs in the RPE cell layer that is adjacent to the ROS photoreceptor cells (Fig. 1.5) (Stiles et al., 2015). Two entry/exit channels were proposed to be the path used by the chromophore to enter/exit the pigment binding pocket (T. Wang & Duan, 2011).

All-*trans*-retinal is transported by the ABCA4 protein (an ATP-binding cassette transporter) from the TM region of the disks to the cytoplasm of the photoreceptor cell (Chen et al., 2013). There, it can be reduced by retinal dehydrogenases 8 and 12 (RDH8 and RDH12) to all-*trans*-retinol by means of NADPH as a reducing factor (Stiles et al., 2015). The RDH activity is considered a limiting factor in the visual cycle (Stiles et al., 2015). Then, retinol diffuses to the RPE via the interphotoreceptor matrix and helped by the interphotoreceptor retinoid-binding protein (IRBP) where it is esterified by lecithin retinol acyltransferase (LRAT) to all-*trans*-retinyl esters. These esters are isomerized by RPE65 (another rate limiting step (Stiles et al., 2015)) to 11-*cis*-retinol which is then oxidized to 11-*cis*-retinal by RDH5, and finally this recycled chromophore is translocated again to the photoreceptor cell by IRBP. Once in the disks of the ROS, 11-*cis*-retinal can combine with free opsin to regenerate Rho and in this way close the cycle (Fig 1.5) (Chen et al., 2013; Perusek & Maeda, 2013; Stiles et al., 2015).

Interestingly, cone opsins use also an alternative pathway, by means of the Müller cells to regenerate the chromophore independent from the RPE. This allows a faster visual cycle recovery and reduces the possibility of

accumulating all-*trans*-retinal or the shortage of 11-*cis*-retinal (Perusek & Maeda, 2013).

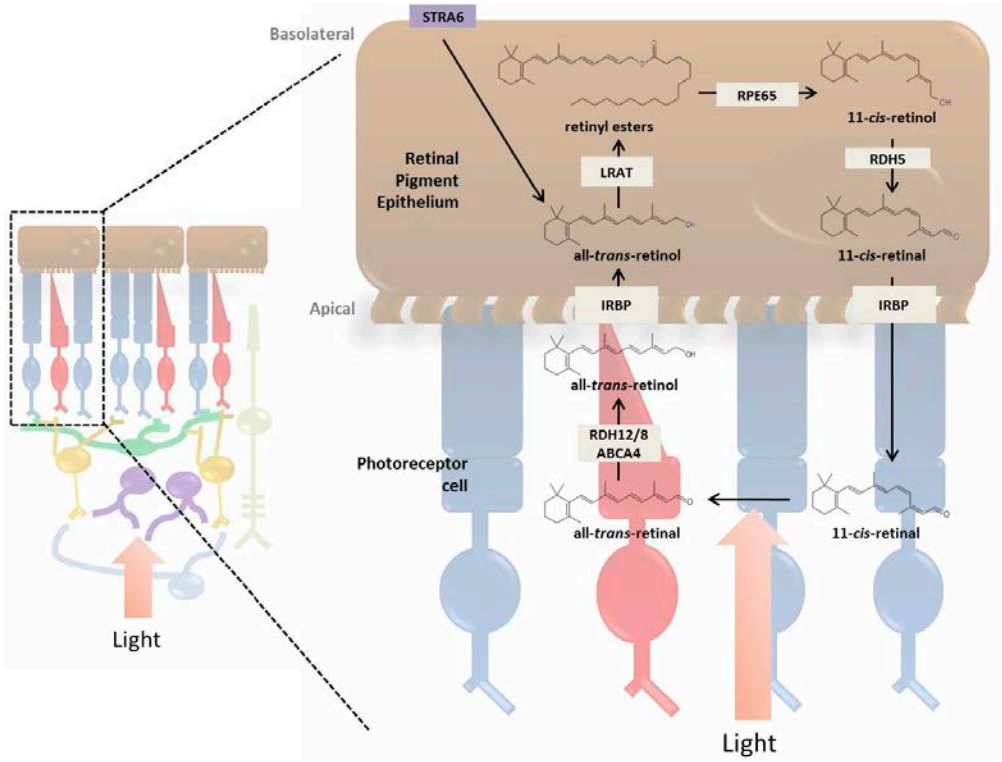

Figure 1.5 Retinoid visual cycle. It is known that experiments with isolated retina in the absence of RPE cannot regenerate Rho. The visual cycle is necessary for the isomerization of all-*trans*-retinal to 11-*cis*-retinal. Although it is possible to induce regeneration by adding fresh 11-*cis*-retinal. Retrieved from (Perusek & Maeda, 2013)

1.2.5 Opsins evolution in mammals

Vertebrate visual pigments emerged about 500 million years ago with four spectrally distinct classes of cone opsins which appeared to have evolved through gene duplication from a common ancestor opsin, being the first division the SWS and LWS opsin genes (Lamb, 2013). The RH1 opsin gene,

corresponding to the dim-light Rho photoreceptor, was the result of gene duplication of green cone opsin, RH2, that at the same time was previously the result of another gene duplication from a SWS opsin gene (Hunt, Carvalho, Cowing, & Davies, 2009). In this way gene duplication has resulted in a high number of opsins as a result of opsin molecular evolution (Bowmaker, 2008).

The ancestor visual pigment complex in tetrapoda was composed by the 4 cone opsins (SWS1, SWS2, LWS and RH2) and one Rho (or RH1) for the dim and nocturnal light (Fig. 1.6). Some amino acid residues in Rho appear to have been positively selected during, in particular, mammalian divergence (Bickelmann et al., 2015). This strong positive selection detected mainly in the therian branch (live-bearing mammals, excluding monotremes such as the platypus) could be related to the loss of RH2 and SWS2 in this lineage. Thus, the therian ancestors were able to absorb just blue/UV (SWS1), red (LWS) and dim light (Rho) (Hunt et al., 2009). This evolutionary loss of visual pigment genes would suggest that the visual systems in early mammals experienced lower light intensities which is consistent with the nocturnal bottleneck hypothesis (Borges et al., 2018; Gerkema, Davies, Foster, Menaker, & Hut, 2013). This hypothesis suggests that the early therian mammals of the Mesozoic era faced competition with diurnal reptiles (like dinosaurs) restricted to diurnal life due to being mainly ectothermic and consequently having the necessity of solar radiation to maintain their body temperature (Gerkema et al., 2013; Maor, Dayan, Ferguson-Gow, & Jones, 2017).

At a later time, a new pigment, MWS, termed green cone opsin appeared, restoring trichromatic vision in some primate lineages and other mammalians, due to a subsequent LWS gene duplication.

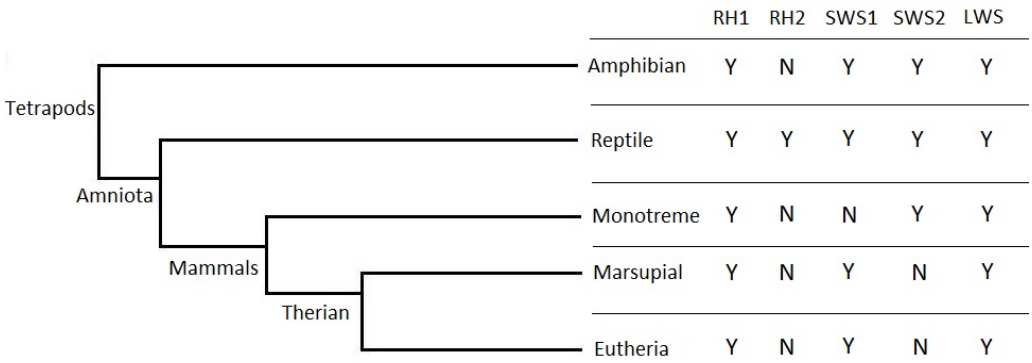

Figure 1.6 Simplified phylogenetic tree of tetrapods and visual opsin presence in the different groups. The bottleneck hypothesis would explain the loss of different cone opsins observed in mammals.

The distribution of both photoreceptor cell types varies enormously depending on the environmental adaptations of each species. A typical mammal retina usually possesses a large quantity of rod photoreceptor cells and a relatively few cone cells, whereas most non-mammal species have cone dominant retinas, and this would also support the bottleneck hypothesis (J. W. Kim et al., 2016). On the other hand, in the case of humans and some primates, although rods are abundant and distributed along the retina, cone cells are concentrated mainly in a central region of the retina called fovea, and this is an adaptation to the diurnal lifestyle (Maor et al., 2017). Other animals have different degrees of rod dominant or cone dominant retinas depending on their degree of nocturnal or diurnal habitat adaptation (Saïdi, Mbarek, Chaouacha-Chekir, & Hicks, 2011).

In addition to the presence of different sets of opsin photoreceptors along evolution, other adaptative characteristics that have being studied include for example the λ_{max} shift in SWS1 from UV to blue (S. Yokoyama et al., 2014)

or the λ_{max} shift in Rho (RH1) that underwent a blue shift in different classes of fishes and cetacean to adapt to the deep water environment (Dungan & Chang, 2017; Luk et al., 2016). Moreover, in the last few years new studies are starting to take into account other functional and biochemical characteristics that could be related to the evolution and adaptation to diurnal or nocturnal niches, as for example the Meta II decay rate (Bickelmann et al., 2015; Dungan & Chang, 2017; Sugawara, Imai, Nikaido, Imamoto, & Okada, 2010).

1.3 Rho associated proteins

1.3.1 G protein (Gt)

Gt is a heterotrimeric protein constituted by three different subunits: α, β and γ. In the inactive state, α subunit binds to GDP forming a complex with β and γ subunits. The agonist effect (all-*trans*-retinal) upon illumination induces a conformational change in Rho leading to the active state whose cytosolic domain interacts with Gt, stimulating GDP release and its exchange by GTP in the α subunit (Fig. 1.7) (Hofmann et al., 2009; Jastrzebska, Orban, Golczak, Engel, & Palczewski, 2013). Some reports have shown that the active Rho forms a 1:1 complex with Gt (Hofmann et al., 2009). Then, the activated α subunit bound to GTP, dissociates from the β and γ subunits (which stay in contact forming the βγ complex). Both complexes, βγ and αGTP interact with their down-stream targets generating an intracellular signalling cascade. Finally, the hydrolysis of GTP to GDP within the α subunit, and the subsequent association of α–GDP with the βγ complex completes the Gt protein cycle.

1.3.2 Rho kinase

Is the protein in charge of the first step in the Meta II inactivation by means of phosphorylation of Ser and Thr at the C-terminal tail of Rho, with each added phosphate partially reducing the rate by which Meta II can activate Gt (Arshavsky & Burns, 2012; Tobin, 2008). Moreover, after the addition of three phosphate groups, the affinity of arrestin for Meta II conformation increases 10 fold (Tobin, 2008)

1.3.3 Arrestin

Arrestins are members of a superfamily of regulator proteins which participate in the termination of the signal transduction in GPCRs. Arrestin-1 is a soluble protein of ~48 kDa found in rod cells. There are other types of arrestins that interact with other GPCRs, being arrestin-4 the protein present in cone cells (Araujo, Sanz-Rodríguez, & Bubis, 2014; Gurevich, Hanson, Song, Vishnivetskiy, & Gurevich, 2011)

The triple phosphorylation of the C-terminal tail of Meta II by Rho kinase is necessary for the high affinity binding of arrestin-1 (Tobin, 2008). Besides interrupting Gt activation, arrestin-1 has other functions not related with GPCR signalling, as calmodulin binding (Huang et al., 2012).

1.3.4 Peripherin

Peripherin/RDS or peripherin-2 (Prph2) is a glycomembrane protein of the family of the tetraspanins and has a molecular mass of 39.3 kDa. It is the second more abundant membrane protein in the disk membranes with about 4 % of the total protein (Molday, 1998).

Prph2 works like an oligomer, formed by dimer subunits to form a tetramer by non-covalent linkages (Loewen, Moritz, & Molday, 2001). Moreover,

besides homotetramers, Prhp2 can also form heterotetramers with the homologous Rom1 protein (Tritarelli et al., 2004). The functional properties of Prph2 suggest that Prph2 is a multifunctional protein, important in disc morphogenesis and maintenance of proper disc alignment (Boon et al., 2008). In this way, the rim region of the disk membrane has a curvature that is facilitated by the presence of Prph2 (Gurevich & Gurevich, 2015)

Recent research provided new insights on this protein showing that Prph2 can interact with Rho, while at the same time demonstrated that Rho is also located in the rim region of the disks (Becirovic et al., 2014) despite previous articles that suggested a compartmental Rho distribution (in the centre) and Prph2 (in the rims) of the ROS disks membranes (Buzhynskyy, Salesse, & Scheuring, 2011). Moreover, Prph2 has also been localized in the RPE (Uhl, Amann, Hauck, & Deeg, 2015)

1.4 Visual signal transduction

1.4.1 Phototransduction cascade

The phototransduction cascade initiates when a photon arrives to the disks of ROS cells and activates the Rho chromophore, inducing the isomerisation from 11-*cis*-retinal to all-*trans*-retinal and a conformational change in the protein. This isomerization results in Rho activation, i.e. formation of the Meta II state. This state catalyses the exchange of GTP for GDP on the α subunit of Gt which in turn stimulates cGMP phosphodiesterase (PDE). This activated PDE is a highly effective enzyme that hydrolyses cGMP to GMP (Stiles et al., 2015). The decline in cGMP concentration in the cytosol leads to closure of the cyclic nucleotide–gated (CNG) ion channel; this has been shown to occur with a sub-millisecond delay. These closed channels ultimately cause the hyperpolarization of the photoreceptor (Field &

Sampath, 2017) (Fig. 1.7) potential to produce the light response. In this way, a series of biochemical reactions, started by the opsins, generate an electrical response to the light stimulus (Burns & Pugh, 2010). The series of biochemical reactions started by the opsins finish in an electrical response.

The deactivation of the pathway is mediated by Rho kinase and arrestin-1 to shut-off the active Meta II conformation. In addition, Gt α-GTP must be eventually deactivated by hydrolysing GTP to GDP, and the cGMP concentration must be restored.

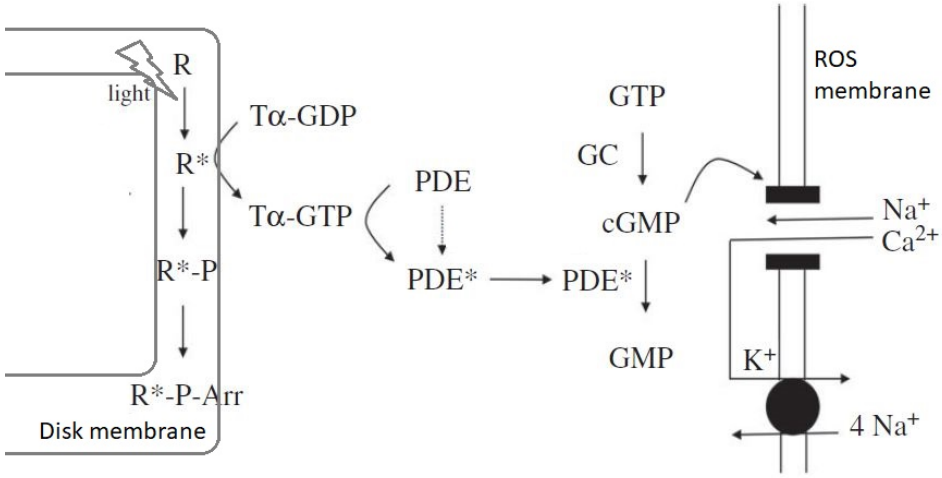

Figure 1.7 Phototransduction scheme. *R** as photoactivated Rho upon photon absorption is deactivated by means of phosphorylation by the Rho kinase and the subsequent arrestin binding. *Tα* as Gt α subunit. Adapted from (Field & Sampath, 2017).

2 Objectives

The main aim of this thesis is to get an insight into the relationship between the molecular features and the physiological specialization of Rho in different species and ancestors to infer potential implications of the occurred biological changes in different aspects (behavioural, environmental, etc.). Furthermore, the link between point mutations in Rho molecular evolution, light adaption and disease is investigated, the present study is also aimed at finding possible relationships between two proteins of photoreceptor which have only been recently associated to each other, Rho and Prph2. For these purposes, the main aim are divided into the following specific objectives:

1. To functionally and biochemically characterize Rho from different species (bovine, mouse and human) to find specific molecular differences among them.
2. To analyse possible strategies to find key point mutations in the differentiation, and molecular evolution, of Rho.
3. To study the RP point mutations in different species backgrounds.
4. To functional and biochemical characterize Rho point mutations, statistically detected of been positively selected during evolution, to try to unveil the importance of the functionality of specific amino acids.
5. To investigate potential common, or divergent, patterns among molecular, environmental and physiologic levels.
6. To apply different strategies for pigment stabilization when needed.
7. To test the functional effects of Prph2 interaction with Rho.

3 Materials and methods

3.1 Materials and chemicals

· L-glutamine and penicillin-streptomycin (Sigma, Spain)

· 11-*cis*-retinal was kindly provided by Dr. R. Crouch (National Eye Institute, National Institutes of Health (USA))

· 9-*cis*-retinal (Sigma, Spain)

· 9-mer peptide corresponding to the last 9 amino acids of Rho was synthesized by Serveis Cientificotècnics (Universitat de Barcelona, Barcelona, Spain)

· Acrilamide/bisacrilamide (Bio-Rad, USA)

· Biodegradable scintillation fluid (GE healthcare life sciences, Spain)

· Cellulose membrane for radioactivity assay (Milipore, France)

· Cyanogen bromide (CNBr)-activated Sepharose 4B Fast Flow (Sigma, Spain).

· Dark adapted bovine retinas (W L Lawson Company, NE, USA).

· DMEM/Ham´s F12 media (Lab clinics, Spain)

· dpnI (Thermo Fisher Scientific- Life Technologies, Spain)

· Dulbecco's Modified Eagle's Medium (DMEM) (Sigma, Spain)

· Fetal bovine serum (FBS) (Sigma, Spain)

· Goat anti-mouse IgG conjugated to horseradish peroxidase (HRP) (Pierce)

· Hi-pure plasmid maxiprep kit (Invitrogen, Carlsbad, CA, USA)

· Hydroxylamine, protease inhibitor cocktail, and phenylmethanesulfonyl fluoride (PMSF) (Sigma, Spain)

· Lysogeny broth (L.B.), formulation Luria (Thermo Fisher Scientific- Life Technologies, Spain)

· Methanol (Panreac, Barcelona, Spain)

· n-Dodecyl-D-maltoside (DM) (Anatrace, Maumee, OH, USA)

· Nitrocellulose membrane 0,45 um (Bio Rad, USA)

· OPTIMEM Reduced Serum Media from (Life Technologies, Madrid, Spain)

· PfuUltra II fusion HS DNA Polymerase (Agilent Technologies, Santa Clara, CA, USA)

· Polyethyleneimine 25 kDa (PEI) (Polysciences,Warrington, PA, USA)

· Primers (Sigma, Spain.)

· Protease inhibitor cocktail and phenylmethanesulfonyl fluoride (PMSF) (Sigma, Spain.)

· Purified mAb rho-1D4 (Cell Essentials. Boston,MA, USA)

· QIAprep spin Miniprep kit (Qiagen, Hilden, Germany)

· QuikChange II (Stratagene)

· Radionucleotide GTPγS^{35} (250μCi) (Perkin Elmer)

· SuperSignal West Pico Chemiluminescent Substrate (Luminol/H2O2) (Thermo Fisher Scientific- Life Technologies, Spain)

All other chemicals and reagents were purchased form Sigma, Spain.

3.2 Positive selected amino acids determination

The bio-statistical analysis explained in section 4.2 was performed by Dr. Brandom Invergo and Dr. Jaume Bertranpetit (Fernández-Sampedro, Invergo, Ramon, Bertranpetit, & Garriga, 2016) as explained below:

The GeneTree alignment for the human Rho gene was fetched from Ensembl Compara (version 7256). The alignment was filtered to include high-quality orthologous sequences from 42 vertebrate species, including paralogs in one-to-many orthologous relationships, resulting in an alignment of 48 sequences. In order to filter out divergent paralogs, which may have evolved under different selective pressures, a phylogenetic gene tree was produced from this alignment using PhyML (version 3.057). The tree was constructed using the GTR substitution model, which produced the highest-likelihood tree out of the different models provided by the software (log-likelihood=-15174); otherwise, the software's default parameters were used. Using this tree, we identified and pruned one Rho paralog each in six fish species, resulting in a final alignment of 42 orthologues with a single ortholog per species.

The rate of evolution undergone by Rho during phylogenetic divergence was first estimated using the M0 site-substitution model as implemented in the codeml program of the PAML package (version 4.758) using the pruned gene tree. This model estimates the rates of non-synonymous substitutions (dN) and synonymous substitutions (dS) during divergence. Their ratio (dN/dS) may be used as an indication of the strength and direction of selection. Under the assumption that synonymous substitutions are nearly selectively neutral, when dN/dS is less than one, the site is taken to have been under purifying (negative) selection; when it is equal to one, the site is evolving neutrally; and when it is greater than one, the site has undergone adaptive

(positive) selection. Because the M0 model uses a single dN/dS ratio for all sites in the sequence alignment, it is not very realistic, however it can be taken as an overall indicator of the strength of purifying selection acting on the gene (A. M. Andrés, De Hemptinne, & Bertranpetit, 2007; Montanucci, Laayouni, Dall'Olio, & Bertranpetit, 2011).

Three tests of positive selection were performed on the alignment. Evidence of pervasive positive selection during phylogenetic divergence was tested using two pairs of nested site-substitution models: M1a versus M2a (Nielsen & Yang, 1998; Ziheng Yang, Wong, & Nielsen, 2005) and M7 versus M8 (Z. Yang, Nielsen, Goldman, & Pedersen, 2000), as implemented in codeml. In both cases, each site in the alignment is assigned a class, which is associated with a given dN/dS ratio. In the null models (M1a, M7), all site classes have dN/dS ratios less than or equal to one (purifying selection or neutral evolution). The alternative models (M2a, M8) include a site class with dN/dS ratio greater than one (positive selection). The maximum likelihoods found by applying the null and alternative models are then compared via a likelihood ratio test with two degrees of freedom and a confidence level of 0.05; a significant test indicates that the alternative model featuring positively selected sites better fits the data. The M1a/M2a test is known to be more robust while M7/M8 is more sensitive (Wong, Yang, Goldman, & Nielsen, 2004).

Evidence of episodic positive selection was inferred via the branch site A model. Under this model, episodic selection is tested on one branch of the phylogeny against a background of neutral or purifying selection on the rest of the tree. In the null model, sites are classified as either being under purifying selection or neutral evolution on all branches of the phylogeny; the alternative model additionally allows sites to be classified as having

undergone positive selection on a single, specific phylogenetic branch. The alternative model was then tested for significance via a likelihood-ratio test with one degree of freedom and a 0.05 confidence level. We hypothesized that Rho would have undergone significant adaptation early in mammalian divergence. Therefore, we marked the branch at the root of the therians as the "foreground" branch, for which positive selection would be tested.

Because gene tree topologies often differ from that of the species tree, the tests of positive selection were performed using the topology of the species tree available from Ensembl, pruned to include only the species used in this study, in order to accurately mark the branch of interest (Figure 1). Branch lengths were estimated directly by codeml. The program was run with three different initial values of the parameter omega (dN/dS) (0.1, 1.0, 2.0), five times each, in order to affirm that the models converge to stable maximum likelihoods. Specific residues that have undergone positive selection were then predicted a posteriori via the Bayes Empirical Bayes method as implemented in codeml (Ziheng Yang et al., 2005).

3.3 Construction of mutants

In order to introduce the selected mutation on the opsins, site-directed mutagenesis was used on the original gene which was previously introduced in a vector as a template. Prph2 and mouse Rho genes were kindly provided by Dr. Elvir Becirovic (Ludwig-Maximilians-University of Munich), human Rho gene was kindly provided by Dr. Robert J. Lucas (University of Manchester) and human green opsin was kindly provided by Prof. Kevin D. Ridge. The bovine Rho F13M mutation was also introduced in the background of the double cysteine mutant N2C/D282C (Xie, Gross, & Oprian, 2003) that was previously constructed in our laboratory by Dr. Eva

Ramon. The oligonucleotide primers that were used are listed on Table 3.1. The numbering of the amino acids in Rho corresponds to bovine Rho.

Table 3.1. List of primers employed in this thesis. Forward and reverse primers for each construct are shown.

Gene template	Vector	Change	Primers
Rho bovine WT	pMT4	Q225R	>Fwd: CGGTGAACACCAGCCGGCC ATAGCAGAAG >Rev: CTTCTGCTATGGCCGGCTGG TGTTCACCG
Rho bovine WT	pMT4	A346S	>Fwd: CTTAGGCAGGGCTCACTTG GCTGGTCTC >Rev: GAGACCAGCCAAGTGAGCC CTGCCTAAG
Rho bovine WT	pMT4	F13M	>Fwd: GCCCGTCTTGTTGGACATA GGAACGTAGAAG >Rev: CTTCTACGTTCCTATGTCCA ACAAGACGGGC
Rho bovine N2C/D282C	pMT4	F13M	>Fwd: GCCCGTCTTGTTGGACATA GGAACGTAGAAG >Rev: CTTCTACGTTCCTATGTCCA ACAAGACGGGC
Rho bovine N2C/D282C /K296G	pMT4	F13M	>Fwd: GCCCGTCTTGTTGGACATA GGAACGTAGAAG >Rev: CTTCTACGTTCCTATGTCCA ACAAGACGGGC
Rho mouse WT	pIRes eGfp	L290I	>Fwd: CGGCCCCATCTTCATGACT ATCCCAGCTTTCTTTGCTAAGAG >Rev: CTCTTAGCAAAGAAAGCTG GGATAGTCATGAAGATGGGGCCG

Rho human WT	pCDNA 3	Y102H	>Fwd: CTCTCTGCATGGACACTTC GTCTTCGG >Rev: CCGAAGACGAAGTGTCCAT GCAGAGAG
Opsin green WT	pMT4	W90C	>Fwd: CCCGCTGAACTGCATCCTG GTGAA >Rev: TTCACCAGGATGCAGTTCAG CGGG
Opsin green WT	pMT4	A169C	>Fwd: GCCAAGCTGCATCGTGGGC ATT >Rev: AATGCCCACGATGCAGCTTG GC
Prph2	pcDNA 3	Insert 1D4 tag	>Fwd: CGGCTCCAGAGGCTGGCAC AGAGACCAGCCAAGTGGCGCCTG CC >Rev: GATGGTGATGATGACCGGT TTAGGCAGGCGCCACTTGGCTGGT CTCTGT

Primers were synthetized by Sigma. The suitable primers were designed to fulfil some conditions:

- Length of the primers should be between 25 and 45 bases.
- Melting temperature (Tm) preferable should be higher than 78°C

$$Tm = 81.5 + 0.41\,(\%GC) - (675/N) - \%mismatch$$

Where N is the primer length in bases.

- The mutation should be in the middle of the primers (10-15 bases on both sides)
- Primers should have a content of GC higher than 40 %, and they should terminate in one or more G or C bases.
- Secondary structure formation on the oligonucleotides should be weak.

The mutated genes were obtained by PCR (polymerase chain reaction) amplification employing Pfu Ultra II Fusion DNA polymerase with the site-directed mutagenesis QuikChange II protocol. At the end of the reaction, 1 µl *DpnI* restriction enzyme (10 U/µl) digestion was performed with 2 h incubation at 37°C in order to eliminate the methylated template vector. Then the DNA was precipitated by 1 h incubation at -80°C with 100 µl ethanol 100 % and 5 µl sodium acetate (pH 5.5) and subsequently subject to centrifugation. Finally the precipitated DNA was resuspended and transformed into E coli DH5α.

3.3.1 Preparation of competent cells

The whole procedure is performed under sterile conditions. All materials and solutions used must be autoclaved and it is necessary to work near the flame to avoid any contamination. The buffers are used at 4°C. Firstly, one colony of E coli DH5α was incubated in 50 ml of LB media at 37°C and 230 rpm overnight. Next morning, 1 ml of this culture was transferred to 100 ml of LB media to incubate it at 37°C, 230 rpm until A600=0.6 (usually between 3-4 h). Then the culture growth was stopped by keeping the culture 25 min on ice, and centrifuged 10 min at 4000 rpm, 4°C. The pellet was resuspended very gently with 40 ml of 100 mM CaCl2 and incubated on ice for 30 min. The cells were centrifuged again for 10 min, 4000 rpm and 4°C and resuspended with 2 ml solution of 80 % 100 mM CaCl2 and 20 % glycerol.

Finally, the culture was divided into aliquots of 50 µl and stored at -80°C until use. 100 ng of DNA was used as control to check the transformation efficiency of the cells.

3.3.2 Transformation of E. coli DH5α competent cells.

These cells have an increased ability to take up extracellular DNA. 50 µL of competent cells were added to the precipitated vector and incubated on ice for 30 min. Subsequently, a heat shock of the sample at 42° for 45 s was applied and then again incubated on ice for 5 min. 300 µL of 2xYT (16 g/L bacto tryptone, 10 g/L bacto yeast extract, 5 g NaCl. autoclaved) was added to the transformed cells and incubated for 1 h at 37°C, 230 rpm. Finally 100µL of cells were plated on LB agar Petri plate supplemented with antibiotic depending on the resistance cassette inserted into the vector transformed (100 µg/ mL of ampicillin for pMT4 and pcDNA3, and 50 µg/mL kanamycin for pIRES eGFP). The agar plate was incubated overnight at 37°C.

3.3.3 DNA miniprep

One unique colony of the transformed plate is picked to amplify the vector. For this, the colony was incubated shaking overnight at 37°C in 6 mL of LB media with antibiotic (100 µg/mL ampicillin or 50 µg/mL kanamycin). Next day the vectors were purified using QIAprep spin Miniprep kit (Qiagen) and at the end the DNA was eluted with 50 µl MiliQ water. The quality of the sample was determined by means of a UV-Vis spectrophotometer with the ratio 260nm/280nm (desirable ratio around 1.8-2) and the concentration determined from the absorbance (A_{260nm}) according with the formula:

$$DNA\ concentration\ (\mu g/ml) = A_{260nm} \quad 50 \ X \ dilution\ factor$$

Where 50 means that 50 µg/ml of pure DNA gives an absorbance of 1.

The plasmids obtained from the mini-prep were sequenced in StabVida (Caparica, Portugal) to verify the correct insertion of the gene modifications.

3.3.4 DNA maxiprep

This method allows to produce large amounts of DNA for cell transfection. Once the sequenced vector was verified, the DNA obtained from the mini-prep was again transformed into DH5α cells as previously described. One colony of the transformation suspension was picked and inoculated into 10 mL of LB media with antibiotic (100 µg/mL ampicillin or 50 µg/mL kanamycin). Then, it was incubated at 37° shaking for 6 h, and later transferred to a 500 mL LB media flask with antibiotic that was incubated at 37°C shaking overnight. The next day, the sample was centrifuged and the supernatant discarded, and the protocol of the Hi-pure plasmid maxiprep kit was performed. The DNA was eluted with 500 µl Mili-Q water. The concentration was determined by spectrophotometry at 260 nm and the quality with the ratio 260nm/280nm as previously described.

3.4 Eukaryotic cell culture

The cells were incubated in specific medium depending on the cell line, with 10 % FBS, 100 units/mL penicillin-streptomycin and 2 mM L-glutamine purchased from Sigma. Cells were grown in a humidified incubator at 37°C under 5 % CO2.

3.4.1 COS-1 cell line (monkey kidney cells)

Cultured in Dulbecco's Modified Eagle's Medium (DMEM) and split every 48-60 hours by removing the old media and washing the plates with phosphate buffered saline (PBS) (137 mM NaCl, 2.7 mM KCl, 10 mM Na_2HPO_4, and 1.8 mM KH_2PO_4) to get rid of the fetal bovine serum (FBS). Then, PBS was added again with 0.8-1 % of trypsin for cell splitting, and the

plates were kept at room temperature for 4-5 min until the cells started to detach helped by gently pipetting. Finally, new media with FBS that stops the trypsin effect was added, and the contents was divided into new plates with fresh media.

3.4.2 HEK293T cell line (human embryonic kidney cells)

These cells are also cultured in DMEM and split every 48-60 hours by removing the old media and washing the plates with PBS, then by gently pipetting the cells until their detachment from the plates. No trypsin is needed in this case, as the cell adherence is weak. Finally, fresh media was added, and the content was divided into new plates with fresh media.

3.4.3 HEK293S GnT I- cell line

These cells are cultured on DMEM + HAMF12. They lack N-acetyl-glucosaminyltransferase I (GnTI) activity and therefore are used to obtain non glycosylated proteins. This strategy is useful for electrophoretic analysis. The same protocol as for HEK293T cell line is applied.

3.4.4 Criopreservation

For long time conservation of a cell line, a protocol for deep freeze in liquid nitrogen was used. The cells were detached from the plates and washed in PBS at 800 rpm for 8 min. Then the pellet was resuspended with 80 % cell media, 10 % FBS and 10 % dimethyl sulfoxide (DMSO) that was previously filtered with 0.22 µm filter. Finally the cells were aliquoted in 1 mL vials and stored at -80°C in a special freezer container with ethanol in the base that allows the sample to decrease the temperature gradually, thereby the next day the tubes were transformed to the -196°C liquid nitrogen container.

For the thawing process, one cryovial of cells in liquid nitrogen was taken out from the liquid nitrogen and immediately incubated at 37°C until totally thaw. It is important to do this process fast as DMSO becomes very toxic to the cells for temperatures above 4°C. Then the content was added by pipetting to a plate with medium depending on the cell line. For better results, after 24 hours the medium was renewed and the plate was washed with PBS to totally eliminate the DMSO reminder.

3.5 Expression and purification of the mutant opsins.

3.5.1 1D4 coupling to CNBr activated-sepharose beads

1.51 g CNBr-activated sepharose powder was dissolved into a final volume of 6 ml of 1 mM HCl (pH 2~3) for 10-15 min until completely dissolved. Then the beads were washed using a filter funnel with G3 porosity (Duran) for 30 min by using 200 ml 1 mM HCl (pH 2~3) per each gram of bead powder. Beads were washed with 3 volumes (18 ml) of coupling buffer (0.1 M $NaHCO_3$ 0.5 NaCl pH 8.3) slowly to increase the pH of beads and to allow antibody coupling. The sepharose beads were mixed with 7.5 ml of 5.3 mg/ml 1D4 antibody by using a spatula and then incubated overnight at 4°C with mild shaking.

The unbound rho-1D4 antibody was washed away by using 2 volumes (12 ml) of coupling buffer. Then, washed rho-1D4 beads were transferred into a 50 ml tube containing 6 ml of 1 mM Tris-HCl pH 8.0 and nutated for 2 h on RT to block any remaining active group. Later a filter funnel porosity G3 was used to remove the 6 ml Tris-HCl (pH 8.0) and the beads were washed slowly with alternative cycles of 5 volumes (30 ml each) of 0.1 M NaAc, 0.5 M NaCl pH 4.0 and 0.1 M Tris-HCl, 0.5 M NaCl pH 8.0, for 4 times each buffer. Finally the beads were transferred to a falcon tube containing 6 ml of

storage buffer (2 mM Na_2PO_4 pH 6.0, 0.004 % (w/v) NaN_3) at 4°C. These beads were used for purification of proteins containing the 1D4 tag.

3.5.2 Protein expression in eukaryotic cells.

The expression and purification were performed as follows. Plasmids encoding the opsin WT or mutant pigment, as well as Prph2 genes were transient transfected into COS-1 or Hek293T cells in 150mm dishes at ≃85 % confluence, by using 0.1 mL of PEI and 30 µg of plasmid DNA per plate (30 µg per each plasmid DNA in the case of co-transfections) in 3mL Opti-MEM. Cells were harvested 48–60 h after transfection, and double washed with PBS by centrifugation for 20 min at 4 000 rpm. Then, the sample was either stored at -80°C or directly purified.

3.5.3 Protein recombinant purification.

From this point, all experiments were conducted in the dark or under dim red light (Kodak number 2 filter). The pigments were reconstituted with 10 µM 11-cis-retinal, or 9-cis-retinal, in PBS by nutating overnight at 4°C in intact cells (In both types of chromophores, a stock solution was prepared in 100 % absolute ethanol). Then, the cells were solubilized for 1 h with 1 % (w/v) DM in PBS pH 7.4, with PMSF and protease inhibitor cocktail. This solubilized sample was ultracentrifuged at 35 000 rpm for 35 min and the pellet was discarded. The pigments were purified by immunoaffinity chromatography on 1D4-Sepharose 4B. For this, the supernatant was incubated for 3 hours by gently nutating at 4°C. All procedures, up to and including binding of the receptor to the immunoaffinity matrix, were performed at 4°C. Therefore subsequent washes and elutions were performed using cold buffer. The resin was washed four times with PBS 0.05 % DM. The receptors were eluted for 30 min (in the case of cone

opsins) to 2 h (for Rho) in the same buffer containing 100 µM rho-1D4 9-mer peptide (TETSQVAPA). This peptide releases the bound protein in DM micelles (Fig. 3.1) by competitive bindings to the 1D4-sepharose beads. These elutions were repeated three times for each purification in order to obtain more purified protein.

Figure 3.1 Schematic model of a DM micelle containing the immunopurified opsin. Image retrieved from (Milic & Veprintsev, 2015)

Experiments of pharmacological chaperone rescue were performed in COS-1 cells transfected with 30 µl of plasmid DNA in the presence of 50 µM of 9-*cis*-retinal. A second addition of 50 µM of 9-*cis*-retinal was performed 24 h later and the cells were collected after 48 h. All the steps were carried out in the dark or under dim red light.

3.6 Membrane preparation of COS-1 cells

Membrane preparation from the transfected COS-1 cells allows to study the proteins in a different background in contrast with the purified proteins. Firstly, the cells were transfected and harvested with PBS as previously described. Then, cells were centrifuged and again resuspended in 2 mL per plate of 15 mM Tris-HCl pH7.5, containing 2 mM $MgCl_2$, 1 mM DTT and 100 µM PMSF. The mix was incubated for 40 min on ice, and the cells were homogenized with a tissue homogenizer and passage through a 23G needle syringe several times. Later, the cell suspension was centrifuged for 30 min at 35 000 rpm (4°C) and the pellet was resuspended in 35 ml PBS.

At this point a sucrose gradient was prepared: with 14 ml of 20 % sucrose in PBS and, with the help of a long needle 14 ml of 50 % sucrose were underlayed to the 20 % sucrose. Then, the sample was added carefully to the top of the gradient and centrifuged at 25 000 rpm 4°C for 30 min, with the centrifuge deceleration brake deactivated. After centrifugation, the interface band between both sucrose layers was pulled out with a syringe and a 18G needle. This band was diluted in PBS and again centrifuged at 35 000 rpm for 30 min at 4°C. Finally, the pellet obtained was resuspended with 2 ml PBS with a 23G needle, divided into 50 to 100 µl aliquots and stored at -80°C until use, when a regeneration with 30 µM 11-*cis*-retinal was carry on. (adapted from Kojima et al., 1996; Robinson, 2000; Terakita et al., 2004).

3.7 Rho solubilization and purification from retinal rod outer segments (ROS)

ROS membranes were obtained from bovine retinas. The solubilization was performed always in the dark in PBS pH 7.4, 1 % (w/v) DM. Membranes were kept nutating for 1 h. The sample was centrifuged at 5 000 rpm for 30 min and the pellet was discarded. At this point, the solubilized ROS were purified by gently nutating with 1D4-Sepharose resin for 3 hours at 4°C. After this, the sample was washed four times with PBS, 0.05 % DM. The receptors were eluted for 2 h in the same buffer containing 100 µM rho-1D4 9-mer peptide that binds to the 1D4-sepharose competitively releasing the protein.

3.8 Subcellular localization of mutant opsins

Pigments cellular localization was performed by means of immunofluorescence microscopy in a Nikon Eclipse Ti microscope. For this purpose, HEK-293S GnT I- cells were transfected in 6 well plates with slide covers inside. They were incubated during 24 h to avoid excessive

overexpression. Cells were washed three times with cold PBS and then immediately fixed with 3.5 % formaldehyde for 30 min at 37°C and permeabilized in 0.5 % Triton X-100 for 10 min. Nonspecific binding in the sample was blocked by adding 5 % milk for 1 h. Then, cells were incubated for 1 h, at room temperature in primary 1D4 mouse IgG antibody (1:2 000 in TBS). Finally, the sample was stained with anti-mouse IgG fluorescein-labelled antibody (FITC) (1:200 in TBS) and incubated for 1 h at room temperature (cells were carefully washed three times with cold TBS in each step). Slide covers with the cells were taken from the plates and mounted into slides with 2 µg/ml DAPI for nuclei counterstaining, and ready for microscopy visualization.

3.9 Electrophoresis

3.9.1 SDS-PAGE

Sodium dodecyl sulphate polyacrylamide gel electrophoresis (SDS-PAGE) analyses proteins based on their electrophoretic mobility on a gel based mainly on their molecular size. Electrophoresis analysis was carried out in order to compare the mobility patterns of the different proteins. SDS-PAGE gels were prepared as detailed in table 3.2.

Table 3.2. Gel preparation for SDS-PAGE.

	Separating gel		**Stacking gel**	
	Stock	Final	Stock	Final
Distilled Water	-	1.25 ml	-	2.9 ml
Acrylamide/bis acrylamide	37.5%/0.8%	12 %	37.5%/0.8%	5 %
Tris/HCl	1.5 M pH 8.8	0.75 M	0.5M pH 6.8	0.125M
SDS	10 %	0.1 %	10 %	0.1 %
APS	10 %	0.1 %	10 %	0.1 %
TEMED	100 %	0.5 %	100 %	0.5 %
Total		10 ml		5 ml

The same amount of purified proteins was loaded onto the gel (to properly compare them) and mixed with 4x protein loading buffer (0.0625 M Tris, 2 % SDS, 10 % glycerol, 0.4 M DTT, 0.1 % bromophenol blue diluted in ddH_2O). Molecular weight marker was loaded as a reference for the proteins samples. The gel was run in a Bio-Rad Mini-PROTEAN 2 system immersed in running buffer (25 mM Tris, 192 mM glycine, 0.1 % SDS) at 125 V until the blue band of the loading buffer almost reached the bottom of the gel.

To be able to visualize the bands, the gel was stained with Coomassie blue overnight. Then the gel was destained in 40 % methanol, 10 % glacial acetic acid diluted in distilled water. The gel image was digitalized with a ChemiDoc XRS + photodocumentation system (Bio-Rad, USA)

3.9.2 Western blot

This technique allows identifying protein targets by means of using specific antibodies. For Western blot analysis, the same protocol that for SDS-PAGE

was used, but instead of SDS-PAGE molecular weight marker, a prestained molecular weight marker was used. Moreover, the Coomassie blue staining was replaced by a different protocol. In this case, after running the gel, the proteins were transferred to a nitrocellulose membrane (100 V for 3 h) and then the membrane was blocked with 5 % (w/v) powder milk in Tris buffered saline (TBS). This prevents the unspecific binding of the antibodies to membrane surface. Next, the membrane was washed 4 times with Tween Tris buffered saline (TTBS) for 10 min each to remove the milk. Right after, the monoclonal Rho-1D4 antibody was added as the primary antibody at a concentration 1:10 000 in TBS for 1 h. Subsequently, a new round of washes with TTBS was performed and a goat anti-mouse IgG conjugated to horseradish peroxidase (HRP) in TBS (1:5 000) as secondary antibody was added for 1 h. Finally, a last round of washes was done to eliminate the unbound antibody. The membrane was stored in TBS.

The membrane was developed using SuperSignal West Pico Chemiluminescent Substrate (Luminol/H_2O_2) and detected with X-ray film in an autoradiography cassette or directly with a ChemiDoc XRS+ system (BioRad, Hercules, CA, USA).

3.10 Ultraviolet-visible (UV-vis) spectrophotometric Rho characterization

All measurements were made on a Cary 100 Bio spectrophotometer (Varian), equipped with water-jacketed cuvette holders connected to a circulating water bath. Temperature was controlled by a Peltier accessory connected to the spectrophotometer. All spectra were recorded in the 250 nm-650 nm range with a bandwidth of 1 nm, a response time of 0.1 s, and a scan speed of 600 nm/min.

Purified samples where photobleached with a 150 Watt power light using a 495 nm cut-off filter (except for green cone opsin) during 30 s; an absorption spectrum was immediately recorded. Acidification was performed immediately after photobleaching by the addition of 2N H_2SO_4 to a final sample pH of 1-2 and the acidified spectrum was measured after 1 min, in order to let the protein spectrum stabilize.

Although the photoresponse of the Rho is a well-studied phenomenon, there are relatively few studies dealing with the behaviour of Rho upon white light illumination (with no 495-nm cut-off filter used). Here, experiments were conducted in order to determine the importance of the use of the cut-off filter and whether there are appreciable differences in the Rho spectral response.

Two experiments were performed, one with solubilized ROS in DM detergent and the other using immunopurified WT Rho. The photobleaching process was followed by means of UV-vis spectroscopy. The illumination of the dark state was performed with a 495-nm cut-off filter or alternatively with white light. Difference spectra between filter versus no filter photobleaching were calculated, and in both experiments a band around 467 nm appeared with a simultaneous decrease at 380 nm (Fig. 3.2C and D insets). These bands would correspond to the formation of Meta III and the decay of Meta II conformation (Lomonosova, Kolesnikov, Kefalov, & Kisselev, 2012) (Fig 3.2D), and to the shift in the equilibrium towards Meta III under white light illumination (Fig. 3.2B).

Different laboratories appear to use diverse approaches in order to photobleach Rho in the *in vitro* characterization experiments. Some studies applied directly white light (Farrens & Khorana, 1995; van Hazel et al., 2016)

meanwhile in other research groups the experiments were conducted using a cut-off filter (λ > 495 nm) or short flash of light (< 1 ms) (Jastrzebska, 2015). Another approach has been photobleaching in the presence of hydroxylamine combined with white light illumination (Fan, Rohrer, Moiseyev, Ma, & Crouch, 2003), considering that this reagent favour the exit of retinal from the binding pocket in the Meta II conformation.

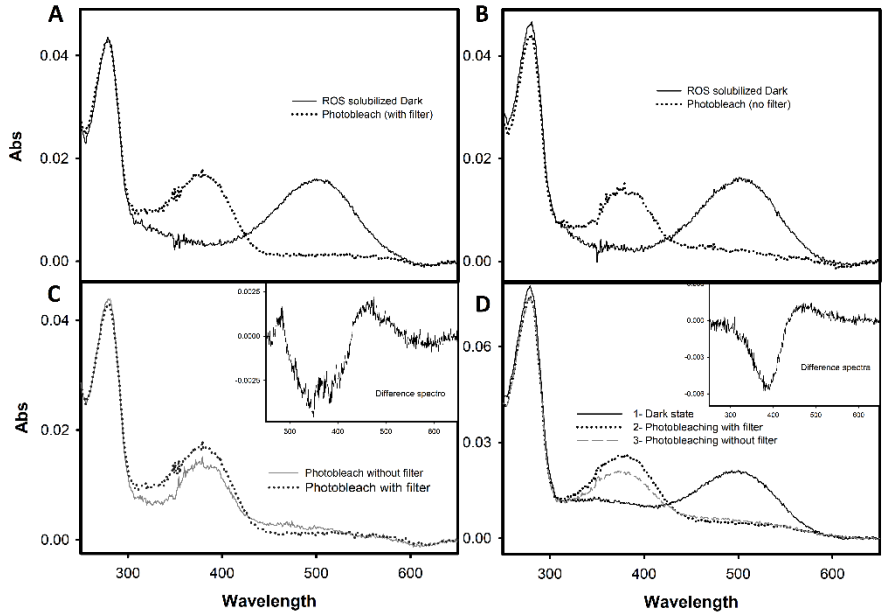

Figure 3.2 Comparative study of Rho photobleaching with white light versus filtered light (λ>495nm). **A and B**) Two samples of ROS solubilized were photobleached and measured. A was illuminated for 30s with 495 nm cut off filter meanwhile B was illuminated with white light. **C)** Comparison of the illuminated states from A and B, the difference spectra is shown in the inset where a band at 467 nm is visible. **D)** A sample of purified Rho WT is photobleached for 30 sec first using the 495 nm filter and subsequently with white light. The difference spectra of both illuminated measurements is shown in the inset where a small band at 467 nm is also visible.

When white light is applied to the active conformation of Rho, Meta III can be generated (Fig. 3.2D), probably as main photoproduct of Meta II illumination with blue light (Bartl & Vogel, 2007; Piechnick et al., 2011). If we take into account also the separate experiments in Fig. 3.2A and 3.2B, we

can argue that white light illumination results in Rho photobleaching and formation of the Meta II active conformation with the light of λ>495nm, and at the same time induces the photoconversion of Meta II to Meta III with the shorter wavelength light.

In summary, in this work the use the yellow filter was chosen since it allows a better characterization of the reactions that occur, at the same time, during Rho photoactivation. Our experiment (Fig. 3.2) reflects the importance of taking into account the use of the filter in order to compare the results with other published studies.

3.10.1 Thermal and chemical stability of Rho

Rho thermal stability in the dark was studied by means of UV-vis spectroscopy at 48°C (or 37°C for green cone opsin) by monitoring the rate of absorbance (A) loss at λ_{max}, and the increase of A_{380} as a function of time. Scan spectra from 250 nm to 650 nm were monitored every 2.5 min.

The chemical stability was measured by adding hydroxylamine (NH_2OH) to the sample and monitoring the decrease in the λ_{max} absorbance band with time at 20°C. NH_2OH from a stock of 1M adjusted to pH 7, was added to the sample to a final concentration of 50 mM and successive scan spectra were recorded every 2.5 min to measure the loss of visible absorbance (A_{max}) and formation of stable oxime with all-trans-retinal, around A_{360} (Stiles et al., 2015).

In both experiments, samples were kept in the dark until the end of the experiment when they were photobleached. For each experiment, three different replicates were carried out. In addition, all the measured spectra were normalized to a value of A=0 at 650 nm.

3.11 Meta II decay determined by fluorescence spectroscopy

Meta II decay was recorded by fluorescence spectroscopy at 20°C. All fluorescence spectra were carried out by exciting the samples for 2 s at 295 nm, with a bandwidth slit of 0.5 nm and measuring Trp emission at 330 nm (Farrens & Khorana, 1995). Rho in PBS 0.05 % DM was kept at 20°C until a stable baseline was obtained and subsequently illuminated for 30 s. The $t_{1/2}$ values for the Trp fluorescence increase (resulting from retinal release from the receptor) were derived from fitting the obtained curves to an exponential function. For each experiment, three different replicates were carried out.

3.12 Isolation of Gt from bovine retinas

Gt was purified from dark adapted bovine retinas purchased from W L Lawson Company (NE, USA). In summary, 50 dark frozen bovine retinas were thawed and exposed to light overnight at 4°C. These retinas were diluted in 150 mL of 47 % sucrose (0.1 mM PMSF and 2 mM DTT) and homogenized with a syringe without needle and a homogenizer.

Then, the sample was centrifuged at 42 000 g for 20 min at 4°C and the orange supernatant containing ROS membranes was immediately diluted with 200 mL of buffer A (20 mM Tris, pH 7.4, 1 mM CaCl2, 2 mM DTT, 0.1 mM PMSF) and homogenized again with a 21-gauge needle per triplicate. This homogenized sample was centrifuged at 30 000 g for 20 min at 4°C, and the pellet obtained was resuspended in 50 mL buffer A and passed through a 23-gauge needle three times. This sample was layered on top of a sucrose density gradient (1.2 mM / 1.0 mM / 0.8 mM) and centrifuged without brake at 42 000 g for 30 min at 4°C. The orange layer was cautiously recollected using a needle and diluted in buffer A and then followed by four centrifugations steps at 42 000 g for 20 min to remove the sucrose,

resuspending the pellet in 100 mL of buffer C (10 mM Tris, pH 7.4, 100 mM NaCl, 5 mM MgCl2, 2 mM DTT, 0.1 mM PMSF) and twice in 100 mL of buffer D (10 mM Tris, pH 7.4, 0.1 mM EDTA 3 mM DTT, 0.1 mM PMSF) respectively.

At the end, the pellet obtained was resuspended in 50mL of buffer D containing 40 µM of GTP and incubated for 30 min at 4°C by shaking. The sample was centrifuged at 180 000 g for 45 min at 4°C and the supernatant was collected and passed through a 0.22 µm filter to remove traces of membranes. This supernatant was concentrated and dialyzed against 900 mL of buffer E (10 mM Tris, pH 7.4, 2 mM MgCl2, 50 % glycerol, 1mM DTT) that was replaced twice.

The concentration and quality of the purified Gt were determined by SDS-PAGE using bovine serum albumin (BSA) as standard. The Gt was stored at 4°C for further use.

3.13 Gt activation

Gt activation was measured with purified proteins expressed in COS-1 cells, and the ability of opsin and Rho to activate Gt was monitored by means of a radionucleotide filter binding assay by measuring the uptake of ^{35S}GTPγS by Gt purified from bovine retinas in a liquid scintillation counter (TRI CARB Packard). The assays were performed by mixing 10 nM mutant or WT Rho with 500 nM Gt in Gt buffer (25 mM Tris, pH 7.5, 100 mM NaCl, 5 mM magnesium acetate, 5 % glycerol), 2.5 mM DTT, and 3µM ^{35S}GTPγS (0.128Ci/mmol) at RT. Reactions were initiated by the addition of Rho in the dark, and samples were filtrated after different incubation times through cellulose membrane, either in the dark or after illumination, to determine the amount of bound ^{35S}GTPγS (Terakita, Yamashita, Nimbari, Kojima, &

Shichida, 2002; Toledo et al., 2011). Each membrane was washed 10 times with Gt buffer, let it dry, and finally placed in scintillation liquid for scintillation counting.

The activity was counted in counts per minute (cpm) and converted to pM by using the formula:

$$Concentration\ in\ pM\ = \frac{cpm\ counted/Counter\ efficiency}{2.22\ x\ 10^{12}\ x\ radioactivity\ of\ S^{35}}$$

Counter efficiency = 55 %

1 Ci = 2.22 x 10^{12} disintegrations per minute (dpm)

Radioactivity of S^{35} = 1250 Ci/mmol

3.14 Determination of free sulfhydryl groups

Ellman's reagent (5,5'-dithio-bis-(2-nitrobenzoic acid), or DTNB) assay is performed to quantify the free sulfhydryls, functional group of cysteines, present and accessible in a given protein. In the case of Rho, as it is an TM protein there are only two free cysteines accessible to the reagent in the dark state (de Grip, van de Laar, Daemen, & Bonting, 1973; K. Yang, Farrens, Altenbach, et al., 1996) as other Cys are buried in the hydrophobic TM domain or forming an extra membrane disulfide bond (Karnik & Khorana, 1990).

The Ellman´s reagent reacts with the free sulfhydryls groups producing a mixed disulfide with the Cys of the protein and 2-nitro-5-thiobenzoic acid (TNB), a measurable yellow-coloured product (Fig. 3.3). TNB has a molar extinction coefficient of 14 150 $M^{-1}cm^{-1}$ at 412 nm allowing its detection by UV-vis spectrophotometry (Riddles, Blakeley, & Zerner, 1983).

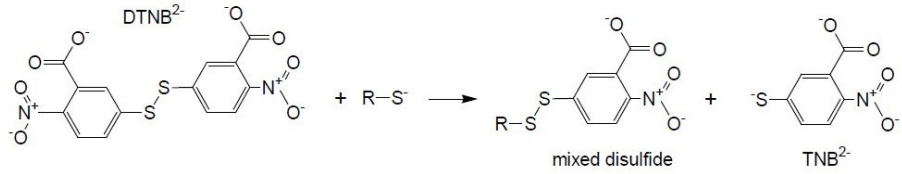

Figure 3.3 Reaction of a free sulfhydryl with the Ellman´s reagent or DTNB.

In the assay, the sample cuvette containing 164 µL of reaction buffer (0.1M sodium phosphate, pH 8.0, containing 1 mM EDTA), 35 µL of purified protein in PBS pH 7.4 with 0.05 % DM and 1 µL DTNB (4 mg/mL freshly prepared in reaction buffer) was measured after 15 min incubation at room temperature. A stock solution was prepared with reaction buffer + DTNB to make sure the concentrations were exactly the same. A blank was determined by using 35 µl of PBS with 0.05 % DM instead of the purified protein used in the sample cuvette. Absorbance increase at 412 nm was measured and the average was calculated.

The concentration of reacting sulfhydryl group was obtained from the Lambert-Beer law with the formula:

$$C = \frac{A}{bE}$$

A = Absorbance at 412 nm, b = path length of the cuvette in cm (here 1 cm). E = 14 150 $M^{-1}cm^{-1}$.

For calculating our actual starting protein concentration we had to take into account the dilution of our protein sample. In our case, since 35 µL of purified protein was added to the total of 200 µL, this means a 1:5.7 dilution.

The final concentration of free sulfhydryls was obtained multiplying by this dilution factor.

4 Results and discussion

4.1 Insights into mammal adaptation to diurnal vision: characterization of mouse, bovine and human Rho

The purpose of this section is to obtain a functional and biochemical characterization of modern Rho in different mammal species and to analyse their relationships in visual pigment evolution. To this aim three Rho species were selected for their relevance in visual and GPCR studies, as well as by their different position on the phylogenetic tree and their diverse ethology in relation with nocturnal/diurnal life. With this idea in mind, the mammals that were selected to be analysed were mouse, cow (bovine) and human.

As described previously by a phylogenetic comparison (Gerkema et al., 2013), each one of the three selected species studied in this chapter have its own dominant temporal niche and, besides the nowadays diversity, the analysed phylogenetic tree reflects the past evolutionary differences. In particular, mouse is classified as a nocturnal animal and there are no reported important phylogenetic changes in the nocturnal behaviour in its rodent ancestors. In contrast, human species is a diurnal mammal whose more distant ancestors were nocturnal, although it is a matter of discussion whether the ancestral primates (our closest ancestors) were nocturnal (Ross, Hall, & Heesy, 2007; Veilleux, Louis, & Bolnick, 2013) or not nocturnal (Tan, Yoder, Yamashita, & Li, 2005). However, cow is not totally diurnal as it is classified as a *"crepuscuplar, cathemeral or arrhythmic animal"* (Gerkema et al., 2013) or alternatively as *"mostly diurnal with some crepuscular activity"* (Solovei et al., 2009). Furthermore, a phylogenetic change from nocturnal to diurnal phenotype occurred in bovine ancestors at a closer time than in the human case (Gerkema et al., 2013).

As explained in the *Introduction* section, the bovine pigment has been thoroughly used as the phototypical model for Rho and GPCRs in structural and functional studies. Likewise, mouse Rho has been often used as a model for *in vitro* and mainly *in vivo* reports in vision studies. Keeping in mind that

a large body of work on human diseases related with opsins was characterized by using these models, the selection of human Rho appears to be a more appropriate candidate if we want the results obtained to have physiological relevance the analysis of human diseases phenotypes and molecular mechanisms. And this approach, at the same time, should allow following a path to continue this work in order to get new insights into the similarities and differences among the different animal models used for the study of diverse Rho mutations causing retinal degenerations in humans. The human pigment, in comparison with the behaviour observed for the bovine and murine pigments can provide novel clues on structure-function relationships, as the inactive conformations and the activation mechanisms could show significant differences and deviations from those of mice. These differences can have physiological relevance and represent important points to consider attentively (Kazmin et al., 2015).

As an example, the characterization of a Rho mutation, Y102H, that in a chemically mutagenized mouse model can lead to light-induced degeneration of photoreceptors similar to that seen in autosomal dominant RP (Budzynski et al., 2010), was carried out in the background of human Rho in the current work. The molecular phenotype of this mutant was compared with the same point mutation, previously studied in our lab, but in the bovine Rho background (Herrera Hernández, 2017). This allowed comparison between our *in vitro* analysis and the bovine *in vitro* in a double cysteine stabilizing N2C and D282C background previously reported (Budzynski et al., 2010).

4.1.1 Sequence analysis

Studying amino acid point mutations in Rho sequences is an interesting approach to understand the biochemical and functional differences of visual

pigments and to provide novel clues for their molecular evolution from their ancestors. Major variants in the visual pigments system can be detected in nocturnal versus non-nocturnal animals, therefore the three corresponding sequences, human, bovine and murine, were aligned (Fig. 4.1.1) to pinpoint the amino acids that are equal in both human and cow, but different in mouse. Thus, the variations found from nocturnal to diurnal niche in these species were: V158A, I162V, F260A, L290I, S299A, L309M, D332E and A337V. Among them, the positions 260, 290 and 299 have been found to be closely associated with the retinal chromophore by their direct proximity or mediated by specific interactions with other amino acid residues.

Interestingly, position 260 is located near an opening between TM helices 5 and 6 in the activated state, that has been suggested to be the passage for retinal during the retinal release process (Piechnick et al., 2012; T. Wang & Duan, 2011), and besides this was found to be one of the positions of amino acid substitutions from inferred ancestral amniota Rho to inferred ancestral mammal Rho (Bickelmann et al., 2015).

The A299S mutation affects an amino acid located in a non-conserved position next to the binding pocket, and was studied in human medical cases as not always causing RP but having the potential to cause it (Chan et al., 2001). Also, previous studies have linked this position to spectral tuning in some vertebrates species (Dungan & Chang, 2017; Huabin Zhao et al., 2009), and it was also recently proposed to have an epistatic interaction with the conserved amino acid at position 83 affecting the kinetics of retinal release in killer whale Rho, accelerating the process in the case of the S299A substitution in this cetacean, and slowing it in the corresponding A299S change in bovine Rho (Dungan & Chang, 2017). In spite of this, no clear

pattern could be found in the diurnal/nocturnal therian mammals related with substitutions at the position 299.

Figure 4.1.1 Amino acid alignment of WT Rho in three different species: mouse, human and cow (bovine). Amino acid differences between the nocturnal (mouse) and the non-nocturnal (human and bovine) are highlight in grey.

More relevant to nocturnality could be the substitution at position 290. This site was found to be positively selected in the evolutionary branch leading to therian from early mammals (Bickelmann et al., 2015). It is worth nothing that the inferred early therian Rho has a slower Meta II decay rate than that of the inferred ancestral mammal Rho (Bickelmann et al., 2015). This change may be explained by ecological diversification on the Mesozoic era, that coincides with the mammalian "nocturnal bottleneck" (Borges et al., 2018;

Gerkema et al., 2013; Heesy & Hall, 2010). Moreover, we have compared the position 290 in 51 mammals pigments phylogenetically differentiated and found a great correlation with the nocturnal and diurnal activity pattern, where L290 is also found in the inferred ancestral therian sequence, supposed to be nocturnal (Table 4.1.1). At this point, it is necessary to emphasize that we had some difficulties in classifying some species due to the fact that they do not show a clear nocturnal or diurnal activity pattern. For this reason, aquatic species were excluded from the analysis.

Interestingly, subterranean rodents like *Heterocephalus glaber* (Table 4.1.1 and Fig. 4.1.2B), that have I290 could be considered as living in almost absolute darkness all their life, and therefore to have underwent an important regression in their visual system (Emerling & Springer, 2014). This may seem contradictory with the correlation of L290 with mammals living in niches with dim light environments but the visual conditions found by the subterranean animals might be very different from those experienced by nocturnal animals (Vega-Zuniga et al., 2017). In the same direction, research on the *Bathyergidae* species (strictly subterranean, coinciding with the rodent species highlighted in brown in Fig. 4.1.2B and with brown background activity pattern in Table 4.1.1) showed that, in spite of these visual deficits and regression, their eyes retained characteristics of diurnal mammals and their visual system is not adapted for low light vision (Kott, Němec, Fremlová, Mazoch, & Šumbera, 2016).

Table 4.1.1 Comparison of position 290 on nocturnal and diurnal therian mammals, along with their diurnal/nocturnal activity. Cathemeral: activity occurs across the 24 h cycle. Sequences retrieved from the NCBI. Primates highlight in red text and rodents in green text. *1 Although reported subterranean, during the night might emerge. Moreover it lacks cones, so this specie is rod monochromatic. (Emerling & Springer, 2014) *2 *Canis lupus* (wolf), the most near ancestor of the dog is primary a nocturnal / crepuscular specie (Merrill & David Mech, 2003). *3 Data corresponding to *Vicugna vicugna*, the wild ancestor of *Vicugna pacos* *4 Wild boar, the ancestor of pig is diurnal by nature but nocturnal in presence of humans in his habitat (Solovei et al., 2009).

Specie	290	Activity pattern
Inferred mammalian ancestor	V	Supposedly diurnal (Bickelmann et al., 2015)
Inferred therian ancestor	L	Supposedly nocturnal (Bickelmann et al., 2015)
>*Sarcophilus harrisii*	L	Nocturnal (Maor et al., 2017)
>*Cricetulus griseus*	L	Nocturnal (Hashimoto, Moritani, & Saito, 2004)
>*Mus musculus*	L	Nocturnal (Solovei et al., 2009)
>*Rattus norvegicus*	L	Nocturnal (Jacobs, Calderone, Fenwick, Krogh, & Williams, 2003)
>*Dipodomys ordii*	L	Nocturnal (Maor et al., 2017)
>*Thryonomys swinderianus*	L	Nocturnal (Maor et al., 2017)
>*Otolemur garnetti*	L	Nocturnal (Wikler & Rakic, 1990)
>*Otolemur crassicaudatus*	L	Nocturnal (Deegan & Jacobs, 1996)
>*Microcebus murinus*	L	Nocturnal (Santini, Rojas, & Donati, 2015)
>*Aotus nancymaae*	L	Nocturnal (Levenson, Fernandez-duque, Evans, & Jacobs, 2007)
>*Tarsius syrichta*	L	Nocturnal /crepuscular (Santini et al., 2015)
>*Sminthopsis crassicaudata*	L	Nocturnal (Maor et al., 2017)
>*Pteropus vampirus*	L	Nocturnal (fruit bat) (Gould, 1978)
>*Macropus eugenii*	L	Nocturnal (Maor et al., 2017)
>*Felis catus*	L	Nocturnal / crepuscular (Solovei et al., 2009)
>*Caluromys philander*	L	Nocturnal (Maor et al., 2017)
>*Dasypus novemcinctus*	L	Nocturnal / crepuscular (Maor et al., 2017)
>*Amblysomus hottentotus* *1	L	Subterranean / nocturnal / crepuscular (Maor et al., 2017)
>*Echinops telfairi*	F	Nocturnal (Lovegrove & Génin, 2008)
>*Canis familiaris*	L	Cathemeral *2 (Maor et al., 2017)
>*Equus caballus*	L	Crepuscular / Cathemeral (Solovei et al., 2009)
>*Loxodonta africana*	L	Cathemeral / diurnal (Maor et al., 2017)
>*Ursus maritimus*	L	Varies / diurnal (living within the Arctic Circle) (Hunter & Caro, 2008; Maor et al., 2017)
>*Vicugna pacos*	L	Diurnal (Maor et al., 2017) *3

>*Procavia capensis*	L	Diurnal (Maor et al., 2017)
>*Oryctolagus cuniculus*	I	Nocturnal / cathemeral (Maor et al., 2017; Solovei et al., 2009)
>*Monodelphis domestica*	I	Nocturnal (Zuri, Su, & Halpern, 2003)
>*Myotis lucifugus*	I	Nocturnal (insectivorous bat) (Maor et al., 2017)
>*Mustela furo*	I	Nocturnal / crepuscular (Solovei et al., 2009)
>*Ailuropoda melanoleuca*	I	Crepuscular / cathemeral (Kelling et al., 2006)
>*Bathyergus suillus*	I	Strictly subterranean (Kott et al., 2016; Huabin Zhao et al., 2009)
>*Heterocephalus glaber*	I	Strictly subterranean (Emerling & Springer, 2014)
>*Fukomys damarensis*	I	Strictly subterranean (Kott et al., 2016; Huabin Zhao et al., 2009)
>*Heliophobus argenteocinereus*	I	Strictly subterranean (Kott et al., 2016)
>*Cavia porcellus*	V	Diurnal / crepuscular (Grant, Delaunay, & Haidarliu, 2017; Solovei et al., 2009)
>*Ictidomys tridecemlineatus*	I	Diurnal (Smale, Nunez, & Schwartz, 2008)
>*Octodon degus*	I	Diurnal (Jacobs et al., 2003)
>*Ochotona princeps*	I	Diurnal (Maor et al., 2017)
>*Ovis aries*	I	Diurnal / crepuscular (Smale et al., 2008; Warren & Mysterud, 1978)
>*Bos taurus*	I	Diurnal / Crepuscular (Solovei et al., 2009)
>*Sus scrofa*	I	Diurnal (Solovei et al., 2009) *4
>*Pongo abelii*	I	Diurnal (Santini et al., 2015)
>*Nomascus leucogenys*	I	Diurnal (Santini et al., 2015)
>*Homo sapiens*	I	Diurnal (Santini et al., 2015)
>*Gorilla gorilla*	I	Diurnal (Santini et al., 2015)
>*Pan troglodytes*	I	Diurnal (Santini et al., 2015)
>*Macaca mulatta*	I	Diurnal (Wikler & Rakic, 1990)
>*Macaca fascicularis*	I	Diurnal (Santini et al., 2015)
>*Callithrix jacchus*	I	Diurnal (Troilo, Rowland, & Judge, 1993)
>*Macroscelides proboscideus*	I	Diurnal / crepuscular (Maor et al., 2017)
>*Camelus dromedarius*	I	Diurnal (Maor et al., 2017)

We decided to construct the phylogenetic trees of rodents and primates to better visualize the data (Fig. 4.1.2). These orders were selected as the phylogenetic studies reported for therian mammals, and related with the

activity pattern, were mainly focused on primates and rodents (Maor et al., 2017). Both orders have a significant degree of specialization in their visual systems (Santini et al., 2015) that shows a more specific and clear dominant temporal niche than in other orders, at least in the species with sequenced Rho that we could use for this study.

In the case of primates (Fig 4.1.2A), although the diurnal or nocturnal nature of the common ancestor is a matter of debate, recent studies point to the nocturnal theory (Maor et al., 2017; Santini et al., 2015). In this theory, the evolution to diurnal would be produced whether in the ancestor of *Haplorrini* (where the Tarsius would have been secondary readapted to nocturnality) or in the ancestor of *Siimiformes*. In any case a secondary return to nocturnality, in genus *Aoutus,* is widely accepted (Santini et al., 2015).

Another diurnal organism, the zebrafish (*Danio rerio)*, was found to have L290 although the phylogenetic evolution and physiological differences with mammals (like body temperature) make direct comparison with mammals difficult. On the other hand, the retinal release in this animal Rho was recently studied, and it was found that the L290I change resulted in a faster Meta II decay (Morrow & Chang, 2015). This result would be consistent with an amino acid change from early therian nocturnal to nowadays diurnal phenotype. Changes in the rate of retinal release were found to depend primarily on the positioning of the chromophore inside the binding pocket, and on the accessibility of bulk water during Schiff base hydrolysis (Piechnick et al., 2012).

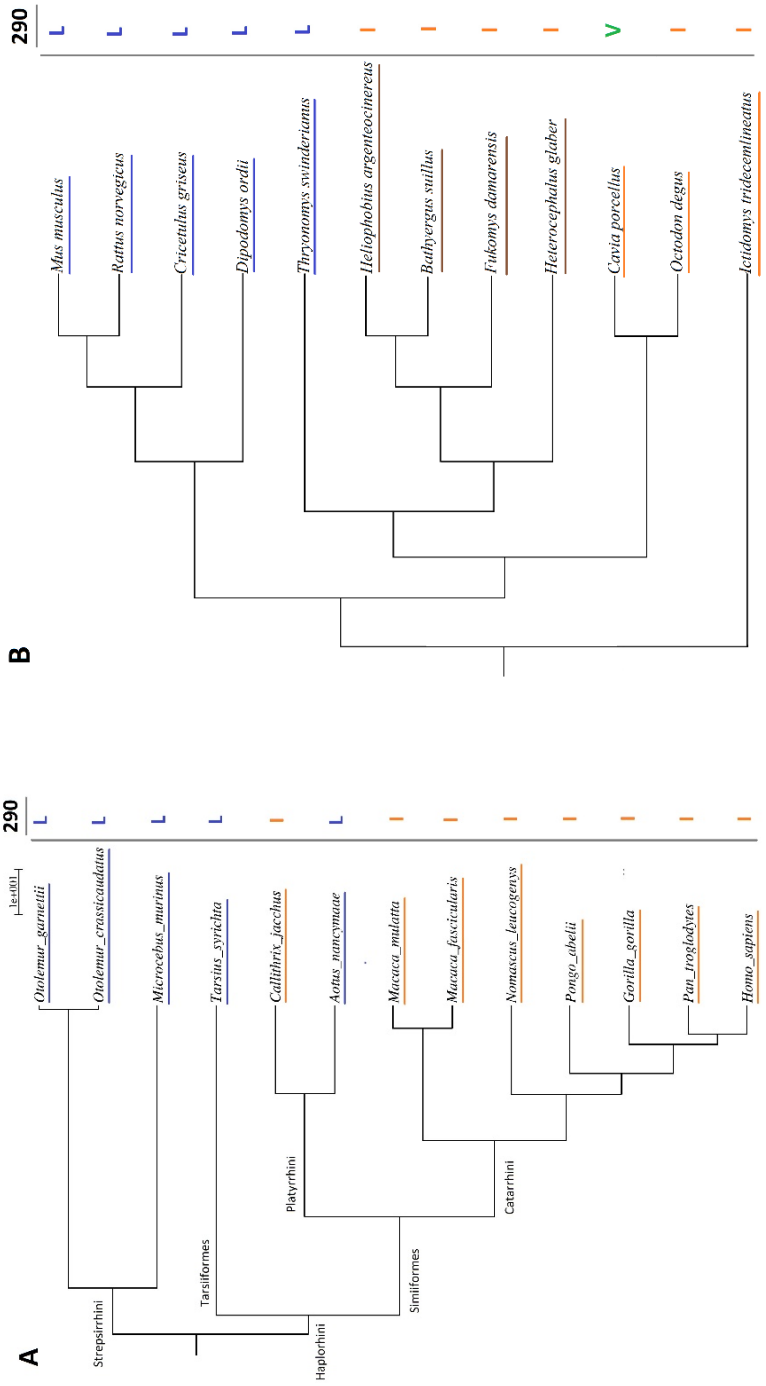

Figure 4.1.2 Phylogenetic trees of the primate (A) and rodent (B) orders. Species analysed in table 4.2.1. Amino acid residues in position 290 are shown in the right side of each specie. Activity pattern is indicated by the underlining colour: **Blue as nocturnal** species, **orange as diurnal** species and **brown** (in rodent) **as strictly subterranean** species which correspond with the *Bathyergidae* family. Tree A was downloaded from 10kTrees Website. Tree B was gently constructed by Dr. Gabriela Aguileta after an analysis of the Rho phylogenetic tree.

Taking all these facts into account, it appears that the introduction of L at position 290 could be one of the important adaptations in scotopic vision of early therians meanwhile L290I could be one of the critical amino acid changes associated with diurnal niches along therian evolution. Furthermore, the L290I substitution is likely to be the result of independent analogous changes, as it appears in therian mammals of different phylogenetic branches that had independently readapted to diurnal vision. In order to test that hypothesis, the experimental analysis and biochemical characterization of this Rho substitution (L290I) was herein performed in a nocturnal species background like that of mouse.

4.1.2 Construction and purification of Rho

The Y102H mutation (associated with retinal degeneration in mouse) was constructed in the human opsin gene and the L290I mutation in the mouse opsin gene by site directed mutagenesis. The correct introduction of the mutations was confirmed by DNA sequencing (Fig 4.1.3).

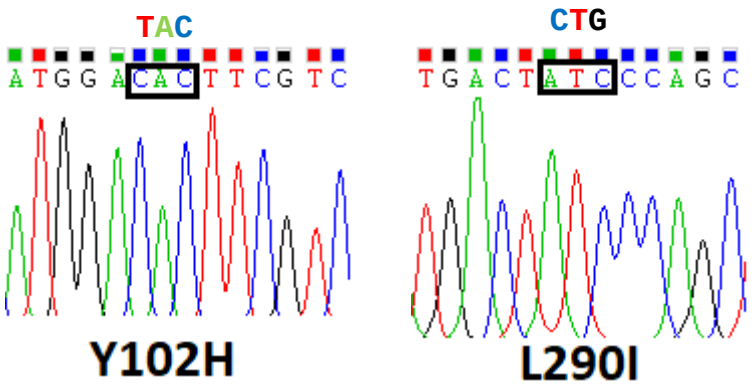

Figure 4.1.3 DNA sequencing for the two Rho, human Y102H and mouse L290I. Amino acid mutation are boxed. Original WT sequence for this mutation is written above.

All Rho genes were expressed in COS-1 cells, the cells were harvested and subsequently regenerated with 11-*cis*-retinal. The regenerated cells were solubilised in 0.05 % DM and immunopurified with the Rho-1D4 antibody as described under *Materials and Methods*. The purified proteins were analysed at 20°C by means of UV-vis spectrophotometry in the wavelength range from 250 nm to 650 nm.

Slight but significant differences can be detected in the wavelength maximum of the visible chromophoric band in the purified protein spectra (Fig. 4.1.4). Besides the common band for the three species at 280 nm representing the opsin apoprotein, the λ_{max} of the spectral chromophoric characteristic band in the visible region is slightly shifted. Thus, human Rho shows a λ_{max} at 495 nm, mouse Rho at 502 nm and bovine Rho at 498 nm. These results point to subtle differences in the retinal binding pocket of the three pigments. On the other hand the Y102H mutation in human Rho produces a slight shift to 494 nm, that is consistent with the data previously observed in our laboratory where the same mutation in bovine Rho showed a blue-shift of 2 nm compared with WT bovine Rho (Herrera Hernández, 2017). A similar behaviour was observed in the L290I on mouse pigment, as it produced a blue-shift of 2 nm to 500 nm.

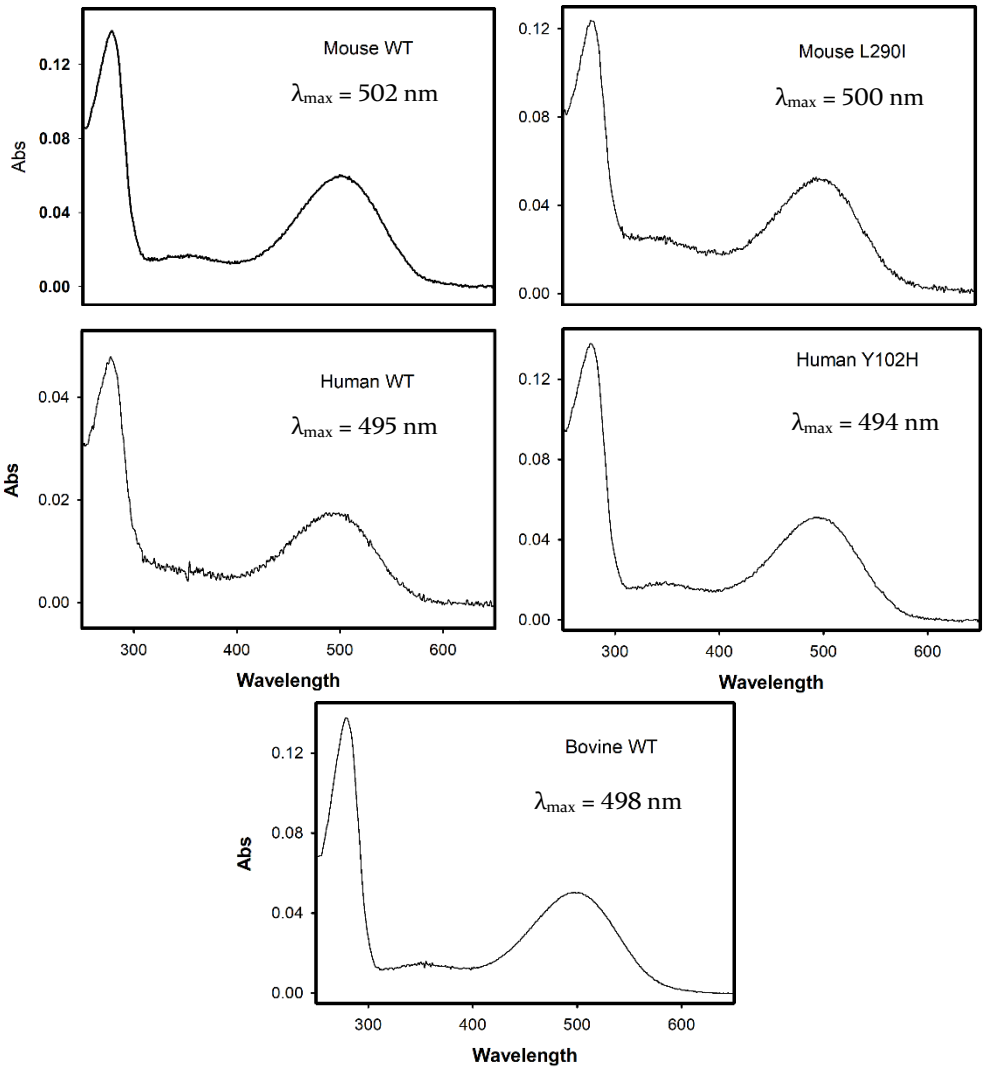

Figure 4.1.4 Purified recombinant Rho UV-vis spectra at 20°C in the dark state. Absorption spectra of immunopurified human, mouse and bovine rhodopsin WTs, and the mouse L290I and human Y102H mutants. All the proteins in PBS pH 7.4 and 0.05 % DM.

The photoresponse of the purified pigments was measured by means of photobleaching the protein samples for 30 s using a 495 nm cut-off filter, and the illuminated sample was subsequently acidified in order to

reprotonate the Schiff base (Figure 4.1.5). No significant differences were observed in the photobleaching and acidification behaviour of all five analysed proteins.

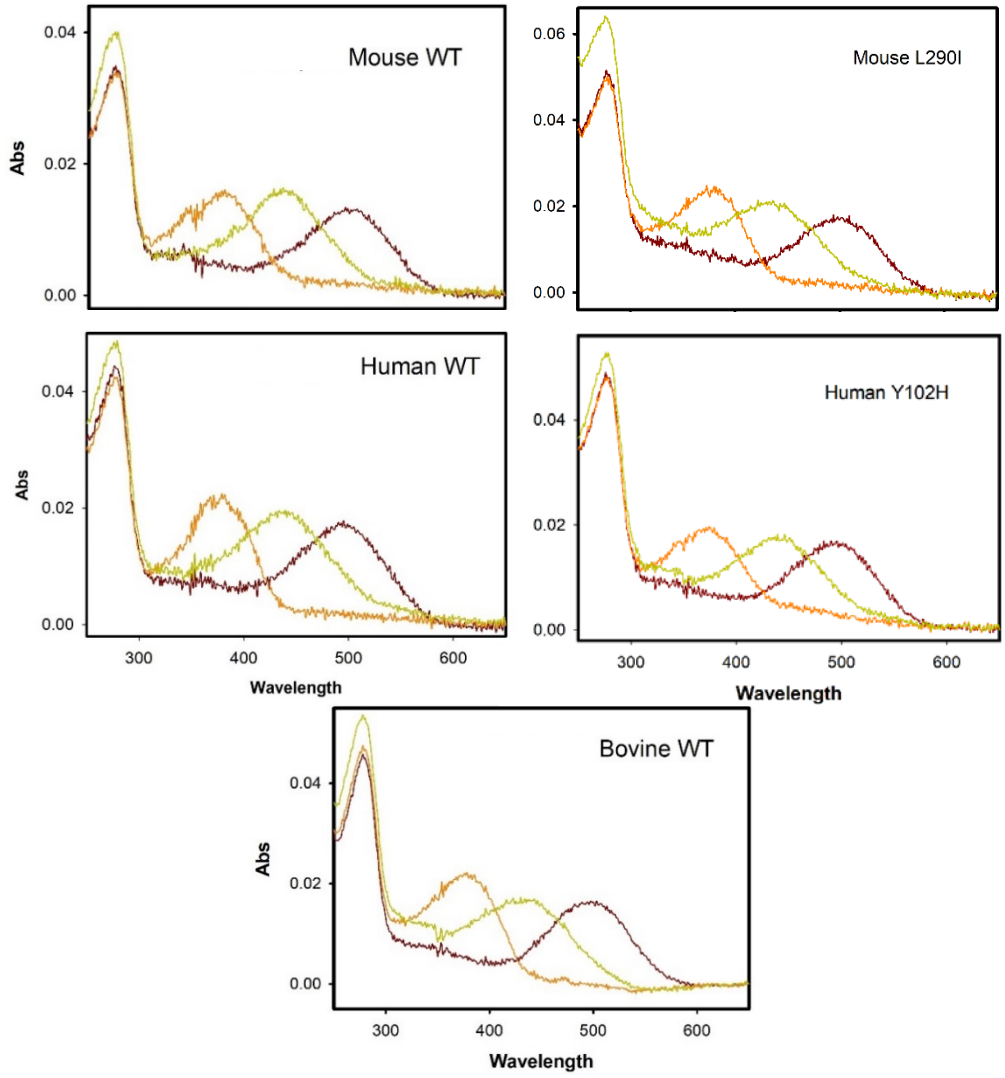

Figure 4.1.5 Photobleaching and acidification behaviour of purified pigments. Absorption spectra of immunopurified human, mouse and bovine Rho in the dark (red), after illumination (orange) and after acidification (green). All the spectra were measured at 20°C.

4.1.3 Dark-state thermal stability

The kinetics of the thermal stability decay process was measured at 48°C by following the decrease in the visible A_{max} for each protein, with time. The temperature used on the thermal decay experiments, 48°C, was selected according to previous experimental studies, and it is under 52°C for which Rho could start to be involved in structural changes related to partial or complete denaturation, that becomes the dominant mechanism producing retinal release without activation of phototransduction (Guo et al., 2014).

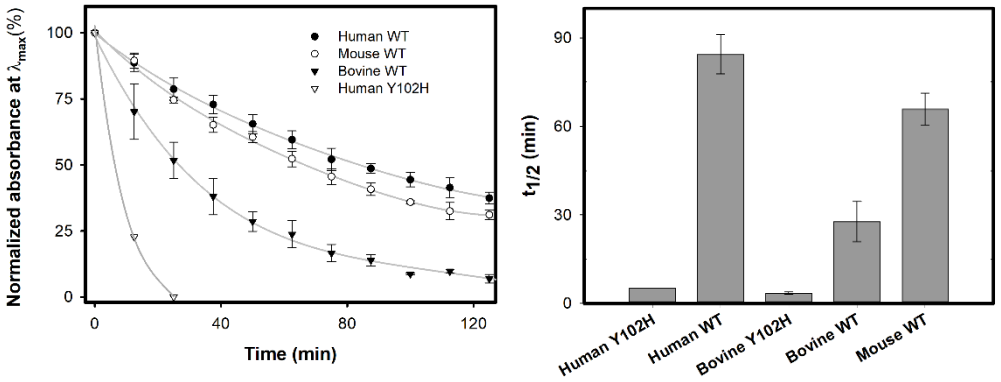

Figure 4.1.6 Thermal stability of purified Rho proteins at 48°C. Average and S.E, with the normalized value in brackets (bovine WT taken as 1.0) are the following: human Y102H: $t_{1/2}$ = 5.1 min (0.2), human WT: $t_{1/2}$ = 84.5± 6.6 min (3.1), mouse WT: $t_{1/2}$ = 65.8±5.4 min (2.4), bovine Y102H: $t_{1/2}$ = 3.4 ± 0.4 (0.1) bovine WT: $t_{1/2}$ = 27.8 ± 6.8 min (1.0). Result from bovine Y102H retrieved from a previous study (Herrera Hernández, 2017).

The half-life ($t_{1/2}$) of the thermal decay process (Fig. 4.1.6) for human and bovine WT Rho was similar to that observed in a very recently published study (Morrow et al., 2017). The comparison of the values for bovine and mouse is also similar to that obtained in a previous work (Yanagawa et al., 2015). In contrast, the human Y102H mutant was very unstable, similarly to

the same mutation studied in our laboratory in the bovine background where the $t_{1/2}$ obtained was 3.4 ± 0.4 min (Herrera Hernández, 2017).

4.1.4 Dark-state chemical stability

Hydroxylamine is a strong nucleophile that has been used in Rho structure-function studies. Bovine Rho is quite stable to hydroxylamine at neutral pH in the dark when the Schiff base is not reactive due to the well-protected retinal binding site. However in the activated state, Meta II, the ligand binding pocket is readily accessible so the hydroxylamine quickly hydrolyses the Schiff base linkage (Beyrière et al., 2015; Farrens & Khorana, 1995) and rapidly forms a stable retinal oxime with all-*trans*-retinal that absorbs around 360 nm (Kawamura & Yokoyama, 1998; Stiles et al., 2015).

The chemical reactivity in the dark state was measured as the reduction in A_{max} in the visible spectral region over time. Hydroxylamine reactivity of the human WT Rho is quite similar to that of bovine WT meanwhile mouse WT is slightly faster (Table 4.1.2). A point of interest is the chemical stability of human Y102H as it is just slightly faster than human WT, in contrast with the previously studied mutation in the bovine background where the initial rate was 0.00530 min^{-1}, that means 4.5 times the initial rate of bovine WT Rho (Herrera Hernández, 2017).

Table 4.1.2 Hydroxylamine reactivity of purified Rho samples. Initial rate of the chemical reactivity process in the presence of hydroxylamine 50 mM at 20°C for the different Rho samples in the dark state. Relative values are shown in brackets and are related to bovine WT taken as 1. [1] Data from bovine proteins obtained from previous work in our laboratory (Herrera Hernández, 2017).

	Initial velocity (min^{-1})
Bovine WT [1]	0,00118 (1)
Bovine Y102H [1]	0.00530 (4.5)
Mouse WT	0,001950 (1,653)
Human WT	0,001306 (1,107)
Human Y102H	0,001957 (1,658)

In the course of these experiments, differential behaviour has repeatedly been observed at the end of the chemical stability assay of human Rho. After 2 h of monitoring Rho spectra in the presence of hydroxylamine in the dark, the sample was photobleached with a λ>495 nm cut-off filter for 30 s, but unlike the response in the case of bovine or murine cases (Fig. 4.1.7C), a distinguishable isoform of opsin around 467 nm was observed (Fig. 4.1.7.A) similar to the 460-470 nm absorbing band previously described as Meta III (Imai et al., 2007; Lewis, Van Kuijk, Carruthers, & Kliger, 1997; Sommer & Farrens, 2006). This is better appreciated when comparing the difference spectrum between spectra obtained immediately and 10 min after illumination (Fig. 4.1.7.B.3). Three bands are noticeable, a positive band at 360 nm associated with the rise of retinal oxime, and two negative bands at 412 nm and 467 nm (the putative Meta III conformation). Here, we propose that the 412 nm band corresponds to a superimposed 380 nm species that was present just after the illumination and shifted towards 360 nm in subsequent scans, as it fits perfectly with a spectrum with λ_{max} at 380 nm

(Fig. 4.1.7 B. 1 and 4). In any case this 380 nm band could correspond to the Meta II formed in constant equilibrium with Meta III (Imai et al., 2007).

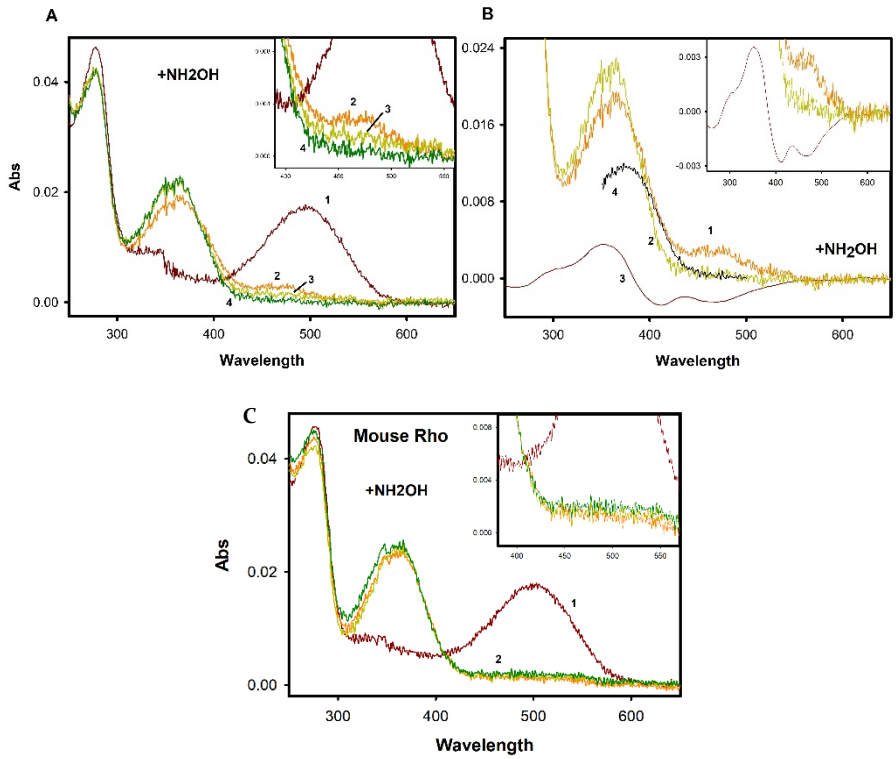

Figure 4.1.7 Purified human Rho (A and B) and mouse Rho (C) photobleaching after hydroxylamine treatment. **A)** Spectrum of human Rho: 1-human Rho in the dark state, 2-immediately after 30s illumination with 495nm cut-off filter, 3-spectrum recorded 5 min after illumination, 4-spectrum recorded 10 min after illumination. *Inset:* detail of the same spectra to better observe the different curves in the visible region. **B)** Detail comparison of spectra in: 1-immediately after illumination, 2- 10 min after illumination, 3-difference spectrum calculated by subtracting the data in 2 from that recorded after 10 min (the spectrum was smoothed with Sigma Plot), 4-normalized detail of an absorbance spectrum of a Meta II state of human Rho in the absence of hydroxylamine. *Inset*: Detail of 1, 2 and 3 were the bands of the difference spectrum can be better visualized. **C)** Spectrum of mouse Rho: 1-mouse Rho in the dark state, 2- overlayed spectra: immediately after 30s illumination and recorded after 5 min and 10 min after illumination. *Inset*: Detail to better observe spectra in the visible region.

The relatively low Meta III band observed in our results, compared with the retinal oxime band could be partially explained by previous studies where it

was found that the decay of Meta I/Meta II into Meta III *in vitro* is related with the pH, where a maximum of 35 % was attained at pH 8.0 (Heck et al., 2003), whereas the band we measured at 467 nm represents around the 18.7 % of the final retinal oxime at pH 7.4. The formation of this band is also affected by DM detergent concentration (Ramon et al., 2003).

An additional experiment was conducted to verify whether this behaviour occurs as well during the photobleaching in the absence of hydroxylamine. For this purpose a sample of human WT Rho was illuminated with a cut-off filter at 495 nm for 30s and successive measurements were recorded each 2 minutes. As observed in Fig. 4.1.8, the result observed is similar to that expected in bovine Rho, were after photoactivation of the dark Rho the Meta II gradually decay to Meta III (Ramon et al., 2003). Not Meta III was visible immediately upon illumination as it was observed in the experiment in the presence of hydroxylamine.

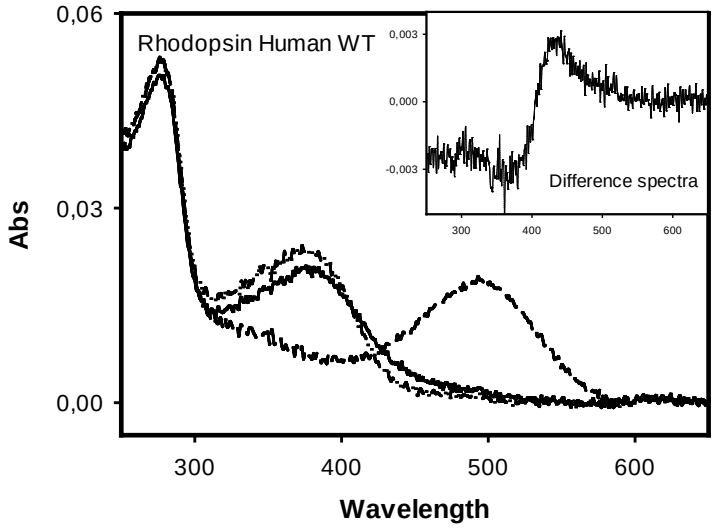

Figure 4.1.8 Purified human WT Rho photobleaching at 20°C. Dashed line: dark state. Dotted-dashed line: measured immediately after photobleaching. Continuous line: measured 28 min after photobleaching. Inset: difference spectrum between the two photobleached spectra obtained after illumination.

4.1.5 Meta II stability

The decay of the Meta II conformation involves hydrolysis of the Schiff base bond followed by release of all-*trans*-retinal from the binding pocket (Lamb, 2013). We have determined the Meta II decay process, and more precisely the associated retinal release, by means of a fluorimetric assay in which tryptophan fluorescence increase is recorded over time after illumination. The $t_{1/2}$ of this process is determined for each Rho sample analysed.

As observed in Fig. 4.1.9, mouse Rho has a clearly slower Meta II decay ($t_{1/2}$ = 25.76 ± 0.37 min) than that obtained for the other two species. When comparing human ($t_{1/2}$ = 12.09 ± 0.72 min) and bovine retinal release ($t_{1/2}$ = 13.9 ± 0.8 min), human Rho apparently has a slightly slower $t_{1/2}$ although our statistical analysis did not find it to be significant. In contrast, similar difference was found to be significant for both Rho in a recent study, (Morrow et al., 2017). Besides, this small difference is consistent with a previous study where a faster Meta II decay in human, compared to bovine Rho, was reported (Lewis et al., 1997).

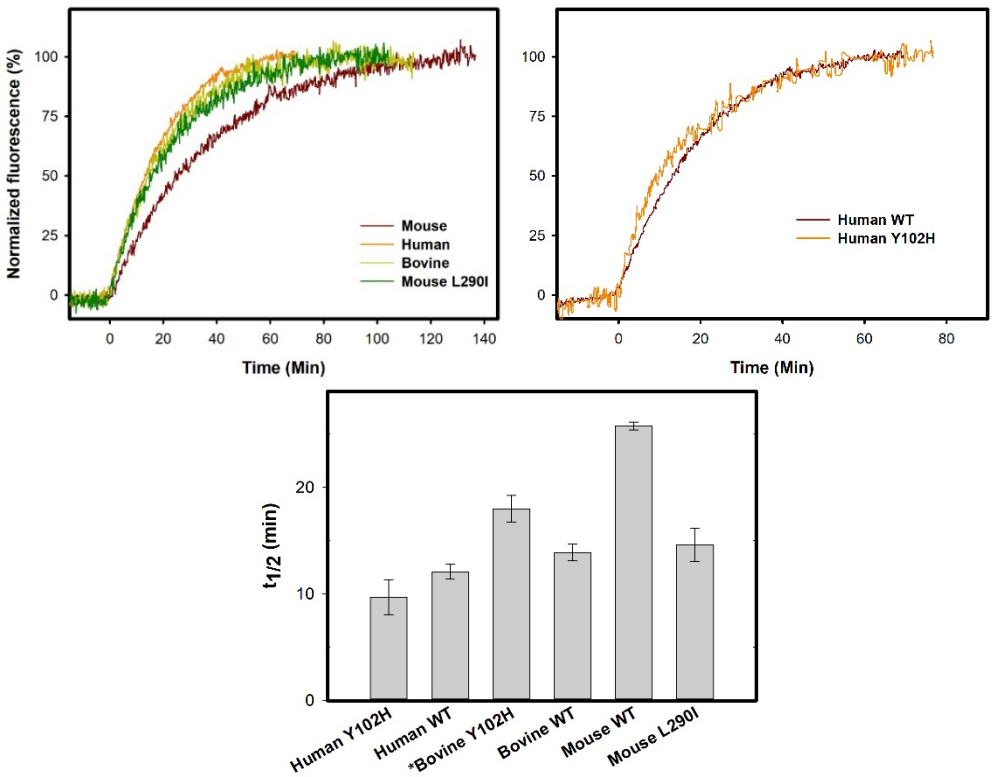

Figure 4.1.9 Meta II decay of photoactivated purified Rho samples at 20°C. The $t_{1/2}$ of retinal release was measured. Illumination was carried out at min = 0. Average data and S.E. are the following: human WT: $t_{1/2}$ = 12.09 ± 0.72 min, bovine WT: $t_{1/2}$ = 13.9 ± 0.8 min, mouse WT: $t_{1/2}$ = 25.76 ± 0.37 min, mouse L290I: $t_{1/2}$ = 14.61 ± 1.55 min, bovine Y102H: $t_{1/2}$ = 18.00 ± 1.25 min, and human Y102H: $t_{1/2}$ = 9.67 ± 1.64 min. *Data from bovine Y102H retrieved from (Herrera Hernández, 2017).

Our results show faster Meta II decay in human WT (diurnal) and bovine WT Rho (diurnal/crepuscular) in contrast with the slower decay for mouse WT Rho (nocturnal) retinal release. Moreover, the L290I mutation introduced in the mouse Rho background reverts the retinal release rate to a faster one (14.61 ± 1.55 min) similar to that for bovine WT Rho.

On the other hand, a slightly faster Meta II decay was observed in the human Y102H mutant (9.67 ± 1.64 min) when compared with human WT (12.09 ±

0.72 min), although this difference appeared not being statistically significant. Similar results between Y102H and WT were obtained in the thermal stabilized bovine N2C/N282C double mutant background (Budzynski et al., 2010) although in that case the presence of a stabilizing engineered disulfide bond and the use of a different methodology prevents the direct comparison with our results. Interestingly, this kinetics values are in contrast with the one obtained for Y102H in the bovine background, where the retinal release $t_{1/2}$ measured previously in our laboratory was 18.00 ± 1.25 min (Herrera Hernández, 2017).

4.1.6 Genotype-phenotype relationship

There is a 93 % sequence identity between human and bovine (Funatogawa, Szundi, & Kliger, 2016), a 94.8 % in mouse/human identity and a 93.5 % between mouse and bovine sequences. In spite of this very high sequence identity, functional differences among these three different Rhos were observed.

The thermal decay results are related on one side, and from a biochemical point of view, with the correctly folded conformation and the thermodynamic properties of the protein. From a physiological point of view, the thermal decay process is linked to the concept of spontaneous thermal activation that could occur, in the absence of light, in the opsins of the retina, that is the so-called dark noise in dim-light vision, (Baylor & Burns, 1998; Lamb, 2013). This phenomenon produces a change in the membrane current indistinguishable from that produced by a single photon photo-activated Rho, as a results of spontaneous thermal activation of Rho. This dark noise can occur even at physiological temperature, at a very low rate. This noise only represents half of the total noise present in rod cells in

the dark, been the other half attributed to the continuous spontaneous activation of downstream signalling molecules, mainly associated with cGMP phosphodiesterase (Field & Sampath, 2017; Tian, Sakmar, & Huber, 2017).

Important considerations appear at this point, as the morphology of the retina largely differs between species in terms of rod converging (e.g. the quantity of rod cells converging its signal to a single retinal ganglion cell is 10 fold higher in the nocturnal cat peripheral retina than in primates (Goodchild, Ghosh, & Martin, 1996)), collecting and amplifying the signals at the cost of visual acuity and more noise. It is also important to highlight that the bipolar pathway (downstream rod cells) has been shown to be involved in the reduction of noise by non-linear threshold mechanisms, although recent studies suggests that this noise is only partially quenched (Field & Sampath, 2017). Based on this, we may assume that is reasonable that a nocturnal species Rho, like mouse, is more stable in the dark than the non-nocturnal bovine Rho. However, it is intriguing why human Rho shows such a high thermal stability in the dark.

The thermal decay process may involve two different pathways, at the molecular level, which are not usually distinguished in the literature:

1- Direct 11-*cis*-retinal release after hydrolysis of the Schiff base, and thus formation of free opsin. Followed by a thermal isomerization from 11-*cis*-retinal to all-*trans*-retinal.
2- Isomerization of 11-*cis*-retinal to all-trans-retinal inside the ligand-binding pocket, producing the active Meta II conformation followed by hydrolysis of the unprotonated Schiff base to give free all-*trans*-retinal (Piechnick et al., 2011).

In previous studies, the spontaneous electrophysiological activation of Rho in the dark state in native disk membranes was mostly attributed to the effect of the second pathway as there was no illumination by photons (Luo, Yue, Ala-Laurila, & Yau, 2011; Tian et al., 2017). Nevertheless, in a recent study with purified bovine Rho, at 37°C, it was found that the main observed pathway actually was the direct retinal release; being three orders of magnitude faster than the thermal isomerization inside the binding pocket (Tian et al., 2017). Other studies found that increasing the temperature of the experiment could shift the main pathway to the isomerization over the 11-*cis*-retinal release pathway (Liu et al., 2013). An interesting question arises here about the balance between both pathways in the different species and how it compares under *in vitro* and *in vivo* conditions. Further research should be carried out in order to clarify this point.

On the other hand, a report strongly suggests a relationship between the wavelength of the A_{max} of the visible chromophoric band and the heat activation energy of the pigments (Luo et al., 2011). This old theory proposed by Barlow in 1957, was also tested in some fish species showing that these variations in thermal activation are noticeable, although they compared larger variations (Luk et al., 2016) than the ones analysed in this section. On this basis, it was suggested that the red-shifted pigment had comparative a lowered thermal activation energy and thus was more susceptible to spontaneous thermal activation. This would represent more noise in night vision. Regarding our results (Fig. 4.1.6), it would appear that the relationship between bovine and human WT Rho or between mouse and human WT Rho would follow this model, although the small λ_{max} difference may preclude deriving a solid conclusion on this.

Finally, a recent work where bovine and human Rho were compared, with a reconstructed ancestral mammalian Rho found a half-life decay of the dark state of this ancestral protein to be in an intermediate point between human and bovine. Therefore, it was concluded that bovine and human Rho evolved in opposite direction, in terms of thermal stability from an ancestral Rho (Morrow et al., 2017).

Taking all this information into account, it is difficult to pinpoint separately the physiological implications of our thermal stability results and thus it is unclear their meaning in terms of evolutionary relationships among species. In spite of this the thermal stability similarities of the mouse Rho with the ancestral mammalian Rho (both of them are in a medium term compared with human and bovine Rho) (Morrow et al., 2017) allow us to infer that this rodent Rho may be a more conserved protein regarding this biochemical feature.

In the presence of **hydroxylamine**, the decay kinetics of the three different WT Rho exhibited a similar behaviour (Table 4.1.2), being the mouse Rho stability only slightly lower than those of bovine and human Rho. This would indicate that the structural compaction around the Schiff base may be similar in the three Rho.

More interesting may be the formation of Meta III that was only observed in the case of human Rho and not in the bovine or the mouse cases. The hydroxylamine reactivity on Meta III was previously reported in detergent-solubilized Rho (Piechnick et al., 2011). The rate of Meta III decay caused by hydroxylamine is significantly slower than the decay rate for Meta II, and this data fits with the human Rho Meta III behaviour observed in our results (Fig. 4.1.7). Hence, the Meta III Schiff base could be less susceptible to hydroxylamine attack by having a structure that excludes it from the binding

pocket or because the protonation state affects the reaction with this chemical compound. Both interpretations are consistent with the idea that Meta III has more similarities with dark-state Rho than Meta II conformation (Piechnick et al., 2011).

In the light of our results, it is important to highlight that we cannot exclude Meta III formation, under given specific conditions, in the case of mouse or bovine, since experiments performed in detergent may favour the Meta II formation (Ramon et al., 2003; Sommer & Farrens, 2006). But it is clear that we cannot observe Meta III formation in bovine and mouse Rho under our experimental conditions. Furthermore, the different behaviour in the formation of Meta III after the hydroxylamine stability experiments, between human and bovine or mouse Rho could have some implications:

a) In different isolated retina studies it was found that referring to production and decay of Meta III, it occurs 3-fold more slowly in mouse than in the human case (Nymark, Frederiksen, Woodruff, Cornwall, & Fain, 2012). These results would be consistent with the results obtained here since mouse Rho would have a delayed Meta III production.
b) Next, about the question why this Meta III, in the presence of hydroxylamine, was observed in human but not in bovine Rho, some mechanisms could have clues to explain this experimental observation. As observed *in vivo* and in detergent solubilized experiments, the formation of deprotonated Schiff base intermediates proceeds faster in the human case , supporting the view that there are structural changes associated with Meta I that forms faster in human Rho (Kazmin et al., 2015). On the other hand, previous works found that the fraction of human Rho converted to

Meta III was higher than in bovine Rho under analogous conditions (Funatogawa et al., 2016; Lewis et al., 1997). Thus in both cases (comparing with bovine and mouse pigments) it is tempting to speculate that this Meta I/Meta II rapid formation in human Rho could favour somehow the subsequent formation of Meta III during the hydroxylamine reaction in the time frame of our experiment.

c) The Meta III decay could have relevance from a physiological point of view by its regulation of the free all-*trans*-retinal concentration in ROS. A recent report suggests that Meta III could be considered as a rate-limiting factor for Rho regeneration by contributing to the homeostasis of free all-*trans*-retinal, essential for the functionality of the visual signal under different light intensities (Chatterjee et al., 2015). Other authors have demonstrated, *in vitro* and in isolated cells, that Meta III decay could be a key intermediate in the recovery of the rod cells after a moderate photobleaching stimulus (Imai et al., 2007), or established a link between the rate of Meta III decay and the rate of dark adaption (Frederiksen et al., 2016). In the literature, Meta III is often associated with storage function by temporarily sequestering all-*trans*-retinal (Bartl & Vogel, 2007; Organisciak & Vaughan, 2010; Ritter, Zimmermann, Heck, Hofmann, & Bartl, 2004).

d) In addition, it was found that the presence of arrestin also prevents Meta III formation (Beyrière et al., 2015; Sommer & Farrens, 2006). This would support the idea that apparently under dim light conditions the shut-off mechanisms occurring in the rod cells would be sufficient to prevent the accumulation of all-*trans*-retinal and its reported toxicity (Funatogawa et al., 2016) and that arrestin already present in ROS could limit Meta III formation. Meanwhile, under

extended illumination conditions, this Meta III conformation was seen to accumulate to a certain amount (Ritter, Elgeti, Hofmann, & Bartl, 2007). Thus this accumulation would play a role in protecting photoreceptor cells by reducing the excess of free all-trans-retinal acting like a storage mechanism (Heck et al., 2003). This would be the main role rather than a delayed dark adaptation, when it is not eliminated (Frederiksen et al., 2016), as it can be deduced from experiments in intact rods of arrestin-deficient mouse where the Meta III decay was substantially reduced compared to that of mouse WT Rho (Frederiksen et al., 2016).

e) Furthermore, from a physiological standpoint, the presence of the Meta III conformation could lower the probability of quantum catch (proportion of incident photons that are captured by the pigments) of rods cells. This would, consequently, reduce the excitation potential of the photoreceptor just saturated by light and could play a significant role in the light adaptation process (Heck et al., 2003).

The Meta II decay. In the last years, an increasing number of studies have focused on the biochemical properties of visual pigments, other than the well-studied spectral tuning, to try to understand the adaptation of the visual process to different living environments. Particularly, different studies have emphasized the importance of the retinal release process in the molecular basis of vision (Dungan & Chang, 2017; Hauser et al., 2017). According with the results obtained (Fig. 4.1.9), a correlation may be inferred between the nocturnality/diurnality of the different species analyzed and the retinal release of the corresponding Rho. Moreover, several aspects can be considered on this topic that can be discussed:

Previously, a nocturnal prototherian mammal Rho, the purified echidna pigment, was reported to have a fast retinal release at 20°C (9.56 ± 2.6 min) (Bickelmann, Morrow, Müller, & Chang, 2012). This result may seem to be in contradiction with our hypothesis, however it could be argued that the Meta II stability could be related with the specific echidna low corporal temperature that is about 30°C (Schmidt-Nielsen, Dawson, & Crawford, 1966). As the Meta II decay kinetics have been shown to be thermally dependent on physiological temperature (Morrow & Chang, 2015; Morrow et al., 2017), this result cannot be directly compared with our Meta II decay results. In the case of our data, bovine, human and mouse have similar body temperatures in the 36-38°C range, so their Rho kinetics can be directly compared. Other studies in immunopurified Rho have resulted in a Meta II decay rate of 33 min in dogs (Zhu et al., 2004), a cathemeral domestic animal that probably preserves nocturnal/crepuscular characteristics from his recent wolf ancestor (Merrill & David Mech, 2003), and 23.6 min for the hippopotamus (Dungan & Chang, 2017), a specie with a peak activity during night-time and a retina specialized to enhance dim light vision compared with other animals of the same order (Coimbra, Bertelsen, & Manger, 2017).

A previous study also recreated the inferred ancestral Rho from early amniota, mammalia and theria and obtained their Meta II decay, 16.5 min, 22.5 min and 27.5 min respectively (Bickelmann et al., 2015) These values, could be related with the nocturnal bottleneck affecting early therians (Bickelmann et al., 2015), and the hypothesized preceding mesopic bottleneck affecting early mammals (Gerkema et al., 2013). This interpretation was recently supported by a study implicating different visual genes where an increased adaptation to dim-light condition was observed in the case of ancestral mammals towards the branch to theria, from an

inferred diurnal amniota (Wu, Wang, & Hadly, 2017). Therefore, the results reported from inferred ancestral Rho would be consistent with our results and with the proposed relationship between retinal release and nocturnal/diurnal animal behaviour.

Meta II decay is related with the deactivation of the Rho visual signal. However, the physiological meaning of the long-lasting Meta II, and its evolutionary meaning, has been reported to be unclear (Bickelmann et al., 2015; Yanagawa et al., 2015). In fact, a simple explanation cannot easily be found, as studies conducted in rod cells have shown that under dim light illumination the presence of arrestin produces a very fast shutoff of the pigment signal after its phosphorylation by Rho kinase (Lohse & Hoffmann, 2014), in the order of 80 ms after illumination (Fu & Yau, 2007). Although later theoretical studies lowered it to values as low as 36 ms (Gross & Burns, 2010) despite that background signal is still generated by these phosphorylated and arrestin-bound photoproducts (Ala-Laurila et al., 2006). This shut-off times highly differ from the Meta II decay times (Fu & Yau, 2007; M. Kim et al., 2011), even if we take into account the stability conferred for the detergent and the temperature used in our measurements, in contrast with the native physiological conditions. In this sense, the shut-off was observed in the order of 3 s after illumination in the absence of Rho kinase (Gross, Pugh, & Burns, 2012) or in the order of 50 s in mouse in absence of arrestin (Kefalov, 2012). Interestingly on transgenic mouse models in absence of arrestin, the mutation E122Q accelerates the retinal release in a comparable ratio than that obtained from biochemical *in vitro* experiments (Kefalov, 2012). A deeper analysis, using in vivo approaches, is needed to unravel the physiological meaning of these photoproducts relative half-lifes related with their belonging to nocturnal/diurnal niches.

Interestingly, different concentrations of monomeric arrestin, the only Rho-binding form, in ROS under dark conditions were found in the three species we are studying: 52.8 μM, 27.6 μM and 15.5 μM in mouse, bovine and human respectively (M. Kim et al., 2011). These results may suggest an arrestin concentration dependence in the nocturnal-diurnal niche, and was predicted by theoretical models to affect the active Rho signal lifetime, where the faster decay would occur in mouse, secondly in bovine and the slowest in human (M. Kim et al., 2011). Some authors also suggest, by means of model studies, that upon arrestin translocation, active Rho would be deactivated even faster (Gross & Burns, 2010). Nevertheless, these changes in the active lifetime of Rho before arrestin desensitization are not supposed to have a great impact in the subsequent photoresponse amplitude, due to the buffering mechanisms found in the downstream calcium feedback mechanism to cGMP synthesis (Gross et al., 2012).

Arrestin is mainly located in the inner segment in dark-adapted rods. When bright and continuous light illuminates rod cells, this pool of arrestins migrate to the ROS, and the $t_{1/2}$ of this translocation process is 5 minutes (Calvert, Strissel, Schiesser, Pugh, & Arshavsky, 2006; Elias, Sezate, Cao, & McGinnis, 2004; Fu & Yau, 2007; Lohse & Hoffmann, 2014). In contrast to that, the return to the inner segment, following dark adaptation, is considerably slower, with a $t_{1/2}$ of 65 min (Lohse & Hoffmann, 2014). Arrestin starts its translocation to the ROS at a light intensity able to activate more than 1 000 Rho per rod cell per second (Calvert et al., 2006; Lohse & Hoffmann, 2014), that is within the upper limit of the mammalian functional range where the rods can detect variations in light. Moreover, on a brighter light, the translocation of Gt is triggered at intensities that are able to activate the order of 4 000 Rho per rod cell per second (Arshavsky & Burns,

2012). Under these light conditions, rods are saturated and vision depends on cones (Calvert et al., 2006).

At this point, is important to highlight that the number of total photoactivated Rho molecules facing similar light intensities differs depending on the species, and reflects the diurnal/nocturnal vision patterns. Thus the level of necessary light for bleaching 50 % of Rho in the mouse retina is ~100–200 cd/m^2, equivalent to a normal room lighting, whereas the light intensity to bleach the same level of Rho in human retina is ~25 000 cd/m^2, equivalent to a bright daylight (Sommer, Hofmann, & Heck, 2014). In order to reach these differential levels, mammals have acquired diverse physiological and morphological conformations. In general, diurnal animals have evolved to have large retinas and small pupils, in contrast with smaller retinas and larger pupils for nocturnal animals (Gerkema et al., 2013) leading, in the case of the mouse eye to a numerical aperture two times larger than that in human in dilated pupils, with increased light collecting (Geng et al., 2011). Besides, other adaptations can be found, like the larger presence of cones in diurnal species or the larger rod density and the presence of the tapetum (tissue behind retina that reflects light back to the photoreceptors) on the retina of nocturnal species. Even the adaptation of the rod nuclear organization in nocturnal mammals was proposed to act like a micro-lens focusing light onto the ROS (Solovei et al., 2009), although some of the diurnal/crepuscular animals, like the cow, have an nuclear conformation intermediate between that of diurnal and nocturnal animals.

As we have seen, some of the evolutional adaptations towards nocturnal vision have been focused in maximizing the intensity of light arriving to the ROS, and therefore to the visual pigments, in order to enhance the photoresponse in dim-light environments. Thus, animals specialized in dark

vision, are more vulnerable to damage by light whereas the diurnal animals are more light-resistant (Domitille L. Boudard, Acar, Bretillon, & Hicks, 2011), as it was demonstrated in experiments with diurnal cone-dominant rodents in contrast with rod-dominant rats and mice (Organisciak & Vaughan, 2010). Moreover, a thorough comparison between diurnal macaque and nocturnal owlmonkey, both rod-dominant primates, brings as a result that under the same light exposure the damage to the retina was catastrophic for the nocturnal species but caused insignificant harm in the diurnal animal (Organisciak & Vaughan, 2010). Taking into account, also, that nocturnal animals are not always restricted to scotopic conditions of light, but that in some cases are able to undergo occasional daytime activity (Gerkema et al., 2013), a different molecular protection mechanism may be present in nocturnal species.

One of the harmful key factors suggested to be implicated in the toxicity for rod cells is the accumulation of all-*trans*-retinal (Maeda, Golczak, & Maeda, 2012; Rozanowska, 2012). Despite that RDH mediates reduction of all-*trans*-retinal to the less toxic all-trans-retinol (H. Wang et al., 2012) all-*trans*-retinal accumulates in ROS after strong photobleaching due to exposure to high light intensity (Bartl & Vogel, 2007; Funatogawa et al., 2016; Organisciak & Vaughan, 2010; Stiles et al., 2015). Furthermore, this all-*trans*-retinal excess is suggested to cause a toxic effect closely related to that observed in age-related retinal macular degeneration and other retinal diseases (Bartl & Vogel, 2007; Funatogawa et al., 2016; Li et al., 2016).

The photodamage toxicity of all-*trans*-retinal involves not only the reactive aldehyde functionality with direct damage to the rods, but other physiological pathways, for example by causing oxidative stress of the RPE where eventually the all-*trans*-retinal could diffuse after delayed clearance

in photoreceptor cells (Li et al., 2016) by insufficient conversion to all-*trans*-retinol by RDH (H. Wang et al., 2012). In addition, phosphatidylethanolamine can react with two molecules of all-*trans*-retinal to form a di-retinoid-pyridinium-ethanolamine (A2E), that accumulates over the time in the RPE by forming lipofuscin granules which can be associated with retinal degeneration (Okano et al., 2012; Sommer et al., 2014). Moreover, it was found that under UVA and blue light irradiation, the resultant free all-*trans*-retinal can be a potent photosensitizer by mediating the generation of different reactive oxygen species (Maeda et al., 2012).

Despite the potential damage of short wavelength light due to its higher energy, and the photoactivation of free all-*trans*-retinal, nocturnal or partially nocturnal therians (like mouse) tend to have lenses transmitting UV, whereas mainly diurnal species (like human) possess lenses preventing short wavelengths to reach the retina (Douglas & Jeffery, 2014), as the short wavelength radiation is mainly present during daytime. Moreover, many scotopic species have the short wavelength cone (SWS1) absorbing in the UV band (the inferred ancestral functionality in mammals (Borges et al., 2018; S. Yokoyama et al., 2014)) instead of being blue sensitive, which suggests a visual relevance to the nocturnal mammal species (Emerling, Huynh, Nguyen, Meredith, & Springer, 2015; Gerkema et al., 2013; H. Zhao et al., 2009). Given these points, along with chronobiological studies, it was suggested that nocturnal species have some lifestyle plasticity, so that the short wavelength cones would be beneficial for the occasional daytime vision (Gerkema et al., 2013). On the other hand other protective mechanisms different from the filter lenses was proposed for scotopic animals like the presence of a UV-absorbing compound in the aqueous humour of the eye like ascorbic acid (Gerkema et al., 2013).

Under these conditions, arrestin will not only be involved in the shut-off of the Rho signal, as previously discussed, but also may be related with a protection function mediating the sequestration of all-*trans*-retinal and thus preventing retinal degeneration by controlling the toxic levels of free all-*trans*-retinal when the light intensity suddenly intensifies (Sommer & Farrens, 2006; Sommer, Hofmann, & Heck, 2012; Sommer et al., 2014). This arrestin binding to Rho may have some structural plasticity allowing arrestin to bind monomeric and dimeric Rho (Sinha et al., 2014) (Fig. 4.1.10A). Likewise, it was proposed that this plasticity could cause the binding of arrestin at the single photon level to the monomeric phosphorylated Meta II, and light increase could also result in dimeric binding. At the same time, all-*trans*-retinal was also shown to re-enter into the binding pocket of half of the phosphorylated opsin population when Meta II was stabilized by arrestin (Sommer et al., 2012) (Fig. 4.1.10B). This entrance was also observed in the case of purified pigment in detergent solution (Schafer, Fay, Janz, & Farrens, 2016). Moreover, this stabilization would occur in half of the pigment population and, would allow the other half to decay at a similar rate to that found in cells lacking arrestin (Beyrière et al., 2015) (Fig. 4.1.10B).

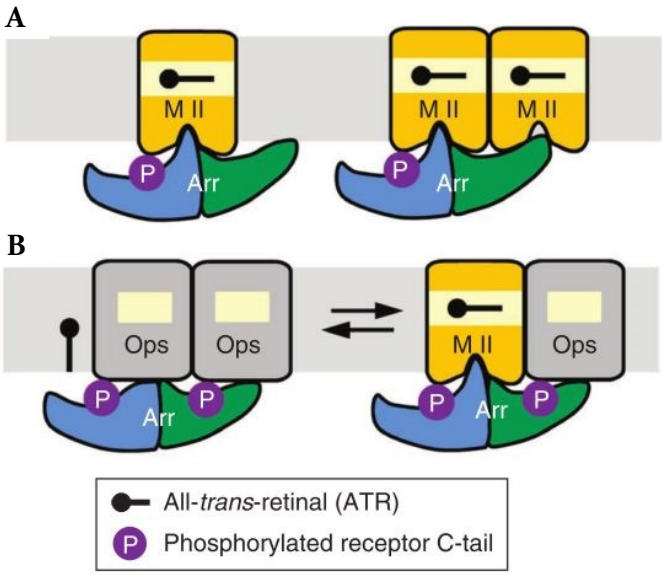

Figure 4.1.10 Scheme of the binding of Arrestin to phosphorylated Meta II conformation of Rho. *A*- Structural plasticity of arrestin (Arr in the figure) allows it to bind monomeric or dimeric Rho. *B*- Arrestin stabilizes half of the population of Rho in its active state by allowing a reversible re-entry of all-*trans*-retinal, and the other half Meta II population decays at a rate similar to that seen in the absence of arrestin. The difference in Meta II decay observed in the different half species could be an important factor in regulating shut-off of the signal. (Image retrieved from Sommer et al., 2012).

Furthermore, some authors propose that arrestin translocation may play a role in adaptation (Arshavsky & Burns, 2012), or as an energy saver system, but other authors argue for a protective role under constant bright light, but this is still an open question (Elias et al., 2004; Gurevich et al., 2011; Sommer et al., 2014). Hence, taking all these facts under consideration, the slower Meta II decay found in nocturnal mammals could also help improve the protection of rod cells by buffering all-*trans*-retinal concentration as arrestin would stabilize half of the photoactivated Rho pool. This proposed mechanism could also be affected by arrestin translocation from the inner to the outer segments.

In the same direction, some aspects were theorized concerning the divergence from cone to rod pigments. In this regard the slower Meta II decay achieved by Rho during its specialization to dim-light vision would provide, among other features related with sensitivity, protection under intense light. This could happen by reducing the toxicity resulting from a huge release and accumulation of all-*trans*-retinal (Lamb, 2013), in comparison with all-*trans*-retinal reduction to all-*trans*-retinol and its posterior clearance that occurs faster in cone cells (Ala-Laurila et al., 2006). In contrast, a slower photoproduct decay would led to a slower regeneration rate that could respond less accurately to light changes and movement detection (Lamb, 2013; Morshedian & Fain, 2017) and result also in a less rapid dark adaption in rod cells compared with cones cells (Ala-Laurila et al., 2006).

The slower regeneration of rod cells and the subsequent less accurate response is, in general, attributed to the rate-limiting availability of 11-*cis*-retinal in ROS (Lamb & Pugh, 2004), although it was also proposed that the rate limiting step would be retinal release from Rho (Heck et al., 2003; McKeown, Pitale, & Kraft, 2016). Importantly, further studies found that the kinetics of dark adaptation after 20 % bleach are rate-limited by the Meta species decay whereas under an intense light (70 % bleach) the limiting factor may be the presence of 11-*cis*-retinal (Imai et al., 2007). This could be explained by the presence of a limited amount of 11-*cis*-retinal in the dark ROS. Therefore, the difference observed between mouse and human Rho behaviour would be connected to a faster regeneration in rod cells after moderate photobleaching. Interestingly, a review comparing results from different studies, found that the regeneration of the pigment in human is faster than in nocturnal mammal species like mouse, although the authors

assumed that the rate-limiting step was 11-*cis*-retinal availability. In this case, however, the comparison should be taken with caution due to the use of chemicals in experiments with non-human animals (Lamb & Pugh, 2004). Thus, these differences in Meta II release rates seen in diurnal mammals may be linked with beneficial effect of a faster dark adaption under dim-light conditions (Bickelmann et al., 2015) and a more relaxed pressure in the protective necessity.

Site 290 in Rho deserves a deeper analysis. The specific amino acid at this position was shown to be importantly correlated with the nocturnal or diurnal activity pattern in therian mammals, especially in the primate and rodent orders (Table 4.1.1 and Fig. 4.1.2). This was experimentally supported by the large shift in the Meta II decay rate observed in the L290I mutant Rho (Fig. 4.1.9) where the nocturnal pigment acquired a behaviour more similar to that of diurnal Rho (e.g. bovine Rho). Moreover, L290I produced a slightly blue-shifted spectral tuning of 2 nm from 502 nm, bring closer to the 498 nm from the bovine Rho (Fig 4.1.4), also taking into account that red shifted pigment was suggested to maximize light absorption in nocturnal light conditions (Wu et al., 2017).

As the key behavioural difference mediated by the position 290 was found in the retinal release, a structural comparison was performed in order to compare the amino acid at this position and the adjacent amino acids in dark-state Rho and in the active Meta II conformation. Furthermore, it is important to emphasize that point mutations may belong to an interacting network, fact that could have a significant impact in the vicinity of the retinal binding pocket through long-range interactions (Piechnick et al., 2012). The change in the decay rate observed is striking since in the amino acid at position 290, either L and I shows a very conservative nature from a

physicochemical an structural standpoint, as both amino acids contain hydrophobic side chains and have the same molecular weight, and a similar molar volume. The difference should be sought in the position of the branching in isoleucine that could allow specific interactions with surrounding amino acids that would not be feasible in the case of leucine.

Despite its location near the opening between TM helix 1 and 7 that is the proposed retinal entry site (T. Wang & Duan, 2011), position 290 is also proximal to the Schiff base linkage in the three-dimensional activated Rho (Morrow & Chang, 2015). Moreover, the contact surface of the amino acid at site 290 with the surrounding amino acids shows other residues in the vicinity that may be closely structurally related (Fig. 4.1.11A). As observed in the active Meta II conformation, these positions correspond to mainly F287, F293 and F294 as well as neighbouring positions T289 and P291. Meanwhile, in the dark conformation these positions correspond mainly to F286, T289, P291 and F294 and neighbouring T289 and P291. These amino acids are also highly conserved in all the 51 therian mammals species analysed in this chapter (except minor variations corresponding to L287). In fact, T289P was found to be a mutation causing RP in humans (Athanasiou et al., 2018). Also, comparison of dark state versus Meta II contact surface shows a closer contact of amino acid at position 290 with those aromatic amino acids at positions 287, 293 and 294, and this can be appreciated in detail in Fig. 4.1.11B and Fig. 4.1.11C.

Importantly, as the retinal chromophore is covalently bound, in the inactive dark state, to K296 in TM7, interaction energy changes affecting this linkage, upon retinal isomerization may be determinant for the retinal release rates. In this way, F293 shows a strong interaction, in the dark state, with the K296 but a weaker interaction with F294 (Kong & Karplus, 2007). Moreover, F293

shows an important conformational change upon receptor activation as seen in Fig. 4.1.10B and C (Piechnick et al., 2012; Ramon et al., 2014). Also, F293 is located in a network including position 29 at TM1, site of a natural mutation causing RP (M39R). This fact, together with its location near the proposed entry retinal opening, has been suggested to be related to a faster retinal release rate observed for the M39R RP mutation (Ramon et al., 2014). On the other hand, mutations at position T289 caused changes in the retinal release rate, but two mutations studied at F293 did not show significant effects in this parameter (Piechnick et al., 2012). This data sheds some light on the structural role of 290 and its molecular relationships with other amino acids in the vicinity of thee retinal binding pocket that may have a profound influence on Meta II stability and on the retinal release rate.

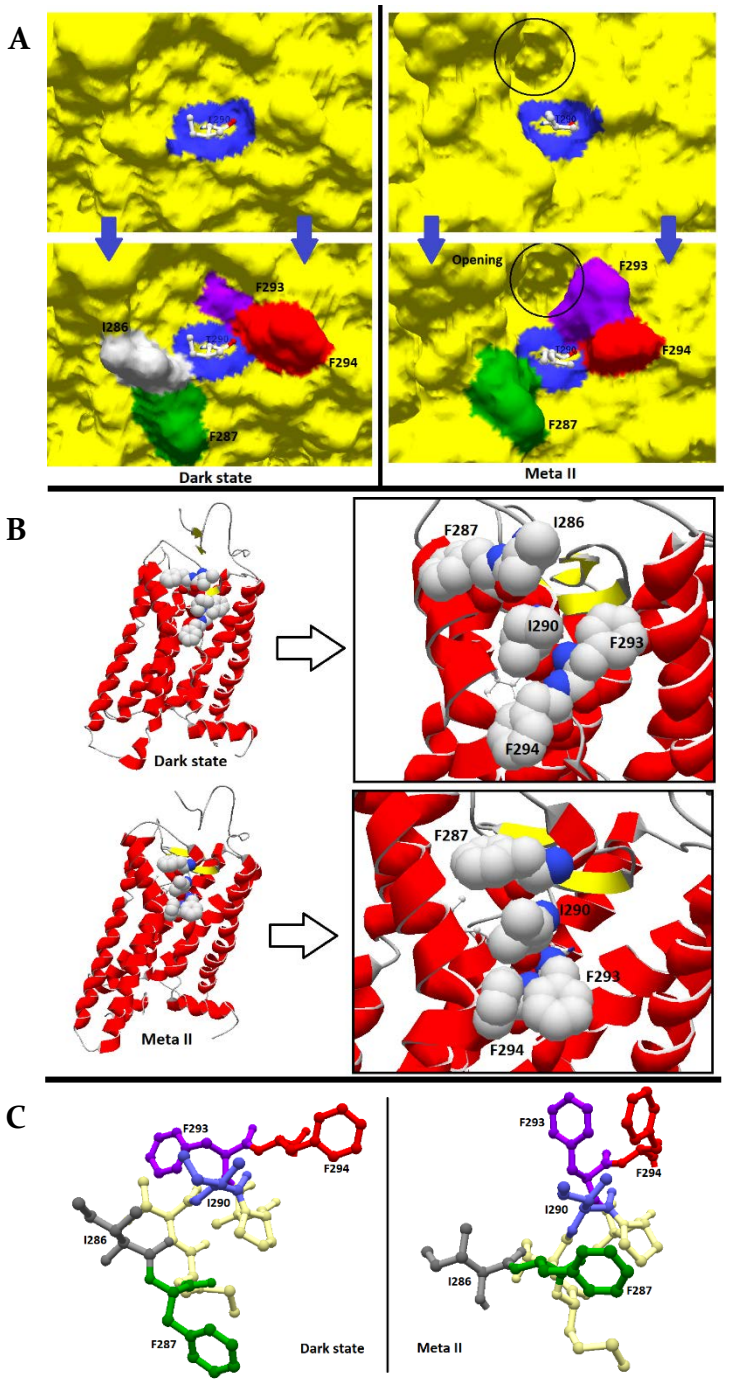

Figure 4.1.11 Three dimensional model of the inactive dark structure (PDB ID 1gzm) and the active Meta II (PDB ID 3pqr) of bovine Rho. ***A***. *Upper panels*, contact surfaces of the pigment with the site 290 in Meta II and dark conformations are highlighted in blue. *Bottom panels*, same figure with the residues F287, F293 and F294 highlight in green, purple and red respectively, and I286 in grey. The remainder blue correspond principally to neighbouring positions T289 and P291 (not shown). The proposed retinal entry site is indicated by a black circle ***B and C.*** Detail of the dark state and Meta II structures, with the same highlighted sites than in A. Visualization program: Swiss PDB viewer.

In summary, the L290I mutation has been shown to cause an important change in the retinal release rate of mouse Rho compared to human and bovine cases. Besides, there may be an important correlation between activity pattern (nocturnal/diurnal) and the amino acid at this position, better appreciated in the more specialized primate and rodent orders.

We propose a systematic explanation for the observed difference of Meta II decay in nocturnal versus diurnal therian mammals by inferring slower Meta II/III kinetics on species with L290 and faster kinetics on species with I290. Thus, taking into account that nocturnal animals tend to maximize the environmental light (including UV wavelengths) that reach the rod cells, and consequently that impinge on Rho, in order to improve their vision under dim-light conditions, and that occasionally these animals can be exposed to bright light potentially harmful to them, different mechanisms of protection could be envisaged. The sequestration of all-*trans*-retinal by a more stable Meta II photointermediate arises as a possible mechanism to this aim, even at the cost of a worse dark adaption. On the other hand, diurnal animals tend to better protect their visual system by different mechanisms that limit the amount of bright light arriving to rod cells and to Rho. Rod regeneration is limited in bright light environments by the supply of fresh 11-*cis*-retinal, but under dim-light conditions the limitation relays on all-*trans*-retinal release from photoactivated Rho. In this case, a faster regeneration of the visual cycle should be expected and thus an improved dark adaptation. In conclusion, a compromise between the prevalence of damage protection under bright light in nocturnal therian mammals (L290), and dark adaptation under dim light in diurnal therian mammals (I290) is proposed to have an important influence in the specialization of Rho (Fig. 4.1.12).

It should be noted, however that some animals have a less clear activity pattern because of low visual specialization or a great plasticity both under nocturnal or diurnal conditions (cathemeral animals), and that it is likely that other positions (in addition to the 290 position reported here) may contribute by epistatic interactions to the adaptation to light conditions.

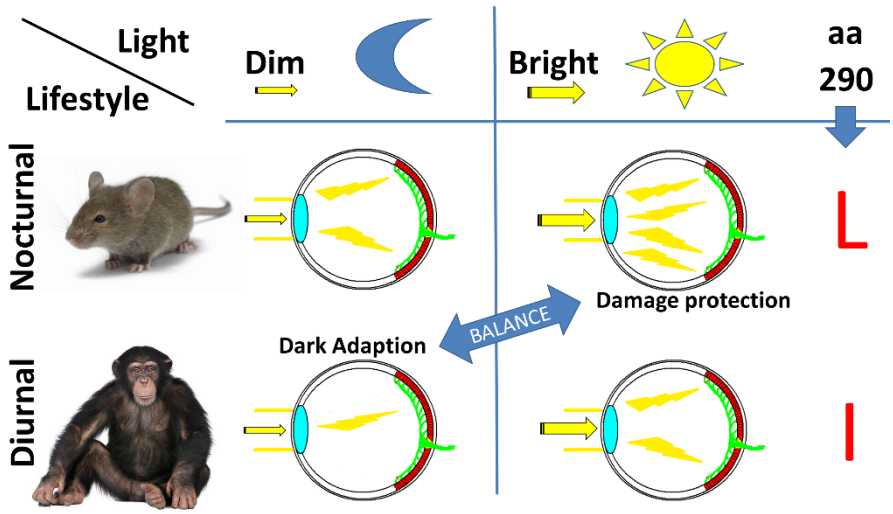

Figure 4.1.12 Schematic representation of the proposed relationship between the amino acid at position 290 and vision specialization. Nocturnal species maximize environmental light transmission to photoreceptors, by different methods, in contrast with diurnal species. In nocturnal species, all-*trans*-retinal sequestration by a more stable Meta II photointermediate associated with the presence of L290 arises like a possible adaption to a damage protection mechanism under bright light. In diurnal species, an improved dark adaptation as a result of faster all-*trans*-retinal release related with the I290 would be expected.

Y102H mutation. The interest of the existence of a chemically mutagenized mouse model carrying Y102H relies on the fact that it does not overexpress WT Rho, in contrast to transgenic mouse models. This provides a better model for retinal degeneration in RP because overexpression by itself can also trigger retinal degeneration (Budzynski et al., 2010). Thus, similarities were found in these mouse models with the phenotype of RP class B1 Rho

mutations, where the disease progression is slower than in class A, but is more focalised in an area of the retina than in the case of the panretinal disease seen in type B2 mutations. Moreover class B1 patients also exhibit impaired deactivation of phototransduction after brief exposure to high light intensity (Budzynski et al., 2010).

On the structure of Rho, Y102 is located in the ECL1 domain that connects TM1 and TM2. This positon was found to be conserved in the whole set of therian mammals studied in this chapter, but a variant (Y102F) causing a spectral shift was detected in some types of deep sea fishes (S. Yokoyama, Tada, Zhang, & Britt, 2008). Besides, Y102 is located near an area that plays a role in the stabilization of the dimeric structure of Rho by polar interactions with Y96 and H100 (Salom et al., 2006).

According to our experimental values, the Meta II decay shows some slight difference in the bovine background (Fig. 4.1.9). The Y102H mutation slows down the retinal release rate in bovine Rho compared with the WT protein, meanwhile an apparently slightly faster Meta II decay, although not statistically significant, was found in the human background. On the other hand, the hydroxylamine stability was found to differ as ration between the initial rates of Y102H Rho and WT Rho was determined to be 1.5 in the human background and 4.5 in the bovine background (Table 4.1.2).

This effect is noticeable but we found more important the high loss in thermal stability produced in the human Y102H, to a similar level to that previously reported in the bovine background (Fig. 4.1.6). A similar reduction was reported also in different studies of RP mutations and was linked, in some of them, to the perturbation of a hydrogen-bond (H-bond) network (Guo et al., 2014). This network is thought to stabilize Rho, and its

perturbation was found to increase the rate of thermal isomerization without greatly affecting the stability of the photoactivated state (Liu et al., 2013). Interestingly, a H-bond was found between Y102 and positions V104 and T97 (yellow in Fig. 4.1.12). It is interesting to note that V104F and T97I are naturally occurring RP mutations in humans (Athanasiou et al., 2018). Other H-bond mediated interactions of ECL1 and the N-terminal domain (Opefi, South, Reynolds, Smith, & Reeves, 2013) involving positions F103 with P23 and G101 with Q28 (orange in Fig. 4.1.12), are also associated with P23A/H/L and Q28H naturally occurring RP mutations that produce thermal instability (Opefi et al., 2013). Similarly, F103 is also H-bonded to G106 (green in Fig 4.1.13), where G106R/W was found also to be RP mutants that generate instability (Athanasiou et al., 2018). The physiological importance of this low thermal stability may be correlated with a higher threshold of light intensity needed for vision and with the early stages of night blindness in RP (Liu et al., 2013).

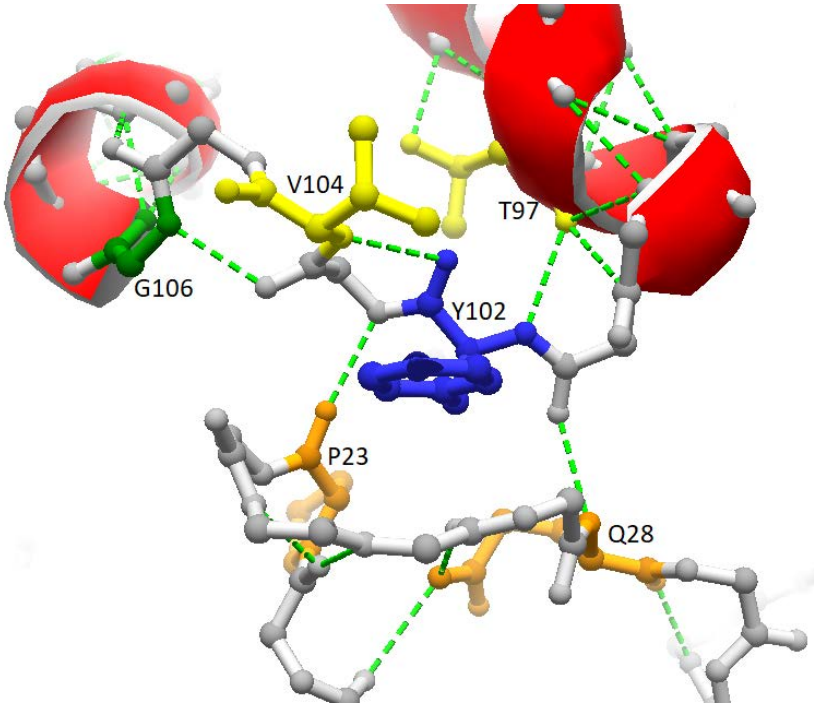

Figure 4.1.13 Three dimensional model of the inactive structure of Rho (PDB ID 1gzm). Detail of the structure centred on the ECL1 and the N-terminal domain (bottom), between TM2 and TM3. Green dashed line represents H-bonds. Y102 is highlight in blue, direct H-bonds from Y102 connect with V104 and T97 (yellow). H-bonds on close positions 103 and 101 (grey) connect with P23 and Q28 (orange) on the N-terminal domain, and with G106 (green). All the highlight positions except Y102 correspond with sites where natural occurring RP mutations where found in humans: P23A/H/L, Q28H, T97I, V104F and G106R/W (Athanasiou et al., 2018)

In summary, we have found significant differences comparing the molecular features of the Y102H RP like mutation with the WT in both the bovine and the human backgrounds. Nevertheless both pigments had a similar behaviour in thermal stability assays. Furthermore, we suggest that the perturbation of a critical H-bond network, in a structurally important region, as a probable cause of this loss in thermal stability.

4.2 Functional role of positively selected amino acid substitutions in mammalian Rho evolution

In order to analyse the evolution of Rho in mammals, an alternative approach to that described on section 4.1 was chosen. In the previous chapter, a functional adaptation was initially inferred from the sequence analysis data, and here a preliminary statistical analysis is conducted to help us in identifying different point mutations that appear to be positively selected in the evolution from a therian ancestor.

4.2.1 Rho molecular evolution

When estimating Rho's evolutionary rate via the simple M0 model, in which a single dN/dS ratio is estimated for the entire sequence (see Materials and Methods), the sequence was found to have evolved, as expected, predominantly under strong purifying selection (dN/dS = 0.045, log-likelihood (lnL) = –12788). Thus, in general, novel non-synonymous nucleotide substitutions in this gene tend to be removed by natural selection. However, positive selection is expected to occur at individual, adaptive sites, which the M0 model cannot be used to detect. We thus performed two tests of positive selection using site-substitution models, which allow each site in the sequence to have evolved at an independent rate. Positive selection is inferred by comparing two nested models in which the alternative model includes sites with dN/dS greater than 1, and significance is determined via a likelihood-ratio test with the p-value derived from the χ^2 distribution. These tests, if significant, would largely provide evidence of sites that have undergone positive selection throughout the phylogenetic divergence. Both tests of pervasive positive selection failed to produce significant evidence (models M1a vs. M2a: M1a log-likelihood (lnL) = –12672, M2a lnL = –12672, degrees of freedom (d.f.) = 2, p = 1; models M7 vs M8: M7 lnL = –12364, M8 lnL = –12364, d.f. = 2, p = 1). Clearly, results of pervasive positive selection should not be used and the detailed analysis

has to concentrate in very specific positions within the protein/DNA sequence.

We next tested the hypothesis that Rho underwent episodic positive selection specifically during therian divergence via a test using a branch-site model (Fig. 4.2.1). This test allows for sites to have undergone positive selection on a specific branch of the phylogeny and significance is determined similarly to the previous tests. Rho was found to have significant evidence of positive selection on the branch leading to the therian mammals (null lnL = –12734, alternative lnL = –12731, d.f. = 1, p = 0.014). The three sites identified as having the highest posterior probability of having been targets of positive selection were (bovine coordinates and posterior probabilities given): M13F (Prob = 0.995), R225Q (Prob = 0.982) and S346A (Prob = 0.888). These three positions (the first two with strong statistical significance) clearly acquired some relevant function that resulted in being positively selected in the basal branch leading to therian mammals.

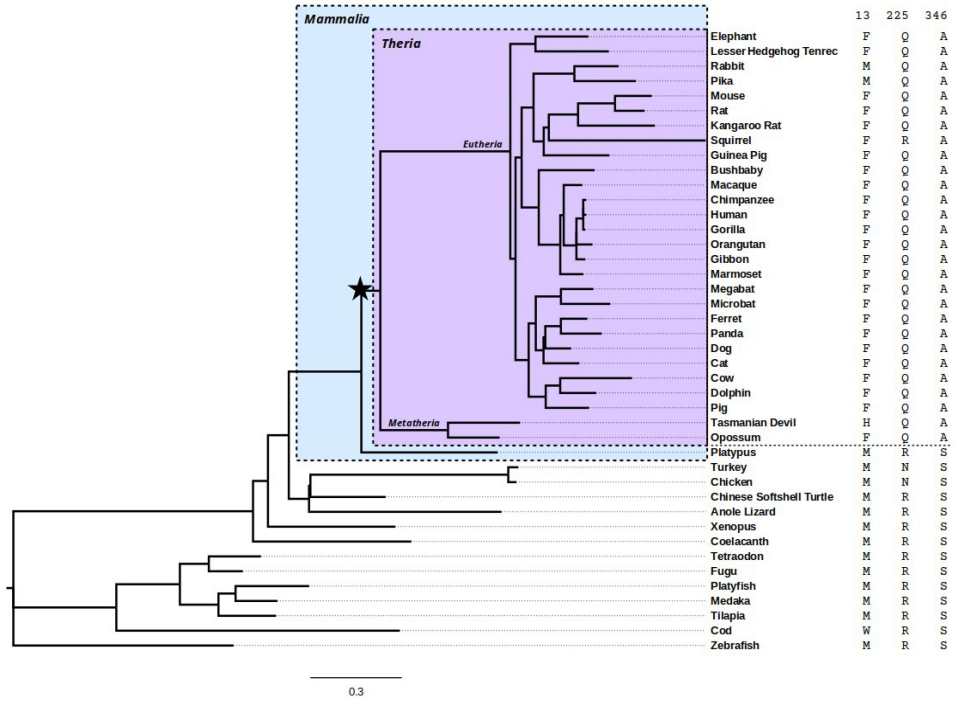

Figure 4.2.1 Rho phylogenetic tree. The topology of the tree, including branch lengths, is derived from the species tree computed for Ensembl Compara. The star indicates the base of the therian branch, on which we found evidence of episodic positive selection. The amino acids present at bovine positions 13, 225 and 346 are shown on the right for each species. Species above the dashed line belong to the therian clade.

4.2.2 Electrophoretic and spectroscopic characterization of the Rho substitutions

These three specific sites (13, 225, and 346 in the bovine opsin background), determined by the statistical analysis, were chosen for experimental characterization due to their high posterior probability of being positively selected. While site 346 does not meet the canonical probability cut-off of 0.95, its location in a region known to be physiologically relevant prompted us to include it in the experimental analysis. The ancestral mutations F13M, Q225R and A346S were constructed in the bovine opsin gene by site directed mutagenesis (Fig. 4.2.2).

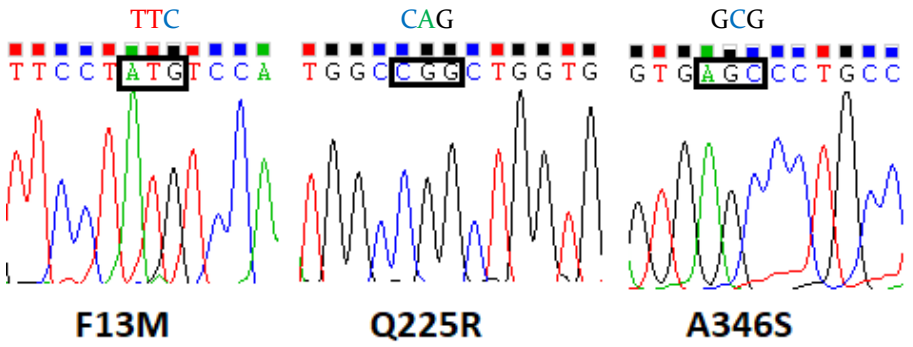

Figure 4.2.2 DNA sequencing for the three Rho mutations studied. Original WT sequence for this mutation is write above.

These amino acids are located at the intradiscal N-terminal domain (F13), the cytoplasmic end of TM helix V (Q225), and the C-terminal tail of the photoreceptor protein opsin (A346), respectively (Fig. 4.2.3).

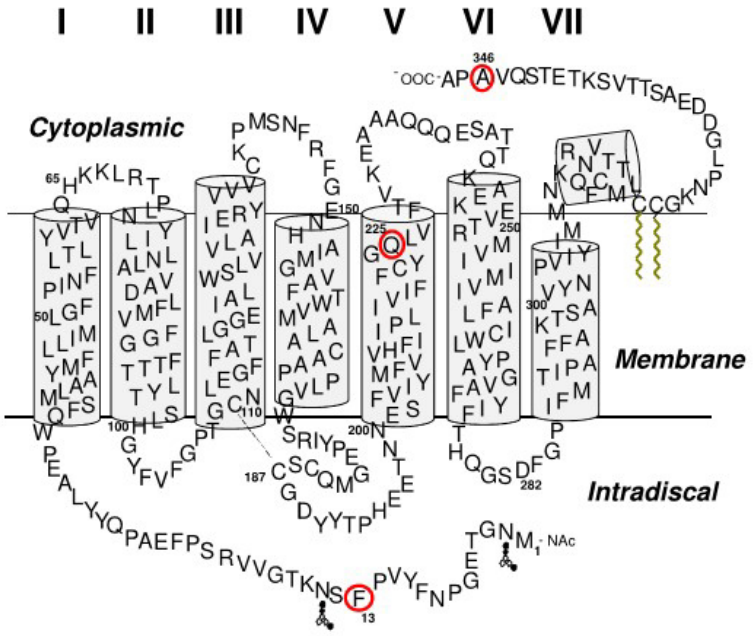

Figure 4.2.3 Rho secondary structure model. Sites mutated in the present study, 13, 225 and 346 are circled in red.

We used electrophoretic analysis in order to determine the glycosylation and oligomerization state of the mutants which are important structural determinants of their functionality. To this end, the recombinant mutated proteins, F13M, Q225R and A346S, were expressed in COS-1 cells, immunopurified and subsequently analyzed by SDS-PAGE. The electrophoretic pattern of Q225R and A346S mutants was very similar to that of the WT (Fig. 4.2.4, left panel) showing the characteristic trailing smear typical of Rho expressed in COS-1 cells and attributed to heterogeneous glycosylation (Reeves, Thurmond, & Khorana, 1996). However, the F13M mutant showed a clearly altered pattern, with a series of discrete bands and the appearance of lower bands below the opsin main band (at about 40 KDa) that can be attributed to non-glycosylated14 or truncated opsin species (Krebs et al., 2010).

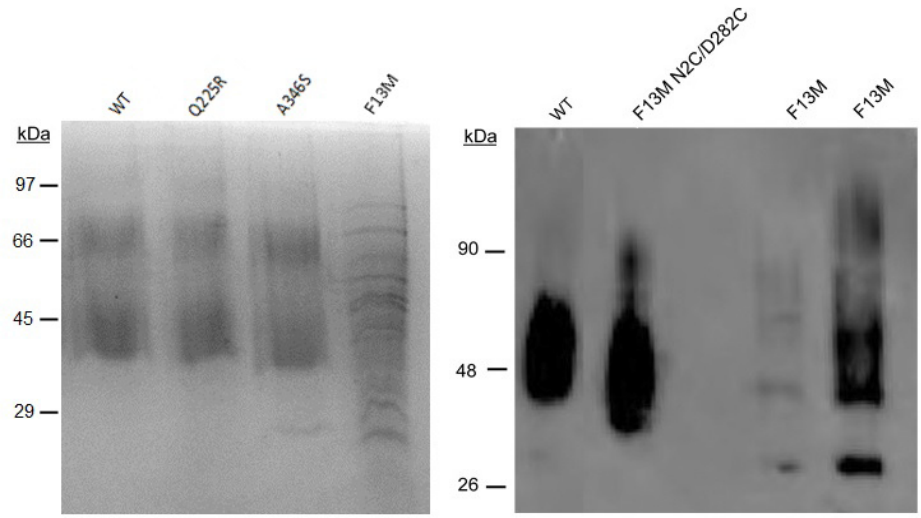

Figure 4.2.4 SDS-PAGE and Western blot of immunopurified WT and mutants Rho. ***Left panel.*** ROS (Rho from rod outer segments), WT Rho and Q225R, A346S and F13M mutants are indicated in the corresponding lanes. All the mutants show a similar electrophoretic behaviour as the WT except for F13M which shows an altered pattern consistent with altered glycosylation. ***Right-panel***. Western Blot of immunopurified protein samples detected with Rho-1D4 monoclonal antibody. WT Rho, F13M in the N2C/D282C background and F13M Rho. Note that a 28kDa band is clearly detectable in the F13M mutant.

Then, the spectral behaviour of the purified proteins was analyzed by UV-vis spectroscopy and its light absorption properties were determined in their dark-adapted state (Fig. 4.2.5 and 4.2.6C). Wild-type (WT) Rho showed the characteristic visible band at 500 nm and the mutants Q225R and A346S showed visible bands at the same wavelength (Fig. 4.2.6). These two mutants showed similar levels of chromophore regeneration with retinal than WT Rho as judged by their A280 nm/A500 nm ratios (see Table 4.2.1).

Table 4.2.1 Spectroscopic properties of bovine WT Rho and mutants. [a]$t_{1/2}$ of the thermal stability measurements of purified samples at 48°C measured at the visible λ_{max}. [b]Chemical stability measured as the decrease rate of the absorbance at the λ_{max} absorbance in the dark in the presence of 50 μM hydroxylamine. Relative values are shown between brackets. [c]Relative initial rates of Gt activation.

	WT	**Q225R**	**A346S**
λ_{max} (dark) (mm)	498 (11-*cis*-retinal)	498 (11-*cis*-retinal)	498 (11-*cis*-retinal)
Ratio 280nm/ λ_{max}	2.66 ± 0.43	2.43 ± 0.19	2.75 ± 0.58
[a]Thermal Stability (48°C) (min)	27.8 ± 6.8	25.9 ± 4.9	19.3 ± 4.2
Meta II Decay (min)	13.9 ± 0.8	13.2 ± 1	14.5 ± 2.7

[b]Hydroxylamine 50 µM	0.000379	0.001068	0.001910
Initial velocity (min^{-1})	(1.00)	(2.82)	(5.04)
[c]Gt activation initial relative rate	1.00 ± 0.179	0.52 ± 0.177	2.58 ± 0.350

The photobleaching and acidification spectra were determined immediately after illumination (with light of $\lambda > 495$ nm) and after acidification respectively. Upon illumination, both mutants showed a typical absorbance band at 380 nm, corresponding to the active Meta II conformation. Subsequent acidification of the samples shifted the absorption maximum from 380 nm to 440 nm which corresponds to the reprotonation of the Schiff base nitrogen. Thus, we find a WT-like behaviour for the Q225R and A346S mutants in the photobleaching and acidification assays (Fig. 4.2.5, insert), suggesting that these amino acid changes did not alter the pathway of photointermediates leading to the activated receptor.

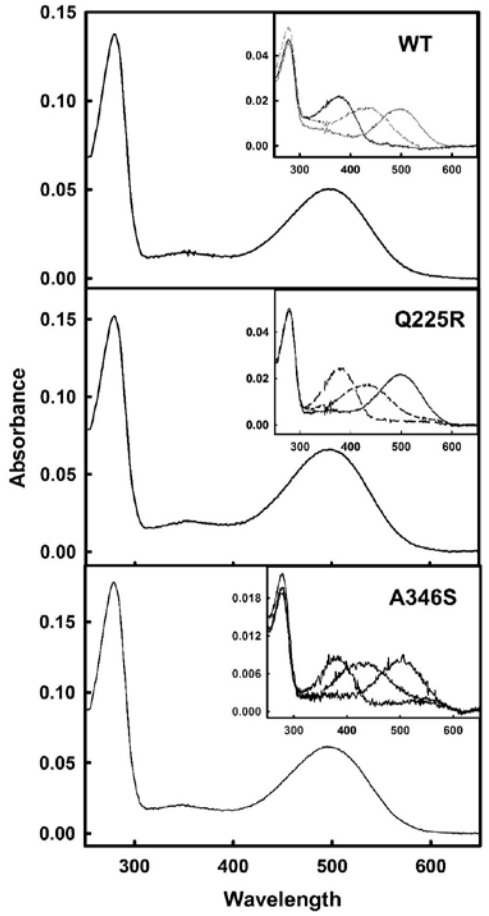

Figure 4.2.5 Spectroscopy UV-vis characterization of the purified proteins. UV-vis spectra of WT, Q225R and A346S in dark. Insets show the corresponding dark (λmax = 498nm), photobleached (λmax = 380nm), and acidified spectra (λmax = 440nm). Note that the mutants show photobleaching and acidification behaviours analogous to those of WT Rho. Experiments conducted at 20°C in PBS pH=7.4 and 0.05 % DM

A specific behaviour was observed in the case of the F13M mutation, at the N-terminal domain of the receptor, which did not show detectable chromophore regeneration as detected by the lack of absorbance in the visible region (Fig. 4.2.6C, upper panel). This lack of chromophore regeneration ability could reflect protein misfolding. It is known that misfolded opsins are retained in the endoplasmic reticulum or can form

intracellular inclusions due to a failure in the intracellular transport to the plasma membrane. Thus, we analyzed the subcellular localization of the F13M mutant, expressed in COS-1 cells, and compared it to that of WT Rho in order to confirm structural misfolding of this mutant. A clearly different pattern was observed in the two cases with WT opsin being trafficked to the plasma membrane (Fig. 4.2.6A), whereas F13M appeared not to be localized effectively to the plasma membrane, and formed intracellular inclusions with higher frequency, in a pattern consistent with protein misfolding (Fig. 4.2.6B).

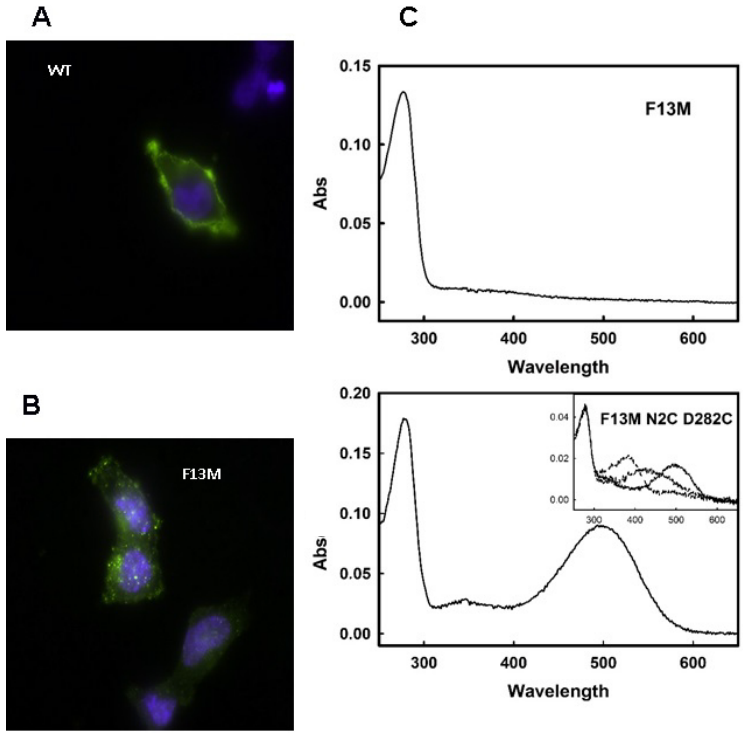

Figure 4.2.6 Fluorescence microscopy and UV-vis spectroscopy behaviour of F13M mutant. Transfected cells with WT Rho (A) and F13M mutant (B) were analyzed by fluorescence microscopy. The blue colour corresponds with the nucleus of the cells, and Rho are labelled in green. C. UV-vis absorption spectra of F13M in the dark (top panel) showing no chromophore regeneration in the visible region. When the mutation is obtained in the background of the N2C/D282C double mutant, then chromophore regeneration can be

rescued to WT levels (lower panel). *Inset*, photobleaching and acidification spectra of the rescued mutant.

4.2.3 Rescue of chromophore regeneration for the F13M mutant

It was of interest to find out if the misfolded phenotype for the F13M could be rescued by means of an experimental strategy. Therefore, pharmacological chaperone rescue was carried out with the F13M mutant. For this, COS-1 cells transfected with this mutant gene where incubated in the presence of 9-*cis*-retinal. Previous studies showed that defective N-terminal mutants supplied with 11-*cis*-retinal or 9-*cis*-retinal, during protein biosynthesis, could recover WT-like Rho chromophore regeneration levels (Noorwez et al., 2004; Opefi et al., 2013). In the case of F13M we could not get any detectable chromophore regeneration for this mutant using this strategy (Figure 4.2.7).

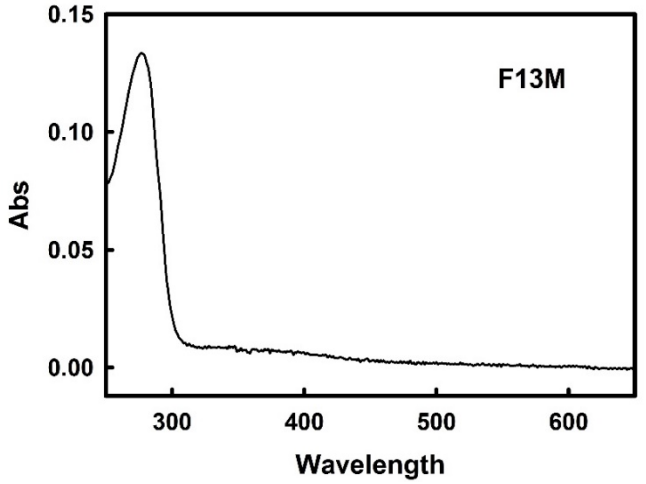

Figure 4.2.7 UV-vis spectrum of purified F13M mutant. The mutant was expressed in COS-1 cells and 9-*cis*-retinal was added to the cell culture during protein expression. No detectable chromophore regeneration can be observed in the 500-nm visible region.

We hypothesized that the inability of the F13M mutant to bind retinal was due to the fact that this mutation, at the N-terminal domain of the receptor, could be destabilizing the protein conformation, thus affecting receptor folding and altering at the same time glycosylation at the proximal N15 residue (Murray, Fliesler, & Al-Ubaidi, 2009). In order to stabilize the structure, we introduced the F13M mutation in the background of the N2C/D282C double mutant that forms a disulfide bond between Cys2 and Cys282 increasing opsin stability (Xie et al., 2003). By using this strategy we could recover full chromophore regeneration for F13M mutant to a similar extent to that of WT Rho (Fig. 4.2.6C, lower panel). Furthermore, Western blot analysis of F13M showed a clear distinctive lower band at approximately 28 KDa that was not detected when the mutant was obtained in the Cys2/Cys282 background (Fig. 4.2.4 right panel). In this latter case a pattern similar to that of WT could be observed, consistent with the rescue observed for chromophore regeneration.

In order to rule out that the retinal could be binding to other Lys residues (Srinivasan, Cordomí, Ramon, & Garriga, 2016) in the F13M mutant (other than the natural K296 at TM helix 7) we constructed the quadruple mutant F13M/N2C/D282C/K296G where the site of retinal attachment was eliminated by the K296G mutation (Zhukovsky, Robinson, & Oprian, 1991). We could not get any chromophore formation for this mutant indicating that retinal was binding to the native K296 in the rescued triple mutant (Figure 4.2.8).

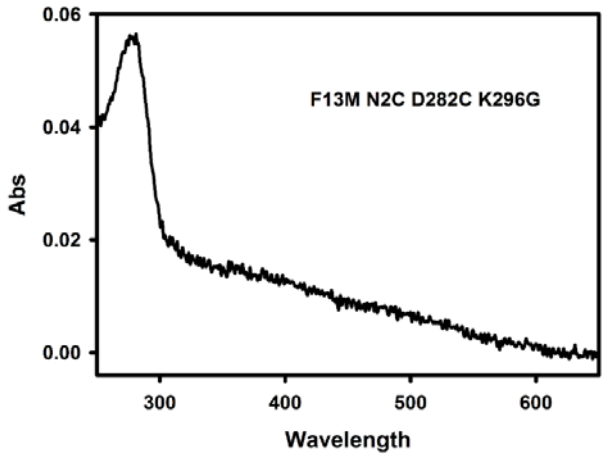

Figure 4.2.8 UV-visible spectrum of the purified quadruple F13N/N2C/D282C/K296G mutant. No detectable chromophore at the visible region could be observed indicating that 11-cis-retinal was binding to the native K296 in the triple F13M/N2C/D282C rescued mutant.

4.2.4 Conformational stability and functionality of WT and mutant opsins

One of the important aspects underlying the functionality of Rho in visual perception is the structural stability of both the dark-adapted and the illuminated photoactivated states. Specific amino acid substitutions can have a profound impact on the stability of the protein so it is of interest to determine their thermal and chemical stabilities in the dark and also the stability of the activated Meta II state. The influence of the mutations on the specific function, i.e. G-protein activation, is also a relevant parameter that can shed light on the importance of a given amino acid position in the molecular evolution of the protein.

4.2.5 Dark-state chemical stability

We determined the hydroxylamine reactivity of WT and the mutants in the dark state. Hydroxylamine cannot access the compact WT Rho binding

pocket in the dark state but if the conformation becomes more open, as in the case of mutation, then it can enter the binding pocket forming a retinal oxime with 11-*cis*-retinal (Kawamura & Yokoyama, 1998). Thus, hydroxylamine is used to indirectly measure the chemical stability of Rho in the dark through the measure of the accessibility of the Schiff base linkage under these conditions. WT has a high stability towards hydroxylamine in the dark (Table 4.1.1) indicating that the retinal Schiff base is not accessible under these conditions. Both Q225R and A346S mutants show a slightly increased sensitivity towards hydroxylamine in the dark (Fig. 4.2.9A) that would reflect a less compact structure around the Schiff base linkage in the chromophore binding pocket.

4.2.6 Dark-state thermal stability

Another assay used to assess the stability in the dark state, is to follow the decay of the visible band at 48°C. At this temperature the Q225R mutant showed similar thermal bleaching kinetics as the Rho WT, while the A346S mutant showed slightly faster bleaching kinetics (Table 4.1.1). On the other hand, the mutant F13M/N2C/D282C has a high stability as expected from the stabilizing effect of the additional engineered disulfide bond ($t_{1/2}$ > 120 min at this temperature) as previously described (Standfuss et al., 2007).

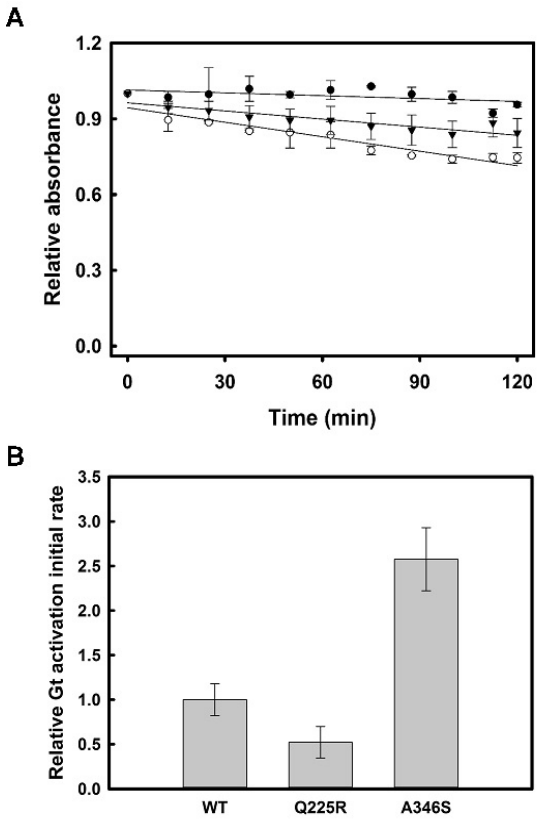

Figure 4.2.9 Molecular properties of immunopurified Rho mutants. A. Chemical stability in the presence of 50 μM hydroxylamine. The decrease in absorbance at the visible λ_{max} was measured over time. WT Rho (●), Q225R (▼) and A346S (○) B. Relative Gt activation initial rate. Error bars represent S.E. in both panels.

4.2.7 Meta II stability

Meta II decay was determined, in real time, by monitoring Trp fluorescence increase upon Rho photoactivation. Our data showed a similar decay time for the Q225R and A346S mutants when compared to WT (Table 4.1.1).

4.2.8 Functional Gt activation

We analyzed the functionality of the mutant Rho by means of a radioactive assay that measures the ability of the mutant Rho to activate the Gt. We

found a lower initial rate for Gt activation for the Q225R mutant compared with the WT. Conversely, A346S mutant showed an increase in Gt activation rate (Fig. 4.2.9B, Table 4.2.1).

4.2.9 Functional implications

The functional variability among vertebrate Rho is not well studied, except for spectral tuning, and little is known about other phenotypic features like glycosylation, G-protein activation and phosphorylation. In this regard, most of the RH1 pigments have λ_{max} values at about 500 nm except for some fishes that have a 10-20 blue-shifted λ_{max} that could reflect an adaptation to the ocean environments (S. Yokoyama, 2000). Some variability has also been found in the kinetics of Rho photointermediates, like the Meta II decay rates that are significantly different in human and bovine Rho compared to other non-mammalian Rhos (Morrow & Chang, 2015). Finally, mathematical models of amphibian (Dell'Orco, Schmidt, Mariani, & Fanelli, 2009) and mammalian (Invergo, Dell'Orco, Montanucci, Koch, & Bertranpetit, 2014) phototransduction suggest that the binding between Rho and Gt and the activation of the G protein occur at significantly faster rates in mammals. All existing information points towards the existence of functional differences in the evolution of vertebrate Rho.

Previous studies suggested that certain specific amino acid positions could be important for vertebrate Rho evolution (Hunt et al., 2009). We have extended these previous analyses by using a larger phylogenetic tree and more opsin sequences that make our analysis more reliable and trustworthy for deep functional analyses. We find that the sites F13, Q225 and A346 are the three sites with the highest posterior probability of having been targets of positive selection after mutating from their ancestral states (M13 → F13,

R225 → Q225 and S346 → A346) during the evolution of mammals. Based on our statistical analysis we have constructed, expressed and immunopurified these three reverse mutations in the bovine opsin background and we have analyzed in detail the structural and functional properties of the purified mutants. We find a clear structural alteration for F13M mutant and stability and functional alterations for the other two mutations, Q225R and A346S that can have importance in the protein molecular evolution process.

Gln225 is located at the cytoplasmic end of TM helix V in the junction region with the ICL3. Previous studies have shown that this loop is directly involved in Gt binding and activation that occurs after Rho photoactivation (Nakatsuma et al., 2011). A different substitution at this position, Q225C was studied in a cysteine-scanning mutagenesis approach where all the amino acids at or near the ICL3 were mutated to Cys (K. Yang, Farrens, Hubbell, & Khorana, 1996). In that case, mutation to Cys did not affect Rho folding but on the contrary it resulted in slightly increased Gt initial activation rate (K. Yang, Farrens, Hubbell, et al., 1996). In our case, the substitution to an Arg in the Q225R mutation would introduce a bulky, charged residue in a domain that is critical for Gt activation. This Arg would likely have a steric clash with Tyr136 of neighbouring helix III (Fig. 4.2.10) that belongs to the conserved ERY motif critical in Gt activation. Arg135 in this conserved triplet was shown to be hydrogen bonded with a Gt-derived peptide (Elgeti et al., 2011; Hofmann et al., 2009; Scheerer et al., 2008). Any change in the structure of this region would cause a change in the coupling efficiency to the G-protein and could explain the decreased Gt activation observed for Q225R when compared to WT Rho as it happened in previous studies studying mutations in close positions (Bosch-Presegué et al., 2011). Recent

studies indicate that the finger loop in arrestin interacts in a similar way with Arg135 (Szczepek et al., 2014) so the Q225R mutation could also potentially affect arrestin binding but establishing this would require further investigation.

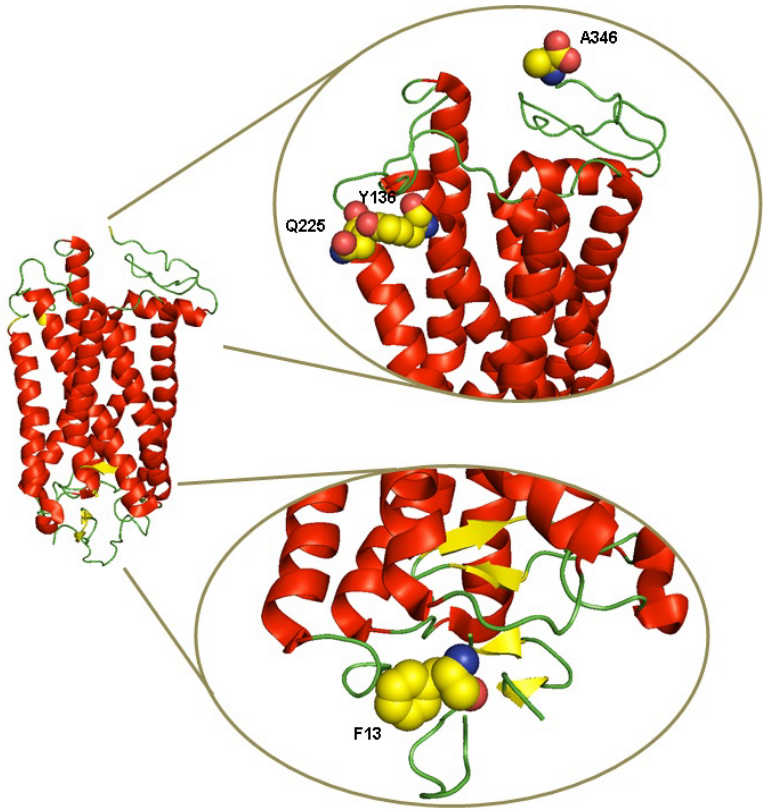

Figure 4.2.10 Three dimensional model of the inactive structure of Rho. The three amino acids studied (positions 13, 225 and 346) are highlighted in yellow. Glu225 is found to be interacting with Tyr136 of the highly conserved Glu134-Arg135-Tyr136 motif which plays a critical role in Rho activation.

In contrast, **A346S**, the other studied mutation that regenerated chromophore, showed increased Gt activation rate (Fig. 4.2.8B). Ala346 is

the site of the naturally-occurring A346P mutation associated with the retinal degenerative disease retinitis pigmentosa (RP) (Borrego, Sánchez, Ruiz, & Antiñolo, 1996; Katagiri et al., 2014) that was studied together with other disease causing mutations (A. Andrés, Garriga, & Manyosa, 2003). In that study some mutants associated with RP were found to have higher Gt activation rates and this was proposed to be the cause of their disease phenotype. Also, other studies demonstrated that some mutations in the C-terminal domain affect the *in vivo* trafficking of Rho, resulting in random delivery to photoreceptor cell membranes (Concepcion & Chen, 2010; Deretic, 2006). Although the C-terminal tail of Rho is believed to be devoid of a defined structure and quite flexible (Langen, Cai, Altenbach, Gobind Khorana, & Hubbell, 1999) we can propose that the C-terminal tail may be covering part of the ICL3 in the dark state that would regulate the Gt activation process. In the case of mutations at this domain, these amino acid changes could affect the conformation of the C-terminal tail of Rho allowing exposure of the ICL3 and facilitating the Rho-G-protein recognition process. Moreover, the specific A346S mutation creates a potential additional phosphorylation site in the protein which would affect Rho phosphorylation after photoactivation (Doan, Mendez, Detwiler, Chen, & Rieke, 2006) and in turn could affect the binding affinity of arrestin, a regulator of Rho deactivation. This could result in a reduction of the amplitude and duration of the flash response since dephosphorylation of Rho correlates with dark adaptation (Baylor & Burns, 1998; Hurley, Spencer, & Niemi, 1998).

Interestingly, it has been recently shown that mutation of Ser to Ala at the C-terminal tail in Rho of transgenic mice results in slowed-down response kinetics (Azevedo et al., 2015). Therefore, this extra phosphorylation site on the ancestral pigment could provide an evolutionary explanation for the

enhanced response in the case of Gt activation that would need a more efficient signal desensitization process.

Both the Q225R and the A346S electrophoretic and spectroscopic patterns were similar to those of WT Rho indicating that both mutants are preferentially in a monomeric state and that the mutations do not alter their UV-vis spectral properties. Thus, the WT-like behaviour for the Q225R and A346S mutants suggests that they did not alter the pathway of photointermediates leading to the activated receptor. The same WT-like behaviour was found in the Meta II decay for both mutants and in the thermal stability for the Q225R Rho, whereas the A346S Rho showed only slightly decreased thermal stability when compared to WT (Table 4.1.1). This minor difference is not believed to play a significant role in its functional performance, and thus in Rho evolution.

In contrast, we found a higher sensitivity to hydroxylamine than WT for both Q225R and A346S mutants (Fig. 4.2.9A). This would reflect a less compact structure for the mutants in the Schiff Base linkage environment; the sensitivity to hydroxylamine has been used in previous studies to distinguish rod opsins from cone opsins, since this reaction is substantially faster in cone opsins (Kawamura & Yokoyama, 1998). Other studies in echidna Rho (the most basal mammals) revealed that these Rho are significantly more sensitive to hydroxylamine than bovine Rho (Bickelmann et al., 2012). And it was also observed in other vertebrates like American Chameleon (Kawamura & Yokoyama, 1998). Thus, the observed increased response to hydroxylamine in the dark state would suggest a phenotype somehow closer to cone opsins for the ancestral state. Cone pigments would require more flexible and conformationally adjustable binding pockets to allow efficient retinal binding for a fast physiological response as observed

when comparing cone pigments and Rho ligand binding properties (Srinivasan, Ramon, Cordomí, & Garriga, 2014). Therefore, the physiological correlate of these results could be found in the known difference between cone and rod opsins that is related with the life-time of their signalling states. Cone opsins can form their signalling states so that they can respond faster (and have a faster dark adaptation) in mediating colour and diurnal vision, but they would actually do so by compromising their sensitivity in comparison to the more sensitive rod opsin. In contrast, rod photoreceptors have a much longer signalling state to account for an amplified response that increases the sensitivity of the photoreceptor, slowing down the physiological response, regulating dark adaptation and making scotopic vision possible (Shichida & Matsuyama, 2009).

In the case of the **F13M**, the poor expression observed is not likely related to problems with trafficking in COS cells because we have also obtained the same results in HEK293T cells. Different vertebrate Rho´s from species that have M at position 13 have been successfully expressed in HEK293T cells (i.e. chicken (Kuwayama, Imai, Morizumi, & Shichida, 2005) and zebrafish (Morrow & Chang, 2015)) or in COS cells (i.e. zebrafish (Chinen, Hamaoka, Yamada, & Kawamura, 2003) and Astyanax (R. Yokoyama, Knox, & Yokoyama, 1995)). In the case of the Astyanax fish, the A280/A500 ratio of the purified pigment was reported to be much higher than that of bovine Rho, and the SDS-PAGE pattern indicated apparent differences in the glycosylation pattern (R. Yokoyama et al., 1995). Therefore, we believe that expressing the protein either in COS cells or in HEK293T cells does not affect trafficking although it can alter the glycosylation pattern of the expressed protein.

In our case, we find that the F13M mutation causes misfolding and alters glycosylation of the protein in spite of the relative conservation of the substitution. Phe13 is near the position of the glycosylation site located at Asn15 (Fig. 4.2.3). Some mutations near this position, like N15S and T17M, are linked to a subset of the retinal degenerative disease RP, known as sector RP, in which the inferior retina appears to be primarily affected (Ramon et al., 2014; Tam & Moritz, 2009; Tam, Noorwez, Kaushal, Kono, & Moritz, 2014). There is another glycosylation position at Asn2. Human disease and animal models suggest that glycosylation plays an important role in the structure and/or function of Rho (Opefi et al., 2013; Tam & Moritz, 2009). In recent years, the importance of the N-terminus in Rho has been emphasized and the importance of including the N-terminus and extracellular loops in structural studies has been highlighted (Belmer et al., 2014). Some studies suggest that glycosylation at Asn15 is essential for Rho structure and/or function (Kaushal, Ridge, & Khorana, 1994), whereas glycosylation at Asn2 had no significant effect on rod viability (Tam & Moritz, 2009).

A prominent electrophoretic 28-kDa band was observed for F13M (Fig. 4.2.4). In previous studies, a similar band has been observed in cell culture and transgenic frog or mouse models of P23H Rho (associated with RP) and other mutations located in the N-terminal in bovine opsin (Krebs et al., 2010). It was thought to correspond to an N-terminal-truncated product of opsin, as it was recognized by a C-terminal antibody but lacked epitopes to N-terminal antibodies and was not glycosylated. Thus, the 28-kDa protein has been assigned to an opsin truncation product (Krebs et al., 2010).

In view that the F13M mutation causes protein misfolding and lack of chromophore regeneration we successfully attempted to rescue the folded

(chromophore binding) phenotype. The results of the spectral characterization of the immunopurified mutant F13M in the N2C/D282C background showed that the mutation phenotype could be rescued in the double cysteine mutant and that in this case it could regenerate chromophore to WT levels. The photobleaching and acidification behaviour of the rescued F13M mutant was also similar to those of WT Rho indicating that the rescued protein was properly folded and had a normal phototransduction process (Fig. 4.2.6C). Moreover, according to a packing analysis using the method of occluded surfaces, Phe13 residue would have van der Waals interactions with the ECL3, where Cys282 is located (Opefi et al., 2013). We could also find differences in the cellular localization in the case of the F13M mutant that formed intracellular inclusions and was not transported efficiently to the plasma membrane (Fig. 4.2.6B). This behaviour was consistent with the known endoplasmic reticulum export efficiency changes that are typically associated with misfolding of membrane proteins in heterologous expression systems (Wiseman, Powers, Buxbaum, Kelly, & Balch, 2007).

In conclusion, we find physiological relevance for specific mutations in Rho derived from statistical evidence of positive selection. We show that position 13 in Rho is very important for the folding of the receptor and also for proper protein glycosylation. Given the deleterious nature of the reverse substitution and our ability to recover a WT phenotype for this mutant, we speculate that the positive selection observed at this site could have been compensatory. In this case, concerted amino acid changes can be related to the fine-tuned network of amino acid interactions that govern the stability and folding of the tightly packed Rho extracellular domain, and particularly its N-terminal tail. It is interesting to note that, among therians, the rabbit

(*Oryctolagus cuniculus*) and the pika (*Ochotona princeps*) both show a reversion to methionine at position 13 (Fig. 4.2.1), making them potential candidates for further investigation of the role of this position.

On the other side, positions 225 and 346 appear to be important for the protein functionality in the G-protein activation process and are likely sites of adaptation. Our results highlight the importance of molecular investigations of positive selected sites in Rho evolution and the relevance of structural and functional analysis of these sites in unravelling the molecular basis of visual pigment evolution. This is also highlighted in a recent experimental study that provides further support to our mutational analysis particularly taking into account that nowadays some evolutionary hypotheses on vision are still based on indirect anatomical inference from fossils (Bickelmann et al., 2015).

Overall, these findings provide a deeper insight into specific amino acids involved in Rho molecular evolution and they may, at the same time, have implications for Rho molecular evolution theories of early mammalian nocturnality, where these mammals would have changed their visual patterns, during the Mesozoic era, in order to avoid competition with diurnal reptiles (Gerkema et al., 2013). Our results are relevant to recent studies suggesting that mechanisms of epistatic interactions between specific amino acids must be understood by studying various orthologues in different species that have adapted to different environments (S. Yokoyama et al., 2014). These findings contribute to the emerging trend that complex non-linear interactions seem to be at the base of phototransduction evolution (Invergo, Montanucci, & Bertranpetit, 2015).

4.3 Human green cone double cysteine mutant

As shown in section 4.2.3, the introduction of a double Cys mutation, in residues close to each other, is an effective technique to study low-stable or non-functional pigments. This method allows stabilizing different kinds of proteins like it was shown in the N2C/D282C double mutant in Rho (Standfuss et al., 2007; Xie et al., 2003).

In this section, an experimental analysis was performed in order to confirm the presence of a disulfide bond in human green cone opsin double mutant that was previously designed and constructed (Srinivasan, 2015). This disulfide bond was obtained by the mutation of positions W90 and A169 that are located respectively on TM2 and TM4 close to ICL1 and ICL2 on the cytoplasmic side of the protein (Fig. 4.3.1) (Gardner et al., 2010) and are not likely to interfere with retinal binding.

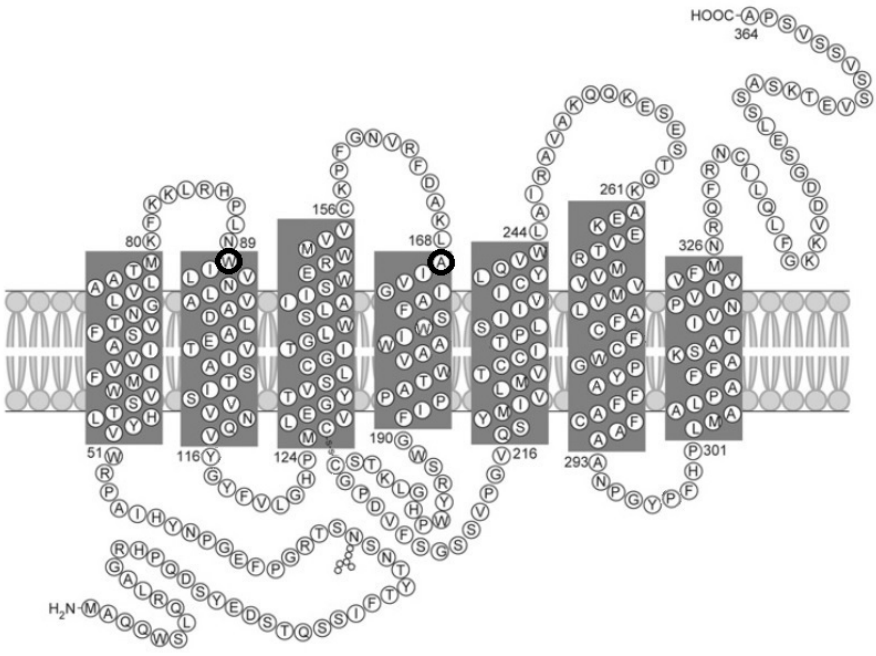

Figure 4.3.1 Secondary structure of the green cone opsin. Positions of the proposed mutants to form a disulfide bond are highlight in black. Figure adapted from (Gardner et al., 2010).

4.3.1 Construction and purification of green cone opsin mutants

Mutations W90C and A169C were individually constructed in the background of the human green cone opsin gene and by site directed mutagenesis. The correct insertion of the mutations was confirmed by DNA sequencing (Fig 4.3.2).

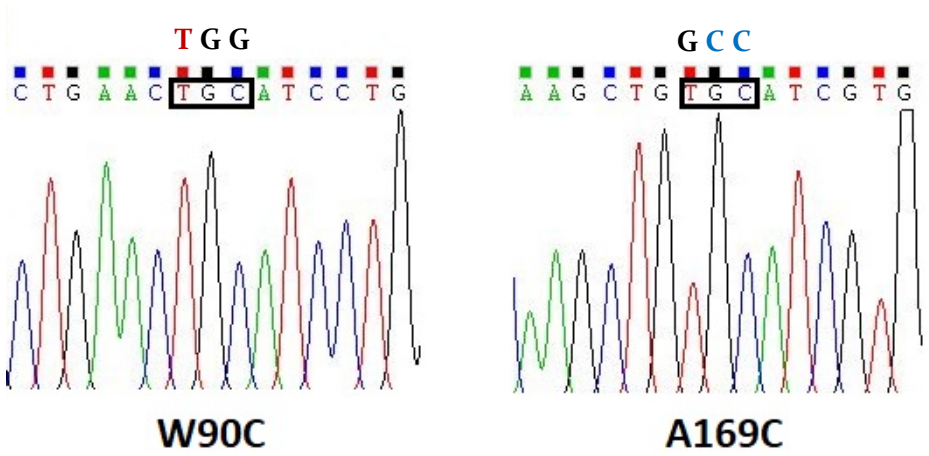

Figure 4.3.2 DNA sequencing for the two human green cone opsins constructed. Amino acid mutation boxed. The original WT sequence for these constructs is written above.

Once the constructs were confirmed, both genes were transfected in COS1 cells, regenerated with 11-*cis*-retinal and immunopurified with Rho-1D4 antibody as previously described. Due to the lower stability compared with Rho, some precautions were taken into account, like always regenerating using freshly transfected cells and reducing the elution time, in the purification process, to 30 min. Green WT and green W90C/A169C (green SS) were also immunopurified as controls.

A similar spectroscopic pattern was observed in the green cone opsin W90C and A169C mutants when compared with green WT and green SS. All of

them had a λ_{max} = 530 nm in the visible wavelength. The main difference found was the lower chromophore yield, measured from the A_{280}/A_{530} ratio, in the case of green W90C (Fig. 4.3.3).

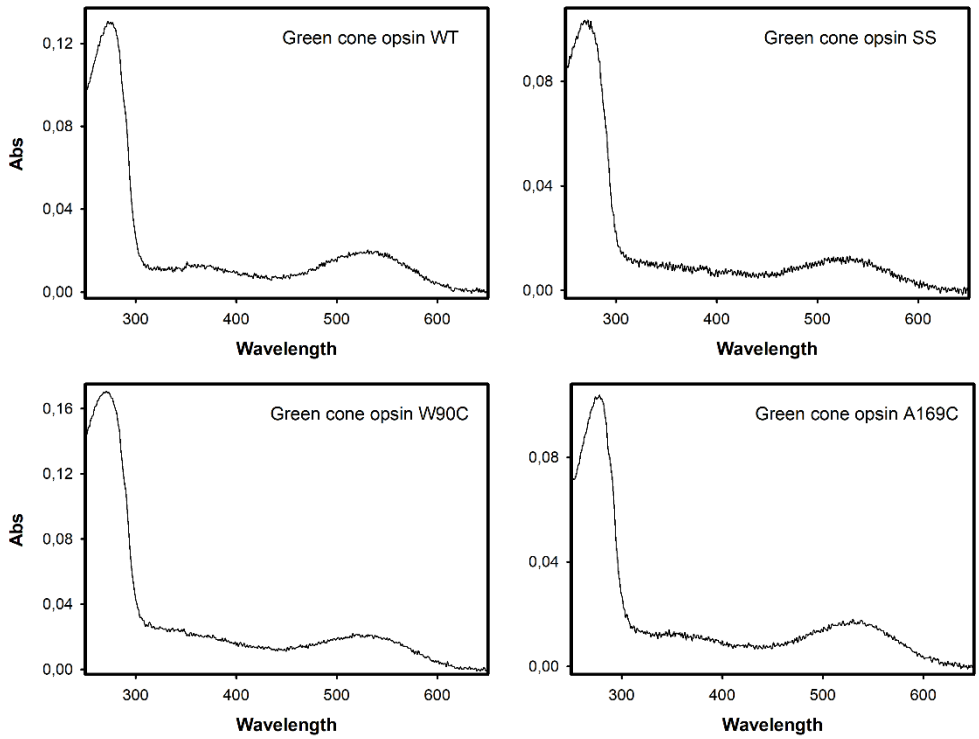

Figure 4.3.3 Dark UV-Vis spectra of immunopurified green cone opsins at 20°C in PBS pH 7.4 and 0.05 % DM. Green cone opsin WT and the mutants green opsin W90C, green opsin A169C and the green opsin double mutant W90C/A169C (SS).

4.3.2 Determination of free sulfhydryl groups

Ellman's reagent (DTNB) assay can quantify the free sulfhydryl groups present in a protein as described in *section 3.14* in the *Materials and Methods* section. Importantly, DTNB cannot access and, consequently, cannot react with Cys buried in the hydrophobic TM domain or with Cys involved in disulfide bonds (Karnik & Khorana, 1990). According to this, the green cone opsin has two residues that can be potentially labelled (Fig. 4.3.1).

The positions of mutated amino acids 90 and 169 are located in the cytoplasmic border of the TM helices (Fig. 4.3.1). Thus, the accessibility of DTNB to these positions is unknown and should be tested by recording the increase of absorbance at 412 nm.

- Free sulfhydryl groups in green WT:

$$C = \frac{0.0106}{14\,150} = 7.49 \times 10^{-7}\ \text{M}$$

35µl of green WT in 200µl total mixture. Dilution 1:5.71

$$7.49 \times 10^{-7}\ \text{M} \times 5.71 = 4.28 \times 10^{-6}\ \text{M} = \mathbf{4.28}\ \boldsymbol{\mu\text{M}}$$

The estimated concentrations of free sulfhydryl groups in green WT is 4.28 µM which accounts from the two Cys accessible residues.

- Free sulfhydryl groups in green W90C:

$$C = \frac{0.0108}{14\,150} = 7.63 \times 10^{-7}\ \text{M}$$

35µl of green WT in 200µl total mixture. Dilution 1:5.71

$$7.63 \times 10^{-7}\ \text{M} \times 5.71 = 4.36 \times 10^{-6}\ \text{M} = \mathbf{4.36}\ \boldsymbol{\mu\text{M}}$$

The estimated concentrations of free sulfhydryl groups in green W90C is 4.36 µM.

- Free sulfhydryl groups in green A169C:

$$C = \frac{0.0136}{14\,150} = 9.61 \times 10^{-7}\ \text{M}$$

As the purified protein was more concentrated in this sample, a larger dilution was prepared: 31µl of sample in 200µl total mixture. Dilution 1:6.45

$$9.61 \times 10^{-7}\ \text{M} \times 6.45 = 6.20 \times 10^{-6}\ \text{M} = \mathbf{6.20}\ \mu\mathbf{M}$$

The estimated concentrations of free sulfhydryl groups in green W90C is 6.20 μM.

Therefore the concentration of free sulfhydryl groups observed in green A169C was 1.45 fold that detected for green WT cone opsin, whereas green W90C mutant had practically the same concentration than WT green cone opsin. These results should be compared with the previously detected concentration in green SS of 1.25 fold over green WT cone opsin (Srinivasan, 2015).

4.3.3 Dark-state thermal stability of green cone opsins

The stability in the dark state was monitored by the spectrophotometric decay of the 530 nm band over the time at 37°C. This temperature was selected becouse green cone opsins have a lower stability than Rho (Owen, Salom, Sun, & Palczewski, 2018).

Opsin experiences an important improvement of its thermal stability in a background of double Cys mutant (N2C/N282C) (Standfuss et al., 2007) as it was also shown in the case of F13M/N2C/N282C Rho studied in section 4.2.3. In contrast, green SS shows a slight stabilization at 37°C in comparison with green WT, with a $t_{1/2}$ of 12.05 ± 3.40 min and 7.17 ± 0.98 min respectively (Srinivasan, 2015).

The study of the decay kinetics of the single green cone opsin mutants can provide further information about the stability of green SS. Thus, the observed thermal stabilities $t_{1/2}$ were 8.91 ± 1.95 min for A169C and 3.47 ± 1.73 min for W90C (Fig. 4.3.4).

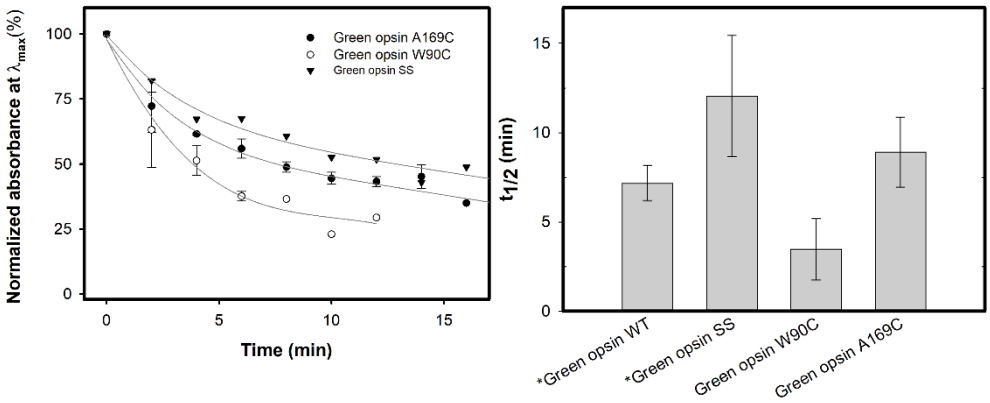

Figure 4.3.4 Thermal stability of purified green cone opsins at 37°C. Green WT $t_{1/2}$ = 7.17±0.98 min, green SS $t_{1/2}$ = 12.05±3.40 min, green W90C $t_{1/2}$ = 3.47±1.73 min, green A169C $t_{1/2}$ = 8.91±1.95 min. Error bars representing SD. *Green cone opsin WT and green SS data retrieved from (Srinivasan, 2015).

4.3.4 The W90C/A169C disulfide bond

Although the comparative analysis of green SS and green WT was previously performed (Srinivasan, 2015), some of the results obtained could be merely attributed to the effect of the single Cys mutations and not to the presence of a disulfide bond. Here this issue is discussed in the light of the experimental data obtained.

An increase of 1.45 fold in TNB could be detected indicating also an increase in free sulfhydryl groups in the case of green A169C mutant with regard to WT green cone opsin. Taking into account that WT green cone opsin showed the presence of two free Cys, this result represents that DTNB reacts, also with position 169 and therefore green A169C may have three free sulfydryl groups. If the introduced Cys formed a disulfide bond with one of the two free Cys of WT green cone opsin, then we would not expect an increase in labelling. In contrast the observed results for the green W90C

mutant showed that the newly mutated position was probably not accessible to the DTNB reagent.

The concentration of free sulfhydryls on green SS was 1.25 fold that of WT green cone opsin, if the disulfide bond was not formed, the expected concentration would have to be 1.5 fold that of the WT green cone opsin, representing 3 free Cys. Therefore, our results suggest the formation, at least partially, of the proposed disulfide bond.

On the three dimensional theoretical model of WT green cone opsin, position 90 is apparently accessible, but it should be noted that it is buried in the membrane bilayer (or the DM micelle in this experiment), as is forming part of the TM2 (Fig. 4.3.5, green). On the other side, position 169 although initially could apparently be buried inside the TM helical core, the view from the cytoplasmic side reveals an aperture to this side. Moreover, the molecular surface in this cytoplasmic side is slightly larger in A169C compared with A169 (Fig. 4.3.5, left panels). In contrast, the W90C mutation causes a reduction in its external molecular surface at the TM side (Fig. 4.3.5, right panels)

Therefore, the structural analysis of the green cone opsin support the analytical results where position 90 appears not to be accessible to DTNB, whereas position 169 appears to be accessible, at least partially, from the cytoplasmic surface of the protein.

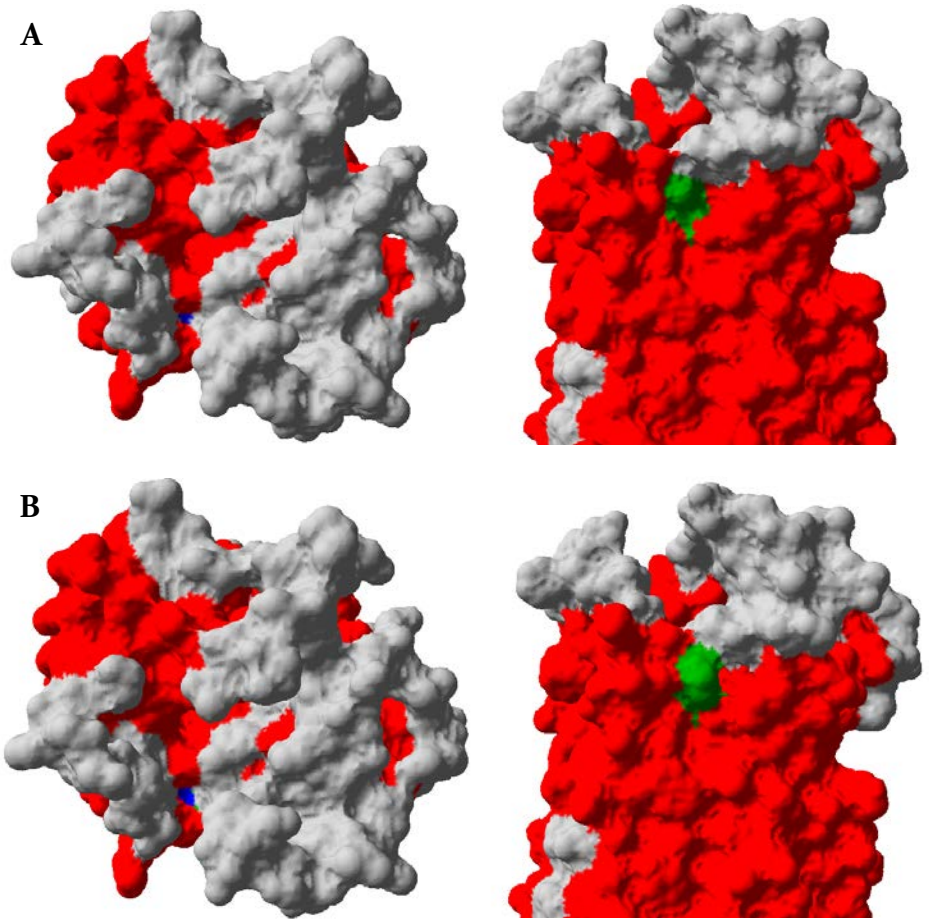

Figure 4.3.5 Molecular surface on the theoretical model of green cone opsin (PDB: 1kpw). TM helices in red and interhelical loops in grey. Cytoplasmic side view with the N-terminal region (left panels) and lateral side view (right panels). *A*- Molecular surface of green opsin W90C mutant. Surface of position 90C is highlight in green, and 169A is highlight in blue. *B*- Molecular surface of green opsin A169C mutant. Surface of position 90W is highlight in green, and 169C is highlight in blue. Visualization program: Swiss PDB viewer.

The difference in thermal stability of W90C and A169C individual mutants indicates that the increased stability observed for green SS was not due to the effect of the single mutations by themselves, as a compensatory effect

was observed in the A169C when the double mutant was tested (Srinivasan, Fernández-Sampedro, Ramon, & Garriga, 2017).

Regarding the thermal stability in the dark, the decreased stability observed for the W90C mutant could be related with a destabilization of the H-bond formed with N94 (Fig. 4.3.6). N94K is a naturally occurring mutation that was reported to cause congenital colour-vision deficiencies (Ueyama et al., 2002), and showed an abnormal spectroscopic behaviour upon acidification (Srinivasan et al., 2017).

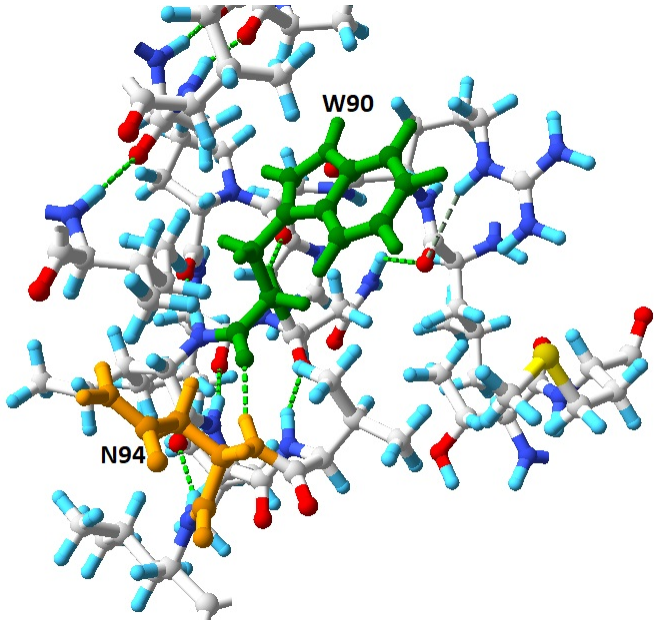

Figure 4.3.6 Residues within 6 Å of W90 in the theoretical model of green cone opsin (PDB: 1kpw). Amino acid W90 highlighted in green and amino acid N94 highlighted in orange. A H-bond connect both residues (green dotted lines).

In summary, additional supporting data was provided about the formation of the disulfide bound (at least partially) by the double Cys mutant W90C/A169C in human green cone opsin. This double mutant background

could be useful in the future for the study of unstable mutations related with different disorders affecting green opsins (Gardner et al., 2010; Ueyama et al., 2002), or studies associated with the molecular evolution of green cone opsin from red cone opsin in primates (Hunt et al., 2009).

4.4 Rho functionality in the presence of Prph-2

Different proteins related with the Rho regulation have been extensively studied by *in vitro* and *in vivo* methods. Proteins with a relevant function on the visual signalling cascade like arrestin, Rho kinase or Gt. In this section another protein, that has only been recently directly associated with Rho, was selected for its study.

As shown in the *Introduction* section, Prph2 plays an essential role in the formation of the outer segments and the structural maintenance of the discs in rod cells. Thus, this protein is necessary for the proper function and viability of rod cells and consequently, of the visual signalling cascade.

Another similar integral membrane protein is Rom1 that, like Prh2, belongs to the tetraspanin superfamily and forms heterotetramers with Prph2. Despite the similarities, Rom1 plays a minor structural role in contrast with that of Prph2. This was revealed by the comparison of a Prhp2 knock-out mouse with the Rom1 knock-out mouse (Loewen, Moritz, & Molday, 2001). In the first case, photoreceptors underwent a slow degeneration process over time whereas in the case of Rom1, the absence of this protein produced limited abnormalities in the ROS. The relevant paper of Prph2 is also demonstrated by the fact that over 90 mutations in its gene have been identified in humans leading to retinal diseases, like macular degeneration or RP (Boon et al., 2008).

On the other hand, it was observed that Prh2 (located in the rim region of disc membranes) interacts with other proteins like the CNG ion channel (Cheng & Molday, 2013; Poetsch, Molday, & Molday, 2001) located in the plasma membrane of the rod cells. This interaction was suggested to play a structural role between the discs and the plasma membranes (Poetsch et al., 2001).

Moreover, a study identified, by means of co-immunoprecipitation assays and mass spectrophotometry, a CNG ion channel interaction with Rho among other proteins like Prph2 (Cheng & Molday, 2013). Interestingly, in a posterior study, this interaction was analysed in depth finding a complex formation between CNG ion channel and Rho through Prph2, i.e. a tripartite interaction involving the three proteins (Becirovic et al., 2014).

This newly reported protein-protein interaction and the implications that Prph2 binding could have on Rho functionality, has been identified as a new interesting field of study.

4.4.1 Non-tagged Prph2 immunopurification

Initially, an experiment was performed to determine whether Prph2 without any tag could be co-purified by means of its complex formation with Rho under our conditions. Co-transfection was conducted by adding two vectors with the genes for both proteins at the same ratio in COS1 cells (Loewen et al., 2001). In parallel, WT bovine Rho was individually transfected under the same conditions. After cell collection and regeneration with 11-*cis*-retinal, both samples were immunopurified with 1D4 antibody and UV-Vis spectra was recorded by UV-vis spectrophotometry at 20°C.

As a result, although a lower yield was observed in the Rho-Prhp2 co-transfection, the ratio $A_{280}/A_{\lambda max}$ was similar to that of the WT bovine Rho transfection (Fig. 4.4.1) and inside the range reported in *Section 4.2* (Table 4.2.1). With this in mind, we could suggest that under these conditions there was not association in a complex of Prph2 and Rho, at least to a significant level, or if such an interaction existed could not have survived the purification process. An increased A_{280}, relative to $A_{\lambda max}$, would be expected due to a larger protein presence if the complex were formed.

Therefore, in our spectra the band at A_{280} principally corresponds with the opsin apoprotein. Consequently, the insertion of the 1D4 tag in the Prph2 background was selected as the strategy to carry out experiments by immunopurification.

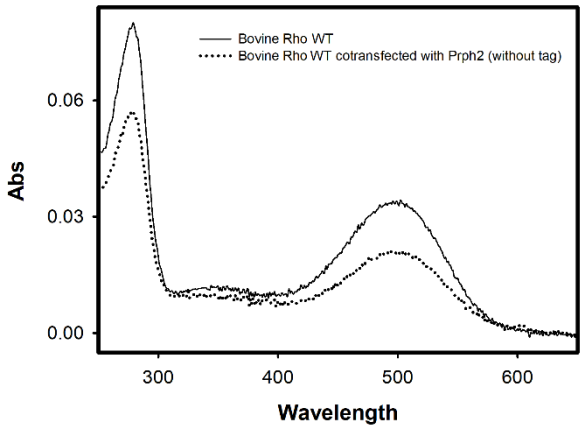

Figure 4.4.1 Immunopurified spectra of individually expressed bovine Rho and Rho co-transfected with untagged Prph2. Samples were at 20°C in PBS pH 7.4, 0.05 %DM. The ratio A_{280} / $A_{\lambda max}$ is similar for Rho WT (A_{280} / $A_{\lambda max}$ = 2.5) and fom Rho WT + Prph2 (A_{280} / $A_{\lambda max}$ = 2.6).

4.4.2 Insertion of the 1D4 tag and immunopurification

In order to immunopurify Prph2, the 1D4 epitope was inserted at the C-terminus of the protein gene by site directed mutagenesis. Then, the mutated gene was sequenced to confirm the correct insertion of the tag (Fig 4.4.2).

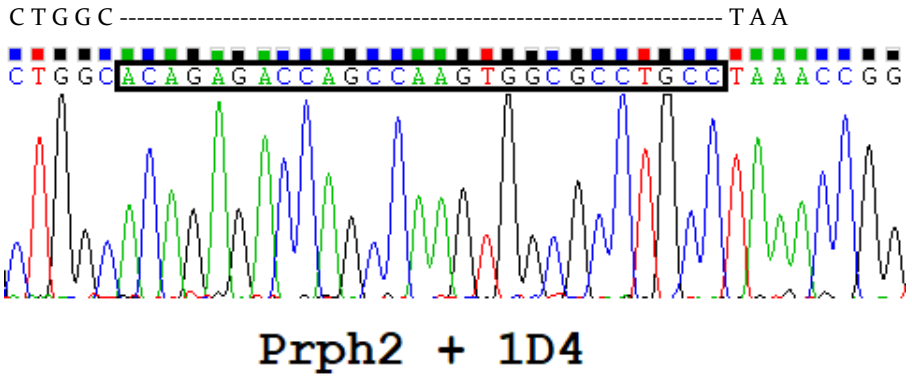

Figure 4.4.2 DNA sequencing for Prph2 with the inserted 9 aminoacids of the 1D4 epitope. Original sequence is indicated above and introduced section corresponding with the 1D4 sequence is boxed.

COS-1 cells were divided in two groups and individually transfected with the mutagenized vector of Prph2 (tagged-Prph2) or with the bovine Rho WT vector. The proteins were immunopurified with 1D4-Sepharose as previously described for the Rho pigment. Then, the purified samples in 0.05 % DM solutions were measured at 20°C by means of UV-vis spectrophotometry. A_{280nm} was determined for both proteins. (Fig. 4.4.3 left panel), and the data supports the absence of Prph2 in Fig. 4.4.1. Moreover, a Western blot was performed by mean of anti-1D4 antibody (Fig. 4.4.3 right panel) where a clear smear was observed that corresponds to the typical pattern seen for proteins expressed in COS1 cells, and usually atributed to heterogeneous glycosylation. As previously described, Rho and Prph2 have a similar molecular weight (Molday, 1998), and Prph2 has tendency to oligomerize (Loewen et al., 2001). This fact was not apparently affected by the addition of Rho at a 1:1 ratio.

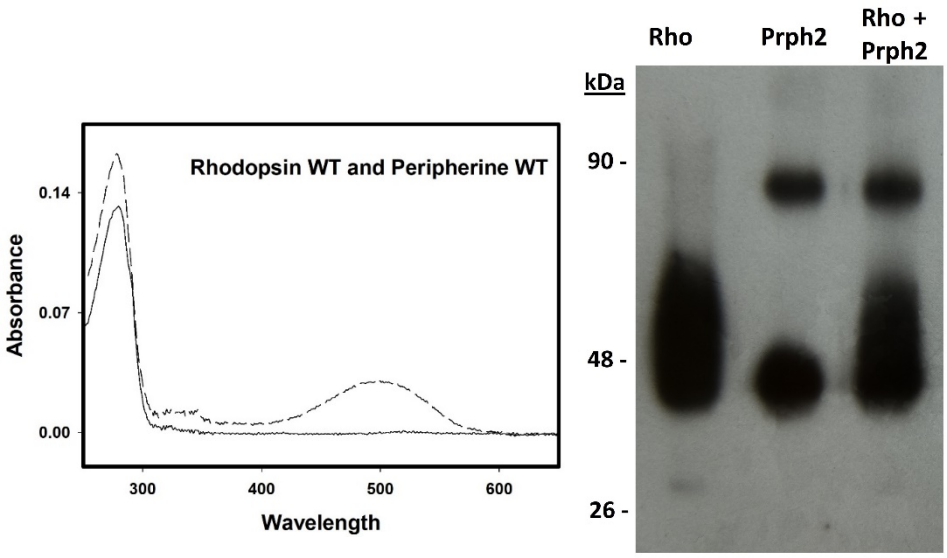

Figure 4.4.3 Parallel immunopurification of Rho and Prph2 and Western blot of the purified proteins. Left panel, spectrum of purified Rho (dashed line) and Prph2 (continued line) in 0.05 % DM. **Right panel,** Western Blot of the immunopurified protein samples detected with Rho-1D4 monoclonal antibody. First lane correspond to purified bovine Rho WT, second lane to purified Prph2 and the third lane to a 1:1 mixture of the proteins from the first and second band.

4.4.3 Co-transfection and Immunopurification

As Prhp2 with the 1D4 tag was correctly immunopurified with 1D4-Sepharose, co-transfection and co-immunopurification with bovine WT Rho was performed. At the same time, the immunopurification of individually expresed Rho was carry out as a control. Both experiments were conducted in parallel under the same experimental conditions throughout the whole process.

The purified samples were analysed by their of UV-vis spectra. Both samples had a similar band at λ_{max} corresponding to Rho, but in contrast with the previous purifications the ratio $A_{280}/A_{\lambda max}$ was found to differ (Fig. 4.4.4 A). Purified Rho had a $A_{280}/A_{\lambda max}$ ratio of 2.55±0.18 that corresponds with the normal ratio previously reported in the same conditions in our laboratory

(Fernández-Sampedro et al., 2016; Ramon et al., 2014) and also to that observed in Fig. 4.4.1. In contrast, the co-transfected and co-purified Rho+Prph2 had an increased ratio of 3.93±0.51, due to the co-purified Prph2 protein.

The proteins spectral behaviour, upon illumination with filter and upon acidification, was also analyzed (Fig. 4.4.4 B). No difference was observed between Rho and Rho+Prph2 samples as they showed similar spectral patterns.

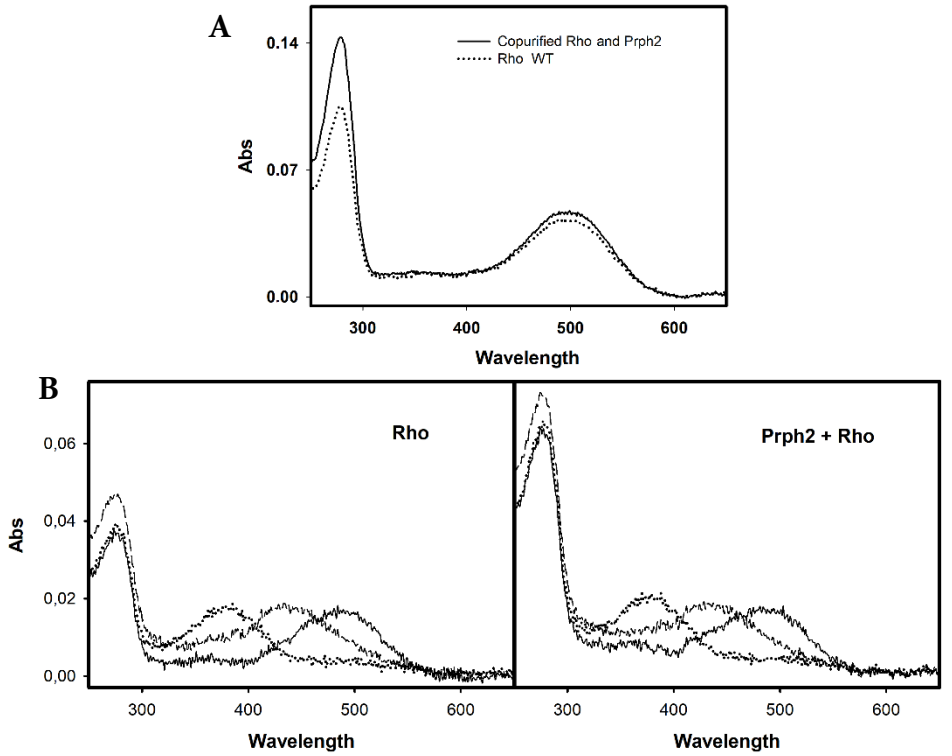

Figure 4.4.4 UV-Vis spectrophotometric analysis of purified Rho in comparison with co-transfected Rho + Prph2. Spectra were measured at 20°C. *A)* Dark state of both samples in PBS and 0.05 %DM. $A_{280}/A_{\lambda max}$ ratio of 2.55±0.18 for Rho, and 3.93±0.51 for Rho+Prph2. *B)* Photobleaching and acidification behaviour. Absorption spectra of dark sample (continuous lines), after 30 s illumination with cut off filter (dotted lines) and after acidification with H_2SO_4 (dashed lines).

Meta II decay

The stability of the active state was compared by Meta II decay determination in real time in the fluorimeter at 20°C. This was carried out by monitoring the Trp fluorescence increase upon Rho illumination as a result of the all-*trans*-retinal release from the binding pocket. Our data showed an almost equal Meta II decay behaviour of Rho in the presence and in the absence of co-transfected Prph2 (Fig. 4.4.5).

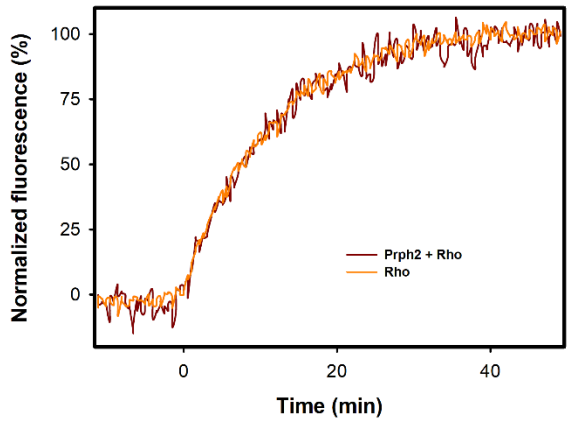

Figure 4.4.5 Meta II decay of the immunopurified proteins, Rho and the cotransfected Rho+Prph2 at 20°C. Normalized fluorescence increase due to the Trp exposure as a result of all-*trans*-retinal release. 30 s illumination with 495 nm cut-off filter at min 0.

Functional Gt activation assay

The functional activation of the Gt by the Rho, upon illumination, initiates the visual signal transduction. This functionality was monitored by calculating the amount of GTPγS^{35} bound by Gt upon photobleaching by means of a radioactive filter binding assay over the time. As in the previous experiments, purified Rho and Rho+Prph2 were measured and compared (Fig 4.4.6).

The Gt activation kinetics were found to be similar in both the Rho and the Rho+Prph2 samples so we conclude that both samples have a similar ability to activate Gt.

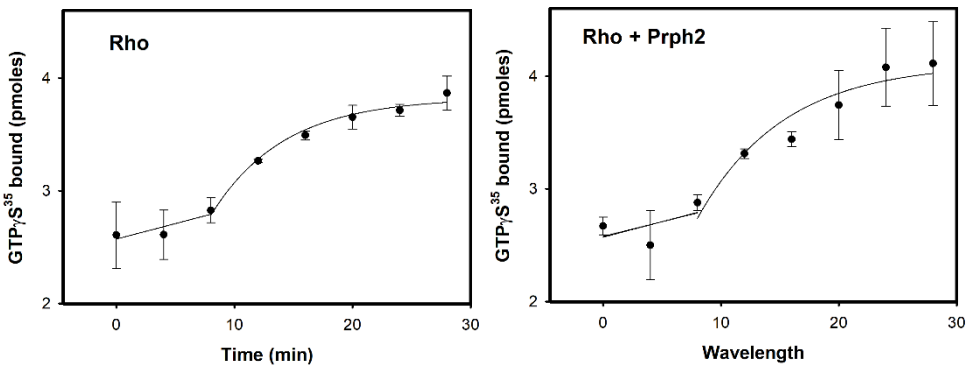

Figure 4.4.6 Gt activation of purified Rho and Rho+Prph2. Measurements were carry out in the dark and at room temperature, at times 0, 4 and 8 min, meanwhile 12, 16, 20, 24 and 28 min were measured after photobleaching.

4.4.4 Cotransfected membrane preparations

The membrane preparation was selected to check whether the protein environment and the purification protocol used could affect the interaction between Rho and Prph2. For this reason, Rho and Rho+Prph2 were separately transfected in COSI cells. Then, COSI cell membranes were prepared as described in *section 3.6*, followed by a solubilization step as described in *section 3.7* but using only 0.1 % DM, as greater DM concentrations can affect formation of dimers seen in the detergent micelles (Jastrzebska et al., 2004). In this way, the formed vesicles were composed of membrane proteins, membrane lipids and detergent (Chattopadhyay, Rao, & Jafurulla, 2015).

At this point, the important contribution of scattering to the spectra in the samples was taken care of by measuring the difference spectra before and after illumination because the signal should then correspond only to Rho.

Moreover, the samples were eventually acidified but a similar spectral pattern was observed in both samples (Fig. 4.4.7).

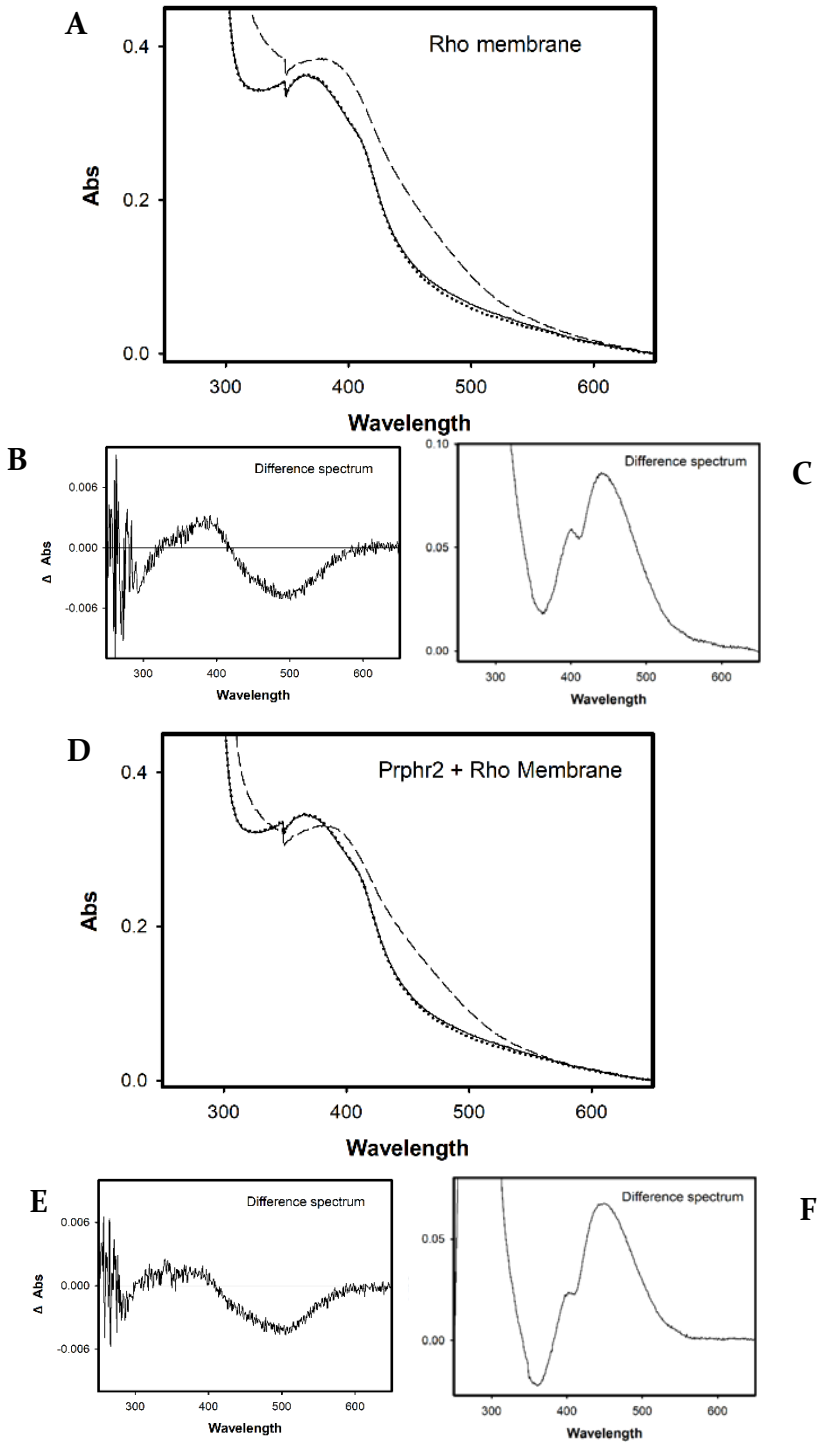

Figure 4.4.7 Solubilized membranes of COS1 cells with transfected Rho (A, B and C) and co-transfected Rho + Prph2 (D, E and F). *A and D,* dark state (continuous lines), photobleached by 30s illumination with filter (dotted lines) and after acidification (dashed lines). *B and E* show difference spectrum obtained by subtracting the photobleached to the dark state. Hence negative values mean absorbance decrease upon illumination. *C and F,* show difference spectrum obtained by subtracting the acidified spectrum to the dark state spectrum.

Functional Gt activation assay

A new Gt activation protocol was performed with the same proteins but this time in partially solubilized membrane environment. In this case, the Gt activation was measured in the dark state 30 min after photobleaching. The results show that in the presence of Prph2 Rho shows a lower ability to activate Gt than in its absence (Fig. 4.4.8).

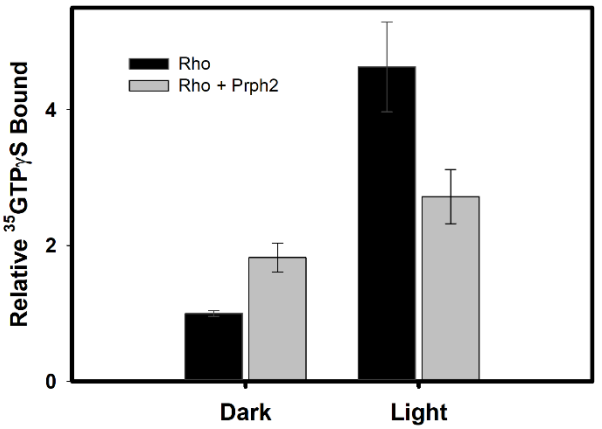

Figure 4.4.8 Gt activation of partially solubilized membranes containing Rho and Rhod+Prph2. Measurements were carried out at room temperature. Initial measurement in the dark and 30 min after 30 s illumination.

4.4.5 Rho-Prph2 interaction analysis

Different strategies were used in order to observe the effect of the complexes of Prph2 and Rho on the functionality of the latter pigment. The usual purification conditions used in our lab failed to detect any effect of the

potential interaction. In this regard Phrp2 could not be co-immunopurified with Rho and when tagged Phph2 was co-transfected and co-purified with Rho no significant functional effect could be observed.

Different factors may explain the observed behaviour that differs from the previous report where the interaction of these two proteins was demonstrated (Becirovic et al., 2014). The first important difference was observed when co-immunoprecipitation and FRET analysis in eukaryotic cells were tested by co-expressing Prph2 and Rho apoprotein without retinal chromophore (Becirovic et al., 2014; Nguyen et al., 2016), as a different protein conformation in the absence of retinal may have some effects. Nevertheless, a FRET assay on isolated ROS also showed the interaction between Prph2 and Rho, but apparently the binding affinity difference from Prph2/Rho to the Rho/Rho dimer was higher in the ROS assays. In any case, some of the experiments carried out with regenerated Rho point to the fact that the presence of chromophore may not be determinant for the interaction. And despite that some authors suggest more prominent interactions of Rho with guanylate cyclase 1 in comparison with Rho and Prph2 (Pearring, Spencer, Lieu, & Arshavsky, 2015), a novel co-localization of Prph2 and Rho in RPE cells also supports the existence of this protein complex (Uhl et al., 2015).

Another important factor on the experiments conducted in this section was the presence and type of detergent used, due to the instability of membrane complexes in detergent solutions (Pearring et al., 2015). In fact, the shorter protocol using a lower DM concentration for the solubilization, instead of the 1 % DM used for the firsts steeps of immunopurification, allow us to obtain functional differences that can be attributed to the presence of Prph2-Rho complex.

In this way, the functional assays (Gt activation and Meta II decay) performed on Rho and Rho+Prph2 co-immunopurified samples, produced non-significant differences (Fig. 4.4.5 and Fig. 4.4.6). Photobleaching and acidification patterns were also similar in the samples (Fig. 4.4.4). In contrast, when using the membrane preparation obtained solubilizing with a lower DM concentration, a clear different behaviour was observed as the presence of prph2 produced a lower Gt activation by Rho (Fig. 4.4.8).

Two scenarios were proposed for the physiological role of this interaction (Becirovic et al., 2014). The first scenario would be the optimization of the visual transduction process by directly connecting Rho and the CNG ion channel through Prph2 and fastening the kinetics of the process. But according to our results this would not be possible as the presence of Prph2 appears to reduce the effectiveness of the transduction at the Gt activation level. Moreover, as discussed in *Section 4.1* the buffering mechanisms found in the downstream calcium feedback mechanism to cGMP synthesis (Gross et al., 2012) may reduce the variations occurring in the first steps of the phototransduction cascade.

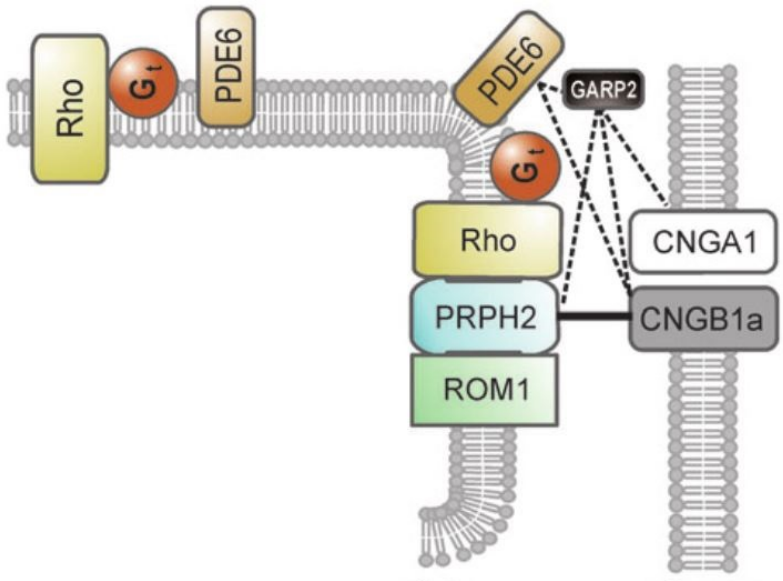

Figure 4.4.9 Proposed model of interaction of Prph2 with Rho and other visual phototransduction proteins. Prph2 bound to Rho and ROM1 in the rim of the discs and at the same time interacting with the subunit of the CNG ion channel located on the cytoplasmic membrane of the rod cell photoreceptor. Image retrieved from Becirovic et al., 2014

The second scenario proposed, was the structural role of this interaction in the formation and maintenance of ROS. In particular, it was suggested that the Rho/Prph2/ROM1/CNG ion channel complex may be relevant for maintaining the ROS structure (Becirovic et al., 2014) (Fig. 4.4.9). Complementary to this idea, a recent study supports the structural role of Rho by forming oligomers and interacting with cytoskeletal filaments (Gunkel et al., 2015). Our results would also point to a structural role of such interaction and in any case a negative regulation of the functionality of a fraction of Rho molecules by reducing its functionality.

5 General discussion

Important divergences in the biochemical behaviour among human, bovine and murine Rho were found, mainly related to their thermal and their Meta II conformation stabilities. Moreover, significant differences were appreciated when comparing the biochemical features of the Y102H RP-like Rho mutation with WT in bovine and human Rho backgrounds.

The relevance of these findings relies on the thorough use of the bovine pigment as the *in vitro* model in different studies of RP and other retinal dystrophies (e.g. Opefi et al., 2013; Toledo et al., 2011; Xie et al., 2003). Keeping in mind that the subject of these studies is the characterization of point mutations in human diseases, and given the differences observed among species, the preferential use of human Rho for *in vitro* RP point mutations characterization studies may be suggested. In the same direction, some authors have conducted *in vitro* experiments dealing with RP mutations with human Rho (Sung, Schneider, Agarwal, Papermaster, & Nathans, 1991; Tam et al., 2014). Furthermore, several recent studies highlight the importance of the characterization of human Rho and its comparison with bovine Rho (Funatogawa et al., 2016; Kazmin et al., 2015; Morrow et al., 2017) to unravel subtle (or even major) phenotypic differences.

Adaptation to scotopic environments is thought to have played an important role in the evolution of vision in vertebrates. When comparing the characterization of diurnal (human and bovine) and nocturnal (mouse) Rho, an important difference was found in the Meta II decay rate. Moreover, by comparing the pigment amino acid sequences a new position, 290, was found to be importantly correlated with the main activity pattern of terrestrial therian mammals. This site mutation from L290I in mouse Rho resulted in the reduction of the retinal release to rates similar to thus of Rho

from diurnal species like cow. Moreover, this mutation produced a slight blue shift of 2 nm, shifting the λ_{max} of mouse Rho WT closer to that of bovine Rho.

Another substitution, D83N, was previously proposed to also to lead to a slower retinal release but was limited to echidna Rho (Bickelmann et al., 2015), cetacean Rho (Dungan & Chang, 2017) and some cichlid fishes Rho (Hauser et al., 2017). In comparison, a potential evolutionary role of the L290I substitution in therian terrestrial mammals (especially in primate and rodents) during photoreceptor adaptation to photic environments was proposed as a new evidence for the relationship between Meta II decay rates and photic environments adaptation. Hence, a deeper analysis using a larger set of mammal Rho species, and even in other clades, would be an interesting topic for further research. In parallel, the search for other sites presumably having epistatic interactions with site 290 would also be an interesting topic of study in visual pigment molecular evolution.

Although the link between Meta II and current physiological aspects of human vision is yet to be clearly stablished, the implications of the Meta II decay rate was found to be important during visual pigment evolution and species differentiation. Deeper analyses by means of an integrative bibliographical research involving different areas as biochemical, physiological, ecological, environmental, would be needed to shed more light into the details of this influence. Thus, the previously suggested effect of a slower retinal release rate, increasing Gt activation by a long-lived Meta II conformation, and consequently increasing rod sensitivity (Bickelmann et al., 2012), was found to be improbable due to the fast shut-off produced by the Rho kinase and arrestin (Fu & Yau, 2007) that was found to be faster than the Meta II decay under physiological conditions (Gross et

al., 2012). Our results, suggest a protective effect of the reported amino acid substitution by sequestrating harmful all-*trans*-retinal excess under bright light in nocturnal Rho therian mammals. This effect would be at the same time, in a compromised balance with the faster dark adaptation, under dim-light conditions, in diurnal Rho therian mammals.

Previous studies have emphasized the differences between *in vivo* visual models from different species, like the biochemically characterized murine and human Rho, for their relevance to human physiology (Domitille L. Boudard et al., 2011; Organisciak & Vaughan, 2010). Yet, the use of diurnal rodent models for retinal damage studies was proposed as the cone/rod cells ratio would be closer to that found in human macula (D.L. Boudard et al., 2010; Jacobs et al., 2003; Saïdi et al., 2011). The differences observed in Rho thermal stability, but mainly in the Meta II decay rates between diurnal and nocturnal species, would suggest that besides the different specific cell photoreceptor types relative abundance, the intrinsically differential behaviour of Rho from different species should also be taken into account for future research.

Despite not directly affecting visual pigments, different diseases have been previously linked to the pathogenic role of free all-*trans*-retinal in retinal cells like dry age-related macular degeneration, Stargardt disease and other degenerative retinal disorders (Maeda et al., 2012), although how this molecule actually triggers retinal degeneration is far from being completely understood (Chen et al., 2013).

Diverse drugs have been proposed in the last years, for prevent, slow down or halt these all-*trans*-retinal linked diseases. Two main approaches were proposed: sequestering of free all-*trans*-retinal by forming Schiff base

adducts that would trap it and, on the other side, the inhibition of the retinoid cycle by for example inhibiting RPE65 enzyme activity (Maeda et al., 2012). This kind of inhibitors are useful in preventing degeneration associated to all-*trans*-retinal, as occurs in the case of retinylamines (Maeda et al., 2012) or in the case of Emixustat, a molecule that is nowadays being tested in clinical trials (J. Zhang et al., 2015). Of these two approaches, the sequestering strategy was suggested to have less adverse effects, as it does not affect the visual cycle regeneration process, being apparently more effective (Maeda et al., 2012; J. Zhang et al., 2015).

Taking into account the photoprotective effect suggested by a slower retinal release, a complementary therapeutic approach for the mentioned diseases could be proposed by temporary slowing all-*trans*-retinal release as would be the case for a more stable Meta II conformation. Similarly, different compounds as for example flavonoids or retinal analogues have being studied in vitro on the stabilization of Rho mutants causing RP or similar congenital diseases (Herrera-Hernández et al., 2017). In this way, the study of compounds that could prolong Meta II stability in WT Rho, by slowing down its decay and subsequent all-trans-retinal release, may proof to be good candidates as therapeutic agents against these retinal diseases, and be the subject of future studies.

An alternative approach was also used to study Rho evolution by means of a statistical analysis that allowed us to obtain three amino acid candidates, in Rho, that could have been positively selected through evolution along the base of the therian branch. These correspond to positions located in the N-terminal region, TM helix and the C-terminal region and we could infer that specific mutations had been positively selected from the ancestral state (M13 → F13, R225 → Q225 and S346 → A346). We used of biochemical and

functional techniques in order to characterize them, and to this aim the reverse mutations to the ancestral state were constructed in the bovine Rho background: F13M, Q225R and A346S.

Mutation F13M was unable to regenerate chromophore with 9-*cis*-retinal or 11-*cis*-retinal under diverse experimental conditions. The introduction of the thermally stable double Cys mutation, N2C/N282C, allowed to obtain a functional Rho by means of the formation of a disulfide bound. Overall, our main conclusion for this mutations is that the amino acid at position 13 is involved in the folding of the receptor and in proper protein glycosylation.

The other two mutations showed a spectral pattern similar to that of bovine WT Rho. Amino acid at position 225 appeared to play a key role in the function of the protein by affecting the G-protein activation process. This Arg of position 225 would likely steric clash with Tyr136 of neighbouring helix III that belongs to the conserved ERY motif critical in Gt activation. Arg135 in this conserved triplet was shown to be hydrogen bonded with a Gt-derived peptide (Elgeti et al., 2011; Hofmann et al., 2009; Scheerer et al., 2008). Any change in the structure of this region would cause a change in the coupling efficiency to the G-protein.

In contrast, amino acid at position 346 would also regulate functionality of the receptor by enhancing G-protein activation and could also alter Rho trafficking (Concepcion & Chen, 2010). Interestingly, the specific A346S Rho mutation creates a potential additional phosphorylation site which would affect Rho phosphorylation after photoactivation (Doan et al., 2006) and in turn may affect the binding affinity of arrestin, a regulator of Rho deactivation.

These findings underscore the importance of molecular analysis of putative positively selected sites in Rho evolution and the relevance of structural and functional analysis of these amino acid substitutions to decipher the molecular clues governing visual pigment evolution. Additional future experiments could be designed involving a series of mutations at positions putatively positively selected in order to detect epistatic effects among those mutations (Dungan & Chang, 2017). Furthermore, it would be interest to insert the inverse mutants in inferred ancestral Rho.

The stabilization, by means of disulfide bond introduction, of Rho mutants incapable of regenerate chromophore with retinal was demonstrated as an effective tool to study this kind of defective receptors. Here, we have confirmed the presence of a disulfide bond (at least partially) in the previously proposed W90C/A169C double mutant (Srinivasan, 2015) in the human green cone opsin system. This disulfide bond strategy could potentially recover other unstable mutations on human cone opsins related with different disorders or help in getting deeper insight into evolutionary questions. A recent study used a different approach to increase protein stability based on the insertion of different thermo-stabilizing proteins (Owen et al., 2018)

The binding interaction of Rho with other proteins non-functionally implicated, at least in principle, in the signal transmission of the visual cascade has been largely unattended. We have undertaken the functional study of the complex formation of Rho and Prph2 because a previous study reported a ternary complex involving Rho, Prph2 and CNG ion channels and in particular Prhp2 with Rho was functionally analysed.

The presence of detergent was found to be determinant in the conditions needed for the study of these protein-protein interactions. In this way, when

Rho and Prph2 were co-transfected and co-purified using the usual purification protocol, no significant differences in Gt activation were detected with regard to Rho alone. This suggested that under such experimental conditions we could not detect any interaction of the two proteins. In contrast, when the proteins were just solubilized in low detergent concentration buffer yielding partially solubilised membranes, we could detect a clear reduction in the Gt activation in sample containing the Prph2+Rho complex as opposed to the sample containing Rho alone.

The reduced functionality of Rho, upon Prph2 interaction suggests a structural role of the Rho molecules located at the rim region of the disc that may be important for the maintenance of ROS integrity mediated by disc interaction with the cytoplasmic membrane where the CNG ion channels are located. This structural role would agree with the structural role for Rho oligomers, and interacting with cytoskeletal filaments, proposed in a recent study (Gunkel et al., 2015).

6 Conclusions

- Important divergences in the biochemical behaviour (folding, stability and function) among human, bovine and murine Rho were found in our *in vitro* conformational analysis. These differences may have physiological relevance and should be taken into account in future studies using *in vitro* and animal models.
- A correlation between the amino acid found at position 290 (in bovine Rho numbering) and diurnal/nocturnal activity along therian terrestrial mammals was found, especially in the primate and the rodent branches. This position is in close contact with other residues forming part of the opening proposed to be the II-*cis*-retinal entry site.
- L290I mutation appears to be a key amino acid change during evolution from nocturnality to diurnality by means of a Meta II stability decrease and a slightly blue-shifted visible λ_{max} in the Rho spectrum. This finding provides further evidence about possible impact of Meta II decay rate changes during the course of Rho evolution.
- The evolutionary-linked results obtained highlight the importance of an integrative comparative analysis that includes ecological, physiological, biochemical, molecular and evolutionary approaches towards the aim of unambiguously determine the phenotype/genotype relationships associated with the evolutionary relevant amino acid changes in the Rho sequence. A new mechanism is proposed involving a compromise between improving rod protection under bright light in nocturnal species by means of a stabilized Meta II conformation, and a faster dark adaption that occurs under dim-light conditions in diurnal species by means of a

faster retinal release. Future studies in drug development could be taking into account this hypothesized rod protection by Meta II stabilization as a strategy for the treatment of different retinal diseases like dry age-related macular degeneration or Stargardt disease.

- The biochemical differences found in WT Rho and the RP-like Y102H mutation, from different species, should be an important issue to consider in research involving point mutation associated with human diseases, and when using *in vitro* bovine Rho or *in vivo* mouse Rho models. Thus, the preferential use of human Rho for *in vitro* RP point mutants characterization can be strongly advised.
- The thermal instability of the RP-like Y102H Rho mutation appears to be the result of structural perturbations of the H-bond network formed by close residues associated with naturally occurring RP mutations along ECL1 and the N-terminal domain.
- The statistical analysis to Rho evolution found three mutations that could be inferred in positively selected sites occurring in the early therian mammal ancestor: M13 to F13, R225 to Q225 and S346 to A346 (in bovine Rho numbering system). The reverse mutations to the ancestor state were individually inserted into the bovine Rho background for *in vitro* characterization.
- The purified F13M protein characterization stresses importance of position 13 for the folding of the receptor and also for proper protein glycosylation by affecting the proximal glycosylation N15 site. Given the deleterious nature of this reverse substitution (F13M), impairing chromophore regeneration and showing the ability to recover a WT phenotype by means of an engineered double Cys mutant

(N2C/N282C), it could be speculated that the positive selection observed at this site could have been compensatory with other sites.

- Position 225 would play a key role in the function of the protein affecting the G-protein activation process. This Arg at position 225 would likely steric clash with Tyr at 136 of neighbouring helix III that belongs to the conserved ERY motif critical in Gt activation. Any change in the structure of this region could cause a decrease in the coupling efficiency to the G-protein as experimentally observed.
- The specific A346S Rho mutation creates a potential additional phosphorylation site which would affect Rho phosphorylation after photoactivation and in turn may affect the binding affinity of arrestin, a regulator of Rho deactivation. Therefore, this extra phosphorylation site on the ancestral pigment could provide an evolutionary explanation for the enhanced response in the case of Gt activation that would need a more efficient signal desensitization process.
- The formation of a disulfide bond (at least partially) in human green cone opsins by the double mutation W90C/A169C was confirmed. This opens up new possibilities for using this stabilizing strategy for further studies of cone opsin pigments.
- Prph2 showed no effect on Rho properties under experimental conditions used for Rho purification (solubilised system in DM solution). However, the functionality of Rho is reduced as measured by a decreased Gt activation level when the two proteins were in a partially solubilised system (with the presence of remaining membrane fragments). The interaction detected between Rho and Prph2 can have implications in the desensitization of Rho on the rim

of the discs (where the Prph2 is located) near to the CNG ion channels. These results provide further support for a structural role of Rho in the rim region at the ROS discs. The Prph2-Rho interaction at this location could serve as an inhibitor of these Rho molecules activity by quenching the outcoming signal upon Rho photoactivation.

Bibliography

Ala-Laurila, P., Kolesnikov, A. V., Crouch, R. K., Tsina, E., Shukolyukov, S. A., Govardovskii, V. I., … Cornwall, M. C. (2006). Visual Cycle: Dependence of Retinol Production and Removal on Photoproduct Decay and Cell Morphology. *The Journal of General Physiology*, *128*(2), 153–169. https://doi.org/10.1085/jgp.200609557

Andrés, A., Garriga, P., & Manyosa, J. (2003). Altered functionality in rhodopsin point mutants associated with retinitis pigmentosa. *Biochemical and Biophysical Research Communications*, *303*(1), 294–301. https://doi.org/10.1016/S0006-291X(03)00328-0

Andrés, A. M., De Hemptinne, C., & Bertranpetit, J. (2007). Heterogeneous rate of protein evolution in serotonin genes. *Molecular Biology and Evolution*, *24*(12), 2707–2715. https://doi.org/10.1093/molbev/msm202

Araujo, N. A., Sanz-Rodríguez, C. E., & Bubis, J. (2014). Binding of rhodopsin and rhodopsin analogues to transducin, rhodopsin kinase and arrestin-1. *World Journal of Biological Chemistry*, *5*(2), 254–68. https://doi.org/10.4331/wjbc.v5.i2.254

Arshavsky, V. Y., & Burns, M. E. (2012). Photoreceptor signaling: Supporting vision across a wide range of light intensities. *Journal of Biological Chemistry*, *287*(3), 1620–1626. https://doi.org/10.1074/jbc.R111.305243

Athanasiou, D., Aguila, M., Bellingham, J., Li, W., McCulley, C., Reeves, P. J., & Cheetham, M. E. (2018). The molecular and cellular basis of rhodopsin retinitis pigmentosa reveals potential strategies for therapy. *Progress in Retinal and Eye Research*, *62*, 1–23. https://doi.org/10.1016/j.preteyeres.2017.10.002

Azevedo, A. W., Doan, T., Moaven, H., Sokal, I., Baameur, F., Vishnivetskiy, S. A., … Rieke, F. (2015). C-terminal threonines and serines play distinct roles in the desensitization of rhodopsin, a G protein-coupled receptor. *ELife*, *4*(7), 2398–2407. https://doi.org/10.7554/eLife.05981

Bartl, F. J., & Vogel, R. (2007). Structural and functional properties of metarhodopsin III: recent spectroscopic studies on deactivation pathways of rhodopsin. *Physical Chemistry Chemical Physics*, *9*(14), 1648–1658. https://doi.org/10.1039/b616365c

Baylor, D. a, & Burns, M. E. (1998). Control of rhodopsin activity in vision. *Eye*, *12*(3), 521–525. https://doi.org/10.1038/eye.1998.140

Becirovic, E., Nguyen, O. N. P., Paparizos, C., Butz, E. S., Stern-Schneider, G., Wolfrum, U., … Biel, M. (2014). Peripherin-2 couples rhodopsin to the CNG channel in outer segments of rod photoreceptors. *Human Molecular Genetics*, *23*(22), 5989–5997. https://doi.org/10.1093/hmg/ddu323

Belmer, A., Doly, S., Setola, V., Banas, S. M., Moutkine, I., Boutourlinsky, K., … Maroteaux, L. (2014). Role of the N-Terminal Region in G Protein – Coupled Receptor Functions : Negative Modulation Revealed by 5-HT 2B Receptor Polymorphisms s. *Molecular Pharmacology*, *85*, 127–138. https://doi.org/1521-0111/85/1/127

Beyrière, F., Sommer, M. E., Szczepek, M., Bartl, F. J., Hofmann, K. P., Heck, M., & Ritter, E. (2015). Formation and Decay of the Arrestin·Rhodopsin Complex in Native Disc Membranes. *Journal of Biological Chemistry*, *290*(20), 12919–12928. https://doi.org/10.1074/jbc.M114.620898

Bickelmann, C., Morrow, J. M., Du, J., Schott, R. K., van Hazel, I., Lim, S., …

Chang, B. S. W. (2015). The molecular origin and evolution of dim-light vision in mammals. *Evolution*, *69*(11), 2995–3003. https://doi.org/10.1111/evo.12794

Bickelmann, C., Morrow, J. M., Müller, J., & Chang, B. S. W. (2012). Functional characterization of the rod visual pigment of the echidna (Tachyglossus aculeatus), a basal mammal. *Visual Neuroscience*, *29*(4–5), 211–217. https://doi.org/10.1017/S0952523812000223

Boon, C. J. F., den Hollander, A. I., Hoyng, C. B., Cremers, F. P. M., Klevering, B. J., & Keunen, J. E. E. (2008). The spectrum of retinal dystrophies caused by mutations in the peripherin/RDS gene. *Progress in Retinal and Eye Research*, *27*(2), 213–235. https://doi.org/10.1016/j.preteyeres.2008.01.002

Borges, R., Johnson, W. E., O'Brien, S. J., Gomes, C., Heesy, C. P., & Antunes, A. (2018). Adaptive genomic evolution of opsins reveals that early mammals flourished in nocturnal environments. *BMC Genomics*, *19*(December), 1–12. https://doi.org/10.1186/s12864-017-4417-8

Borrego, S., Sánchez, B., Ruiz, A., & Antiñolo, G. (1996). Missense mutation A346P in the rhodopsin gene in one family with autosomal dominant retinitis pigmentosa. *Human Mutation*, *7*(2), 180–1. https://doi.org/10.1002/humu.1380070202

Bosch-Presegué, L., Iarriccio, L., Aguil, M., Toledo, D., Ramon, E., Cordomí, A., & Garriga, P. (2011). Hydrophobic amino acids at the cytoplasmic ends of helices 3 and 6 of rhodopsin conjointly modulate transducin activation. *Archives of Biochemistry and Biophysics*, *506*(2), 142–149. https://doi.org/10.1016/j.abb.2010.11.019

Boudard, D. L., Acar, N., Bretillon, L., & Hicks, D. (2011). Retinas of the diurnal rodent Arvicanthis ansorgei are highly resistant to experimentally induced stress and degeneration. *Investigative Ophthalmology and Visual Science*, *52*(12), 8686–8700. https://doi.org/10.1167/iovs.11-8162

Boudard, D. L., Tanimoto, N., Huber, G., Beck, S. C., Seeliger, M. W., & Hicks, D. (2010). Cone loss is delayed relative to rod loss during induced retinal degeneration in the diurnal cone-rich rodent Arvicanthis ansorgei. *Neuroscience*, *169*(4), 1815–1830. https://doi.org/10.1016/j.neuroscience.2010.06.037

Bowmaker, J. K. (2008). Evolution of vertebrate visual pigments. *Vision Research*, *48*(20), 2022–2041. https://doi.org/10.1016/j.visres.2008.03.025

Budzynski, E., Gross, A. K., McAlear, S. D., Peachey, N. S., Shukla, M., He, F., … Nishina, P. M. (2010). Mutations of the opsin gene (Y102H and I307N) lead to light-induced degeneration of photoreceptors and constitutive activation of phototransduction in mice. *Journal of Biological Chemistry*, *285*(19), 14521–14533. https://doi.org/10.1074/jbc.M110.112409

Burns, M. E., & Pugh, E. N. (2010). Lessons from Photoreceptors: Turning Off G-Protein Signaling in Living Cells. *Physiology*, *25*(2), 72–84. https://doi.org/10.1152/physiol.00001.2010

Buzhynskyy, N., Salesse, C., & Scheuring, S. (2011). Rhodopsin is spatially heterogeneously distributed in rod outer segment disk membranes. *Journal of Molecular Recognition*, *24*(3), 483–489. https://doi.org/10.1002/jmr.1086

Calvert, P. D., Strissel, K. J., Schiesser, W. E., Pugh, E. N., & Arshavsky, V. Y. (2006). Light-driven translocation of signaling proteins in vertebrate photoreceptors. *Trends in Cell Biology*, *16*(11), 560–568. https://doi.org/10.1016/j.tcb.2006.09.001

Chan, W. M., Yeung, K. Y., Pang, C. P., Baum, L., Lau, T. C., Kwok, A. K., & Lam, D. S. (2001). Rhodopsin mutations in Chinese patients with retinitis pigmentosa. *The British Journal of Ophthalmology*, *85*, 1046–1048. https://doi.org/10.1136/bjo.85.9.1046

Chatterjee, D., Eckert, C. E., Slavov, C., Saxena, K., Fürtig, B., Sanders, C. R., … Schwalbe, H. (2015). Influence of Arrestin on the Photodecay of Bovine Rhodopsin. *Angewandte Chemie - International Edition*, *54*(46), 13555–13560. https://doi.org/10.1002/anie.201505798

Chattopadhyay, A., Rao, B. D., & Jafurulla, M. (2015). Solubilization of G Protein-Coupled Receptors: A Convenient Strategy to Explore Lipid–Receptor Interaction. In *Methods in Enzymology* (1st ed., Vol. 557, pp. 117–134). Elsevier Inc. https://doi.org/10.1016/bs.mie.2015.01.001

Chen, Y., Palczewska, G., Mustafi, D., Golczak, M., Dong, Z., Sawada, O., … Palczewski, K. (2013). Systems pharmacology identifies drug targets for Stargardt disease-associated retinal degeneration. *The Journal of Clinical Investigation*, *123*(12), 5119–34. https://doi.org/10.1172/JCI69076

Cheng, C. L., & Molday, R. S. (2013). Interaction of 4.1G and cGMP-gated channels in rod photoreceptor outer segments. *Journal of Cell Science*, *126*(Pt 24), 5725–34. https://doi.org/10.1242/jcs.137679

Chinen, A., Hamaoka, T., Yamada, Y., & Kawamura, S. (2003). Gene

duplication and spectral diversification of cone visual pigments of zebrafish. *Genetics*, *163*(2), 663–675.

Coimbra, J. P., Bertelsen, M. F., & Manger, P. R. (2017). Retinal ganglion cell topography and spatial resolving power in the river hippopotamus (Hippopotamus amphibius). *Journal of Comparative Neurology*, *525*(11), 2499–2513. https://doi.org/10.1002/cne.24179

Concepcion, F., & Chen, J. (2010). Q344ter mutation causes mislocalization of rhodopsin molecules that are catalytically active: a mouse model of Q344ter-induced retinal degeneration. *PloS One*, *5*(6), e10904. https://doi.org/10.1371/journal.pone.0010904

de Grip, W. J., van de Laar, G. L., Daemen, F. J., & Bonting, S. L. (1973). Biochemical aspects of the visual process. 23. Sulfhydryl groups and rhodopsin photolysis. *Biochimica et Biophysica Acta*, *325*(2), 315–22. Retrieved from http://www.ncbi.nlm.nih.gov/pubmed/4796923

Deegan, J. F., & Jacobs, G. H. (1996). Spectral sensitivity and photopigments of a nocturnal prosimian, the bushbaby (Otolemur crassicaudatus). *American Journal of Primatology*, *40*(1), 55–66. https://doi.org/10.1002/(SICI)1098-2345(1996)40:1<55::AID-AJP4>3.0.CO;2-#

Dell'Orco, D., Schmidt, H., Mariani, S., & Fanelli, F. (2009). Network-level analysis of light adaptation in rod cells under normal and altered conditions. *Molecular BioSystems*, *5*(10), 1232. https://doi.org/10.1039/b908123b

Deretic, D. (2006). A role for rhodopsin in a signal transduction cascade that regulates membrane trafficking and photoreceptor polarity. *Vision*

Research, *46*(27), 4427–4433. https://doi.org/10.1016/j.visres.2006.07.028

Doan, T., Mendez, A., Detwiler, P. B., Chen, J., & Rieke, F. (2006). Multiple phosphorylation sites confer reproducibility of the rod's single-photon responses. *Science*, *313*(5786), 530–3. https://doi.org/10.1126/science.1126612

Douglas, R. H., & Jeffery, G. (2014). The spectral transmission of ocular media suggests ultraviolet sensitivity is widespread among mammals. *Proceedings of the Royal Society B: Biological Sciences*, *281*(1780), 20132995–20132995. https://doi.org/10.1098/rspb.2013.2995

Dungan, S. Z., & Chang, B. S. W. (2017). Epistatic interactions influence terrestrial–marine functional shifts in cetacean rhodopsin. *Proceedings of the Royal Society B: Biological Sciences*, *284*(1850), 20162743. https://doi.org/10.1098/rspb.2016.2743

Elgeti, M., Kazmin, R., Heck, M., Morizumi, T., Ritter, E., Scheerer, P., … Bartl, F. J. (2011). Conserved Tyr2235.58 plays different roles in the activation and G-protein interaction of rhodopsin. *Journal of the American Chemical Society*, *133*(18), 7159–7165. https://doi.org/10.1021/ja200545n

Elias, R. V, Sezate, S. S., Cao, W., & McGinnis, J. F. (2004). Temporal kinetics of the light/dark translocation and compartmentation of arrestin and alpha-transducin in mouse photoreceptor cells. *Molecular Vision*, *10*(May), 672–81. https://doi.org/v10/a81 [pii] ET - 2004/10/07

Emerling, C. A., Huynh, H. T., Nguyen, M. A., Meredith, R. W., & Springer, M. S. (2015). Spectral shifts of mammalian ultraviolet-sensitive

pigments (short wavelength-sensitive opsin 1) are associated with eye length and photic niche evolution. *Proceedings of the Royal Society B: Biological Sciences*, *282*(1819), 20151817. https://doi.org/10.1098/rspb.2015.1817

Emerling, C. A., & Springer, M. S. (2014). Eyes underground: Regression of visual protein networks in subterranean mammals. *Molecular Phylogenetics and Evolution*, *78*(1), 260–270. https://doi.org/10.1016/j.ympev.2014.05.016

Fan, J., Rohrer, B., Moiseyev, G., Ma, J.-X., & Crouch, R. K. (2003). Isorhodopsin rather than rhodopsin mediates rod function in RPE65 knock-out mice. *Proceedings of the National Academy of Sciences*, *100*(23), 13662–7. https://doi.org/10.1073/pnas.2234461100

Farrens, D. L., & Khorana, H. G. (1995). Structure and function in rhodopsin: Measurement of the rate of metarhodopsin II decay by fluorescence spectroscopy. *Journal of Biological Chemistry*, *270*(10), 5073–5076. https://doi.org/10.1073/pnas.91.16.7643

Fernández-Sampedro, M. A., Invergo, B. M., Ramon, E., Bertranpetit, J., & Garriga, P. (2016). Functional role of positively selected amino acid substitutions in mammalian rhodopsin evolution. *Scientific Reports*, *6*(1), 21570. https://doi.org/10.1038/srep21570

Field, G. D., & Sampath, A. P. (2017). Behavioural and physiological limits to vision in mammals. *Philosophical Transactions of the Royal Society of London B: Biological Sciences*, *372*(1717). https://doi.org/10.1098/rstb.2016.0072

Flock, T., Hauser, A. S., Lund, N., Gloriam, D. E., Balaji, S., & Babu, M. M.

(2017). Selectivity determinants of GPCR-G-protein binding. *Nature*, *545*(7654), 317–322. https://doi.org/10.1038/nature22070

Frederiksen, R., Nymark, S., Kolesnikov, A. V, Berry, J. D., Adler, L., Koutalos, Y., … Cornwall, M. C. (2016). Rhodopsin kinase and arrestin binding control the decay of photoactivated rhodopsin and dark adaptation of mouse rods. *The Journal of General Physiology*, *148*(1), 1–11. https://doi.org/10.1085/jgp.201511538

Fredriksson, R., & Schio, H. B. (2005). The Repertoire of G-Protein – Coupled Receptors in Fully. *Molecular Pharmacology*, *67*(5), 1414–1425. https://doi.org/10.1124/mol.104.009001.sequenced

Fu, Y., & Yau, K. W. (2007). Phototransduction in mouse rods and cones. *Pflugers Archiv European Journal of Physiology*, *454*(5), 805–819. https://doi.org/10.1007/s00424-006-0194-y

Funatogawa, C., Szundi, I., & Kliger, D. S. (2016). A Comparison between the Photoactivation Kinetics of Human and Bovine Rhodopsins. *Biochemistry*, *55*(50), 7005–7013. https://doi.org/10.1021/acs.biochem.6b00953

Gardner, J. C., Webb, T. R., Kanuga, N., Robson, A. G., Holder, G. E., Stockman, A., … Hardcastle, A. J. (2010). X-linked cone dystrophy caused by mutation of the red and green cone opsins. *American Journal of Human Genetics*, *87*(1), 26–39. https://doi.org/10.1016/j.ajhg.2010.05.019

Geng, Y., Schery, L. A., Sharma, R., Dubra, A., Ahmad, K., Libby, R. T., & Williams, D. R. (2011). Optical properties of the mouse eye. *Biomedical Optics Express*, *2*(4), 717. https://doi.org/10.1364/BOE.2.000717

Gerkema, M. P., Davies, W. I. L., Foster, R. G., Menaker, M., & Hut, R. A. (2013). The nocturnal bottleneck and the evolution of activity patterns in mammals. *Proceedings of the Royal Society B: Biological Sciences*, *280*(1765), 20130508. https://doi.org/10.1098/rspb.2013.0508

Goodchild, A. K., Ghosh, K. K., & Martin, P. R. (1996). Comparison of photoreceptor spatial density and ganglion cell morphology in the retina of human, macaque monkey, cat, and the marmoset Callithrix jacchus. *Journal of Comparative Neurology*, *366*(1), 55–75. https://doi.org/10.1002/(SICI)1096-9861(19960226)366:1<55::AID-CNE5>3.0.CO;2-J

Gould, E. (1978). Foraging Behavior of Malaysian Nectar-Feeding Bats. *Biotropica*, *10*(3), 184. https://doi.org/10.2307/2387904

Grant, R. A., Delaunay, M. G., & Haidarliu, S. (2017). Mystacial Whisker Layout and Musculature in the Guinea Pig (Cavia porcellus): A Social, Diurnal Mammal. *Anatomical Record*, *300*(3), 527–536. https://doi.org/10.1002/ar.23504

Gross, O. P., & Burns, M. E. (2010). Control of Rhodopsin's Active Lifetime by Arrestin-1 Expression in Mammalian Rods. *Journal of Neuroscience*, *30*(9), 3450–3457. https://doi.org/10.1523/JNEUROSCI.5391-09.2010

Gross, O. P., Pugh, E. N., & Burns, M. E. (2012). Calcium Feedback to cGMP Synthesis Strongly Attenuates Single-Photon Responses Driven by Long Rhodopsin Lifetimes. *Neuron*, *76*(2), 370–382. https://doi.org/10.1016/j.neuron.2012.07.029

Gunkel, M., Schöneberg, J., Alkhaldi, W., Irsen, S., Noé, F., Kaupp, U. B., … Al-Amoudi, A. (2015). Higher-order architecture of rhodopsin in intact

photoreceptors and its implication for phototransduction kinetics. *Structure*, *23*(4), 628–638. https://doi.org/10.1016/j.str.2015.01.015

Guo, Y., Sekharan, S., Liu, J., Batista, V. S., Tully, J. C., & Yan, E. C. Y. (2014). Unusual kinetics of thermal decay of dim-light photoreceptors in vertebrate vision. *Proceedings of the National Academy of Sciences*, *111*(29), 10438–10443. https://doi.org/10.1073/pnas.1410826111

Gurevich, V. V., & Gurevich, E. V. (2015). Arrestins; Critical Players in Trafficking of Many GPCRs. In G. Wu (Ed.), *Trafficking of GPCRs* (First edit, pp. 1–14). Academic Press. https://doi.org/10.1016/bs.pmbts.2015.02.010

Gurevich, V. V., Hanson, S. M., Song, X., Vishnivetskiy, S. A., & Gurevich, E. V. (2011). The functional cycle of visual arrestins in photoreceptor cells. *Progress in Retinal and Eye Research*, *30*(6), 405–430. https://doi.org/10.1016/j.preteyeres.2011.07.002

Hashimoto, H., Moritani, N., & Saito, T. R. (2004). Comparative study on circadian rhythms of body temperature, heart rate, and locomotor activity in three species hamsters. *Experimental Animals*, *53*(1), 43–6. Retrieved from http://www.ncbi.nlm.nih.gov/pubmed/14993740

Hauser, F. E., Ilves, K. L., Schott, R. K., Castiglione, G. M., López-Fernández, H., & Chang, B. S. W. (2017). Accelerated Evolution and Functional Divergence of the Dim Light Visual Pigment Accompanies Cichlid Colonization of Central America. *Molecular Biology and Evolution*, *34*(10), 2650–2664. https://doi.org/10.1093/molbev/msx192

Heck, M., Schädel, S. A., Maretzki, D., Bartl, F. J., Ritter, E., Palczewski, K., & Hofmann, K. P. (2003). Signaling states of rhodopsin. Formation of

the storage form, metarhodopsin III, from active metarhodopsin II. *Journal of Biological Chemistry*, *278*(5), 3162–3169. https://doi.org/10.1074/jbc.M209675200

Heesy, C. P., & Hall, M. I. (2010). The Nocturnal Bottleneck and the Evolution of Mammalian Vision. *Brain, Behavior and Evolution*, *75*(3), 195–203. https://doi.org/10.1159/000314278

Herrera-Hernández, M. G., Ramon, E., Lupala, C. S., Tena-Campos, M., Pérez, J. J., & Garriga, P. (2017). Flavonoid allosteric modulation of mutated visual rhodopsin associated with retinitis pigmentosa. *Scientific Reports*, *7*(1), 1–13. https://doi.org/10.1038/s41598-017-11391-x

Herrera Hernández, M. G. (2017). *Structural and functional effects of natural phenolic compounds on rhodopsin mutants associated with retinitis pigmentosa*. Universitat Politècnica de Catalunya. Retrieved from http://hdl.handle.net/2117/113677

Hofmann, K. P., Scheerer, P., Hildebrand, P. W., Choe, H. W., Park, J. H., Heck, M., & Ernst, O. P. (2009). A G protein-coupled receptor at work: the rhodopsin model. *Trends in Biochemical Sciences*, *34*(11), 540–552. https://doi.org/10.1016/j.tibs.2009.07.005

Hu, G. M., Mai, T. L., & Chen, C. M. (2017). Visualizing the GPCR Network: Classification and Evolution. *Scientific Reports*, *7*(1), 1–15. https://doi.org/10.1038/s41598-017-15707-9

Hunt, D. M., Carvalho, L. S., Cowing, J. A., & Davies, W. L. (2009). Evolution and spectral tuning of visual pigments in birds and mammals. *Philosophical Transactions of the Royal Society of London. Series B, Biological*, *364*(1531), 2941–2955.

https://doi.org/10.1098/rstb.2009.0044

Hunter, J., & Caro, T. (2008). Interspecific competition and predation in American carnivore families. *Ethology Ecology and Evolution*, *20*(4), 295–324. https://doi.org/10.1080/08927014.2008.9522514

Hurley, J. B., Spencer, M., & Niemi, G. A. (1998). Rhodopsin phosphorylation and its role in photoreceptor function. *Vision Research*, *38*(10), 1341–52. Retrieved from https://www.ncbi.nlm.nih.gov/pubmed/9667002

Imai, H., Kefalov, V., Sakurai, K., Chisaka, O., Ueda, Y., Onishi, A., … Shichida, Y. (2007). Molecular Properties of Rhodopsin and Rod Function. *Journal of Biological Chemistry*, *282*(9), 6677–6684. https://doi.org/10.1074/jbc.M610086200

Imamoto, Y., & Shichida, Y. (2014). Cone visual pigments. *Biochimica et Biophysica Acta - Bioenergetics*, *1837*(5), 664–673. https://doi.org/10.1016/j.bbabio.2013.08.009

Invergo, B. M., Dell'Orco, D., Montanucci, L., Koch, K., & Bertranpetit, J. (2014). A comprehensive model of the phototransduction cascade in mouse rod cells. *Molecular BioSystems*, *10*(6), 1481–9. https://doi.org/10.1039/c3mb70584f

Invergo, B. M., Montanucci, L., & Bertranpetit, J. (2015). Dynamic sensitivity and nonlinear interactions influence the system-level evolutionary patterns of phototransduction proteins. *Proceedings of the Royal Society B: Biological Sciences*, *282*(1820), 20152215. https://doi.org/10.1098/rspb.2015.2215

Jacobs, G. H., Calderone, J. B., Fenwick, J. a, Krogh, K., & Williams, G. a. (2003). Visual adaptations in a diurnal rodent, Octodon degus. *Journal*

of Comparative Physiology. A, Neuroethology, Sensory, Neural, and Behavioral Physiology, *189*(5), 347–61. https://doi.org/10.1007/s00359-003-0408-0

Jastrzebska, B. (2015). *Rhodopsin Methods and Protocols*. (B. Jastrzebska, Ed.) (Vol. 1271). New York, NY: Springer New York. https://doi.org/10.1007/978-1-4939-2330-4

Jastrzebska, B., Maeda, T., Zhu, L., Fotiadis, D., Filipek, S., Engel, A., … Palczewski, K. (2004). Functional characterization of rhodopsin monomers and dimers in detergents. *Journal of Biological Chemistry*, *279*(52), 54663–54675. https://doi.org/10.1074/jbc.M408691200

Jastrzebska, B., Orban, T., Golczak, M., Engel, A., & Palczewski, K. (2013). Asymmetry of the rhodopsin dimer in complex with transducin. *FASEB Journal*, *27*(4), 1572–1584. https://doi.org/10.1096/fj.12-225383

Karnik, S. S., & Khorana, H. G. (1990). Assembly of functional rhodopsin requires a disulfide bond between cysteine residues 110 and 187. *Journal of Biological Chemistry*, *265*(29), 17520–17524.

Katagiri, S., Hayashi, T., Akahori, M., Itabashi, T., Nishino, J., Yoshitake, K., … Iwata, T. (2014). RHO Mutations (p.W126L and p.A346P) in Two Japanese Families with Autosomal Dominant Retinitis Pigmentosa. *Journal of Ophthalmology*, *2014*, 1–10. https://doi.org/10.1155/2014/210947

Katritch, V., Cherezov, V., & Stevens, R. C. (2013). Structure-Function of the G Protein–Coupled Receptor Superfamily. *Annual Review of Pharmacology and Toxicology*, *53*(1), 531–556. https://doi.org/10.1146/annurev-pharmtox-032112-135923

Kaushal, S., Ridge, K. D., & Khorana, H. G. (1994). Structure and function in rhodopsin: the role of asparagine-linked glycosylation. *Proceedings of the National Academy of Sciences*, *91*(9), 4024–8. https://doi.org/10.1073/pnas.91.9.4024

Kawamura, S., & Yokoyama, S. (1998). Functional characterization of visual and nonvisual pigments of American chameleon (Anolis carolinensis). *Vision Research*, *38*(1), 37–44. https://doi.org/10.1016/S0042-6989(97)00160-0

Kazmin, R., Rose, A., Szczepek, M., Elgeti, M., Ritter, E., Piechnick, R., … Bartl, F. J. (2015). The activation pathway of human rhodopsin in comparison to bovine rhodopsin. *Journal of Biological Chemistry*, *290*(33), 20117–20127. https://doi.org/10.1074/jbc.M115.652172

Kefalov, V. J. (2012). Rod and cone visual pigments and phototransduction through pharmacological, genetic, and physiological approaches. *Journal of Biological Chemistry*, *287*(3), 1635–1641. https://doi.org/10.1074/jbc.R111.303008

Kelling, A. S., Snyder, R. J., Marr, M. J., Bloomsmith, M. a, Gardner, W., & Maple, T. L. (2006). Color vision in the giant panda (Ailuropoda melanoleuca). *Learning & Behavior: A Psychonomic Society Publication*, *34*(2), 154–161.

Kim, J. W., Yang, H. J., Oel, A. P., Brooks, M. J., Jia, L., Plachetzki, D. C., … Swaroop, A. (2016). Recruitment of Rod Photoreceptors from Short-Wavelength-Sensitive Cones during the Evolution of Nocturnal Vision in Mammals. *Developmental Cell*, *37*(6), 520–532. https://doi.org/10.1016/j.devcel.2016.05.023

Kim, M., Hanson, S. M., Vishnivetskiy, S. A., Song, X., Cleghorn, W. M., Hubbell, W. L., & Gurevich, V. V. (2011). Robust Self-Association Is a Common Feature of Mammalian Visual Arrestin-1. *Biochemistry*, *50*(12), 2235–2242. https://doi.org/10.1021/bi1018607

Kojima, D., Oura, T., Hisatomi, O., Tokunaga, F., Fukada, Y., Yoshizawa, T., & Shichida, Y. (1996). Molecular properties of chimerical mutants of gecko blue and bovine rhodopsin. *Biochemistry*, *35*(8), 2625–9. https://doi.org/10.1021/bi9511548

Kong, Y., & Karplus, M. (2007). The Signaling Pathway of Rhodopsin. *Structure*, *15*(5), 611–623. https://doi.org/10.1016/j.str.2007.04.002

Kott, O., Němec, P., Fremlová, A., Mazoch, V., & Šumbera, R. (2016). Behavioural Tests Reveal Severe Visual Deficits in the Strictly Subterranean African Mole-Rats (Bathyergidae) but Efficient Vision in the Fossorial Rodent Coruro (Spalacopus cyanus, Octodontidae). *Ethology*, *122*(8), 682–694. https://doi.org/10.1111/eth.12515

Krebs, M. P., Holden, D. C., Joshi, P., Clark, C. L., Lee, A. H., & Kaushal, S. (2010). Molecular Mechanisms of Rhodopsin Retinitis Pigmentosa and the Efficacy of Pharmacological Rescue. *Journal of Molecular Biology*, *395*(5), 1063–1078. https://doi.org/10.1016/j.jmb.2009.11.015

Kuwayama, S., Imai, H., Morizumi, T., & Shichida, Y. (2005). Amino acid residues responsible for the meta-III decay rates in rod and cone visual pigments. *Biochemistry*, *44*(6), 2208–15. https://doi.org/10.1021/bi047994g

Lamb, T. D. (2013). Evolution of phototransduction, vertebrate photoreceptors and retina. *Progress in Retinal and Eye Research*, *36*, 52–

119. https://doi.org/10.1016/j.preteyeres.2013.06.001

Lamb, T. D., & Pugh, E. N. (2004). Dark adaptation and the retinoid cycle of vision. *Progress in Retinal and Eye Research*, *23*(3), 307–380. https://doi.org/10.1016/j.preteyeres.2004.03.001

Langen, R., Cai, K., Altenbach, C., Gobind Khorana, H., & Hubbell, W. L. (1999). Structural features of the C-terminal domain of bovine rhodopsin: A site-directed spin-labeling study. *Biochemistry*, *38*(25), 7918–7924. https://doi.org/10.1021/bi990010g

Levenson, D. H., Fernandez-duque, E., Evans, S., & Jacobs, G. H. (2007). Mutational changes in S-cone opsin genes common to both nocturnal and cathemeralAotus monkeys. *American Journal of Primatology*, *69*(7), 757–765. https://doi.org/10.1002/ajp.20402

Lewis, J. W., Van Kuijk, F. J. G. M., Carruthers, J. A., & Kliger, D. S. (1997). Metarhodopsin III formation and decay kinetics: Comparison of bovine and human rhodopsin. *Vision Research*, *37*(1), 1–8. https://doi.org/10.1016/S0042-6989(96)00138-1

Li, J., Zhang, Y., Cai, X., Xia, Q., Chen, J., Liao, Y., … Wu, Y. (2016). All-trans-retinal dimer formation alleviates the cytotoxicity of all-trans-retinal in human retinal pigment epithelial cells. *Toxicology*, *371*, 41–48. https://doi.org/10.1016/j.tox.2016.10.005

Liu, M. Y., Liu, J., Mehrotra, D., Liu, Y., Guo, Y., Baldera-Aguayo, P. A., … Yan, E. C. Y. (2013). Thermal stability of rhodopsin and progression of retinitis pigmentosa: Comparison of S186W and D190N rhodopsin mutants. *Journal of Biological Chemistry*, *288*(24), 17698–17712. https://doi.org/10.1074/jbc.M112.397257

Loewen, C. J. R., Moritz, O. L., & Molday, R. S. (2001). Molecular Characterization of Peripherin-2 and Rom-1 Mutants Responsible for Digenic Retinitis Pigmentosa. *Journal of Biological Chemistry*, *276*(25), 22388–22396. https://doi.org/10.1074/jbc.M011710200

Lohse, M. J., & Hoffmann, C. (2014). *Arrestins - Pharmacology and Therapeutic Potential*. (V. V. Gurevich, Ed.) (Vol. 219). Berlin, Heidelberg: Springer Berlin Heidelberg. https://doi.org/10.1007/978-3-642-41199-1

Lomonosova, E., Kolesnikov, A. V., Kefalov, V. J., & Kisselev, O. G. (2012). Signaling states of rhodopsin in rod disk membranes lacking transducin βγ-Complex. *Investigative Ophthalmology and Visual Science*, *53*(3), 1225–1233. https://doi.org/10.1167/iovs.11-9350

Lovegrove, B. G., & Génin, F. (2008). Torpor and hibernation in a basal placental mammal, the Lesser Hedgehog Tenrec Echinops telfairi. *Journal of Comparative Physiology B: Biochemical, Systemic, and Environmental Physiology*, *178*(6), 691–698. https://doi.org/10.1007/s00360-008-0257-9

Luk, H. L., Bhattacharyya, N., Montisci, F., Morrow, J. M., Melaccio, F., Wada, A., … Olivucci, M. (2016). Modulation of thermal noise and spectral sensitivity in Lake Baikal cottoid fish rhodopsins. *Scientific Reports*, *6*(October), 38425. https://doi.org/10.1038/srep38425

Luo, D.-G., Yue, W. W. S., Ala-Laurila, P., & Yau, K.-W. (2011). Activation of Visual Pigments by Light and Heat. *Science*, *332*(6035), 1307–1312. https://doi.org/10.1126/science.1200172

Maeda, T., Golczak, M., & Maeda, A. (2012). Retinal photodamage mediated

by all-trans-retinal. *Photochemistry and Photobiology*, *88*(6), 1309–1319. https://doi.org/10.1111/j.1751-1097.2012.01143.x

Mahalingam, M., & Vogel, R. (2006). The all-trans-15-syn-retinal chromophore of metarhodopsin III is a partial agonist and not an inverse agonist. *Biochemistry*, *45*(51), 15624–15632. https://doi.org/10.1021/bi061970n

Maor, R., Dayan, T., Ferguson-Gow, H., & Jones, K. E. (2017). Temporal niche expansion in mammals from a nocturnal ancestor after dinosaur extinction. *Nature Ecology and Evolution*, *1*(12), 1889–1895. https://doi.org/10.1038/s41559-017-0366-5

McKeown, A. S., Pitale, P. M., & Kraft, T. W. (2016). Signalling beyond photon absorption: extracellular retinoids and growth factors modulate rod photoreceptor sensitivity. *The Journal of Physiology*, *594*(7), 1841–1854. https://doi.org/10.1113/JP271650

Merrill, S. B., & David Mech, L. (2003). The usefulness of GPS telemetry to study wolf circadian and social activity. *Wildlife Society Bulletin*, *31*(4), 947–960. https://doi.org/10.2307/3784439

Milic, D., & Veprintsev, D. B. (2015). Large-scale production and protein engineering of G protein-coupled receptors for structural studies. *Frontiers in Pharmacology*, *6*(MAR), 1–24. https://doi.org/10.3389/fphar.2015.00066

Molday, R. S. (1998). Photoreceptor membrane proteins, phototransduction, and retinal degenerative diseases: The Friedenwald Lecture. *Investigative Ophthalmology and Visual Science*, *39*(13), 2493–2513.

Montanucci, L., Laayouni, H., Dall'Olio, G. M., & Bertranpetit, J. (2011).

Molecular evolution and network-level analysis of the N-glycosylation metabolic pathway across primates. *Molecular Biology and Evolution*, *28*(1), 813–823. https://doi.org/10.1093/molbev/msq259

Morrow, J. M., Castiglione, G. M., Dungan, S. Z., Tang, P. L., Bhattacharyya, N., Hauser, F. E., & Chang, B. S. W. (2017). An experimental comparison of human and bovine rhodopsin provides insight into the molecular basis of retinal disease. *FEBS Letters*, *591*(12), 1720–1731. https://doi.org/10.1002/1873-3468.12637

Morrow, J. M., & Chang, B. S. W. (2015). Comparative Mutagenesis Studies of Retinal Release in Light-Activated Zebrafish Rhodopsin Using Fluorescence Spectroscopy. *Biochemistry*, *54*(29), 4507–4518. https://doi.org/10.1021/bi501377b

Morshedian, A., & Fain, G. L. (2017). Light adaptation and the evolution of vertebrate photoreceptors. *The Journal of Physiology*, *595*(14), 4947–4960. https://doi.org/10.1113/JP274211

Murray, A. R., Fliesler, S. J., & Al-Ubaidi, M. R. (2009). Rhodopsin: the functional significance of asn-linked glycosylation and other post-translational modifications. *Ophthalmic Genetics*, *30*(3), 109–20. https://doi.org/10.1080/13816810902962405

Nakatsuma, A., Yamashita, T., Sasaki, K., Kawanabe, A., Inoue, K., Furutani, Y., … Kandori, H. (2011). Chimeric microbial rhodopsins containing the third cytoplasmic loop of bovine rhodopsin. *Biophysical Journal*, *100*(8), 1874–1882. https://doi.org/10.1016/j.bpj.2011.02.054

Nguyen, O. N. P., Böhm, S., Gießl, A., Butz, E. S., Wolfrum, U., Brandstätter, J. H., … Becirovic, E. (2016). Peripherin-2 differentially interacts with

cone opsins in outer segments of cone photoreceptors. *Human Molecular Genetics*, *25*(12), ddw103. https://doi.org/10.1093/hmg/ddw103

Nielsen, R., & Yang, Z. (1998). Likelihood models for detecting positively selected amino acid sites and applications to the HIV-1 envelope gene. *Genetics*, *148*(3), 929–936.

Noorwez, S. M., Malhotra, R., McDowell, J. H., Smith, K. A., Krebs, M. P., & Kaushal, S. (2004). Retinoids Assist the Cellular Folding of the Autosomal Dominant Retinitis Pigmentosa Opsin Mutant P23H. *Journal of Biological Chemistry*, *279*(16), 16278–16284. https://doi.org/10.1074/jbc.M312101200

Nymark, S., Frederiksen, R., Woodruff, M. L., Cornwall, M. C., & Fain, G. L. (2012). Bleaching of mouse rods: microspectrophotometry and suction-electrode recording. *The Journal of Physiology*, *590*(10), 2353–2364. https://doi.org/10.1113/jphysiol.2012.228627

Okano, K., Maeda, A., Chen, Y., Chauhan, V., Tang, J., Palczewska, G., … Maeda, T. (2012). Retinal cone and rod photoreceptor cells exhibit differential susceptibility to light-induced damage. *Journal of Neurochemistry*, *121*(1), 146–156. https://doi.org/10.1111/j.1471-4159.2012.07647.x

Opefi, C. A., South, K., Reynolds, C. A., Smith, S. O., & Reeves, P. J. (2013). Retinitis pigmentosa mutants provide insight into the role of the N-terminal cap in rhodopsin folding, structure, and function. *Journal of Biological Chemistry*, *288*(47), 33912–33926. https://doi.org/10.1074/jbc.M113.483032

Organisciak, D. T., & Vaughan, D. K. (2010). Retinal light damage: Mechanisms and protection. *Progress in Retinal and Eye Research*, *29*(2), 113–134. https://doi.org/10.1016/j.preteyeres.2009.11.004

Owen, T. S., Salom, D., Sun, W., & Palczewski, K. (2018). Increasing the Stability of Recombinant Human Green Cone Pigment. *Biochemistry*, acs.biochem.7b01118. https://doi.org/10.1021/acs.biochem.7b01118

Palczewski, K. (2006). G Protein–Coupled Receptor Rhodopsin. *Annual Review of Biochemistry*, *75*(1), 743–767. https://doi.org/10.1146/annurev.biochem.75.103004.142743

Palczewski, K., Kumasaka, T., Hori, T., Behnke, C. A., Motoshima, H., Fox, B. A., … Miyano, M. (2000). Crystal structure of rhodopsin: A G protein-coupled receptor. *Science*, *289*(5480), 739–45. Retrieved from http://www.sciencemag.org/cgi/doi/10.1126/science.289.5480.739

Parmley, S. (2014). GPCRs' grand plans. *Science-Business EXchange*, *7*(46), 1–3. https://doi.org/10.1038/scibx.2014.1337

Pearring, J. N., Spencer, W. J., Lieu, E. C., & Arshavsky, V. Y. (2015). Guanylate cyclase 1 relies on rhodopsin for intracellular stability and ciliary trafficking. *ELife*, *4*(November2015). https://doi.org/10.7554/eLife.12058

Perusek, L., & Maeda, T. (2013). Vitamin a derivatives as treatment options for retinal degenerative diseases. *Nutrients*, *5*(7), 2466–2666. https://doi.org/10.1016/j.exer.2013.02.003

Piechnick, R., Heck, M., & Sommer, M. E. (2011). Alkylated hydroxylamine derivatives eliminate peripheral retinylidene schiff bases but cannot enter the retinal binding pocket of light-activated rhodopsin.

Biochemistry, *50*(33), 7168–7176. https://doi.org/10.1021/bi200675y

Piechnick, R., Ritter, E., Hildebrand, P. W., Ernst, O. P., Scheerer, P., Hofmann, K. P., & Heck, M. (2012). Effect of channel mutations on the uptake and release of the retinal ligand in opsin. *Proceedings of the National Academy of Sciences*, *109*(14), 5247–5252. https://doi.org/10.1073/pnas.1117268109

Poetsch, A., Molday, L. L., & Molday, R. S. (2001). The cGMP-gated Channel and Related Glutamic Acid-rich Proteins Interact with Peripherin-2 at the Rim Region of Rod Photoreceptor Disc Membranes. *Journal of Biological Chemistry*, *276*(51), 48009–48016. https://doi.org/10.1074/jbc.M108941200

Ramon, E., Cordomi, A., Aguila, M., Srinivasan, S., Dong, X., Moore, A. T., … Garriga, P. (2014). Differential Light-induced Responses in Sectorial Inherited Retinal Degeneration. *Journal of Biological Chemistry*, *289*(52), 35918–35928. https://doi.org/10.1074/jbc.M114.609958

Ramon, E., Marron, J., Del Valle, L., Bosch, L., Andrés, A., Manyosa, J., & Garriga, P. (2003). Effect of dodecyl maltoside detergent on rhodopsin stability and function. *Vision Research*, *43*(28), 3055–3061. https://doi.org/10.1016/j.visres.2003.08.009

Reeves, P. J., Thurmond, R. L., & Khorana, H. G. (1996). Structure and function in rhodopsin: high level expression of a synthetic bovine opsin gene and its mutants in stable mammalian cell lines. *Proceedings of the National Academy of Sciences*, *93*(21), 11487–11492. https://doi.org/10.1073/pnas.93.21.11487

Riddles, P. W., Blakeley, R. L., & Zerner, B. (1983). Reassessment of Ellman's

reagent. *Methods in Enzymology*, *91*, 49–60. Retrieved from http://www.ncbi.nlm.nih.gov/pubmed/6855597

Ritter, E., Elgeti, M., Hofmann, K. P., & Bartl, F. J. (2007). Deactivation and proton transfer in light-induced metarhodopsin II/metarhodopsin III conversion: A time-resolved fourier transform infrared spectroscopic study. *Journal of Biological Chemistry*, *282*(14), 10720–10730. https://doi.org/10.1074/jbc.M610658200

Ritter, E., Zimmermann, K., Heck, M., Hofmann, K. P., & Bartl, F. J. (2004). Transition of Rhodopsin into the Active Metarhodopsin II State Opens a New Light-induced Pathway Linked to Schiff Base Isomerization. *Journal of Biological Chemistry*, *279*(46), 48102–48111. https://doi.org/10.1074/jbc.M406857200

Robinson, P. R. (2000). Assays for Detection of Constitutively Active Opsins. In K. Palczewski, John Abelson, & Melvin Simon (Eds.), *Vertebrate Phototransduction and the Visual Cycle, Part A, Volume 315* (Vol. 315, pp. 207–218).

Ross, C. F., Hall, M. I., & Heesy, C. P. (2007). Were Basal Primates Nocturnal? Evidence From Eye and Orbit Shape. In *PRIMATE ORIGINS: Adaptations and Evolution* (pp. 233–256). Boston, MA: Springer US. https://doi.org/10.1007/978-0-387-33507-0_7

Rozanowska, M. B. (2012). Light-induced damage to the retina: Current understanding of the mechanisms and unresolved questions: A symposium-in-print. *Photochemistry and Photobiology*, *88*(6), 1303–1308. https://doi.org/10.1111/j.1751-1097.2012.01240.x

Saïdi, T., Mbarek, S., Chaouacha-Chekir, R. Ben, & Hicks, D. (2011). Diurnal

rodents as animal models of human central vision: Characterisation of the retina of the sand rat Psammomys obsesus. *Graefe's Archive for Clinical and Experimental Ophthalmology*, *249*(7), 1029–1037. https://doi.org/10.1007/s00417-011-1641-9

Salesse, C. (2017). Physiologie du signal visuel rétinien : de la phototransduction jusqu'au cycle visuel. *Journal Francais d'Ophtalmologie*, *40*(3), 239–250. https://doi.org/10.1016/j.jfo.2016.12.006

Salom, D., Lodowski, D. T., Stenkamp, R. E., Trong, I. L., Golczak, M., Jastrzebska, B., … Palczewski, K. (2006). Crystal structure of a photoactivated deprotonated intermediate of rhodopsin. *Proceedings of the National Academy of Sciences*, *103*(44), 16123–16128. https://doi.org/10.1073/pnas.0608022103

Santini, L., Rojas, D., & Donati, G. (2015). Evolving through day and night: Origin and diversification of activity pattern in modern primates. *Behavioral Ecology*, *26*(3), 789–796. https://doi.org/10.1093/beheco/arv012

Schafer, C. T., Fay, J. F., Janz, J. M., & Farrens, D. L. (2016). Decay of an active GPCR: Conformational dynamics govern agonist rebinding and persistence of an active, yet empty, receptor state. *Proceedings of the National Academy of Sciences*, *113*(42), 11961–11966. https://doi.org/10.1073/pnas.1606347113

Scheerer, P., Park, J. H., Hildebrand, P. W., Kim, Y. J., Krauss, N., Choe, H., … Ernst, O. P. (2008). Crystal structure of opsin in its G-protein-interacting conformation. *Nature*, *455*(7212), 497–502. https://doi.org/10.1038/nature07330

Schmidt-Nielsen, K., Dawson, T. J., & Crawford, E. C. (1966). Temperature regulation in the echidna (Tachyglossus aculeatus). *Journal of Cellular Physiology*, *67*(1), 63–71. https://doi.org/10.1002/jcp.1040670108

Shichida, Y., & Matsuyama, T. (2009). Evolution of opsins and phototransduction. *Philosophical Transactions of the Royal Society of London. Series B, Biological Sciences*, *364*(1531), 2881–2895. https://doi.org/10.1098/rstb.2009.0051

Sinha, A., Jones Brunette, A. M., Fay, J. F., Schafer, C. T., & Farrens, D. L. (2014). Rhodopsin TM6 Can Interact with Two Separate and Distinct Sites on Arrestin: Evidence for Structural Plasticity and Multiple Docking Modes in Arrestin–Rhodopsin Binding. *Biochemistry*, *53*(20), 3294–3307. https://doi.org/10.1021/bi401534y

Smale, L., Nunez, A. A., & Schwartz, M. D. (2008). Rhythms in a diurnal brain. *Biological Rhythm Research*, *39*(3), 305–318. https://doi.org/10.1080/09291010701682666

Solovei, I., Kreysing, M., Lanctôt, C., Kösem, S., Peichl, L., Cremer, T., … Joffe, B. (2009). Nuclear Architecture of Rod Photoreceptor Cells Adapts to Vision in Mammalian Evolution. *Cell*, *137*(2), 356–368. https://doi.org/10.1016/j.cell.2009.01.052

Sommer, M. E., & Farrens, D. L. (2006). Arrestin can act as a regulator of rhodopsin photochemistry. *Vision Research*, *46*(27), 4532–4546. https://doi.org/10.1016/j.visres.2006.08.031

Sommer, M. E., Hofmann, K. P., & Heck, M. (2012). Distinct loops in arrestin differentially regulate ligand binding within the GPCR opsin. *Nature Communications*, *3*(1), 995. https://doi.org/10.1038/ncomms2000

Sommer, M. E., Hofmann, K. P., & Heck, M. (2014). Not Just Signal Shutoff: The Protective Role of Arrestin-1 in Rod Cells. In V. V. Gurevich (Ed.), *Arrestins - Pharmacology and Therapeutic Potential* (Vol. 219, pp. 101–116). Springer. https://doi.org/10.1007/978-3-642-41199-1

Srinivasan, S. (2015). *Stability and ligand binding properties of human cone visual pigments*. Universitat Politècnica de Catalunya. Retrieved from http://hdl.handle.net/2117/95839

Srinivasan, S., Cordomí, A., Ramon, E., & Garriga, P. (2016). Beyond spectral tuning: Human cone visual pigments adopt different transient conformations for chromophore regeneration. *Cellular and Molecular Life Sciences*, *73*(6), 1253–1263. https://doi.org/10.1007/s00018-015-2043-7

Srinivasan, S., Fernández-Sampedro, M. A., Ramon, E., & Garriga, P. (2017). Structural and functional alterations associated with deutan N94K and R330Q mutations of green cone opsin. *Biochimica et Biophysica Acta (BBA) - Molecular Basis of Disease*, *1863*(7), 1840–1847. https://doi.org/10.1016/j.bbadis.2017.05.006

Srinivasan, S., Ramon, E., Cordomí, A., & Garriga, P. (2014). Binding specificity of retinal analogs to photoactivated visual pigments suggest mechanism for fine-tuning GPCR-ligand interactions. *Chemistry and Biology*, *21*(3), 369–378. https://doi.org/10.1016/j.chembiol.2014.01.006

Standfuss, J., Xie, G., Edwards, P. C., Burghammer, M., Oprian, D. D., & Schertler, G. F. X. (2007). Crystal Structure of a Thermally Stable Rhodopsin Mutant. *Journal of Molecular Biology*, *372*(5), 1179–1188. https://doi.org/10.1016/j.jmb.2007.03.007

Stehle, J., Silvers, R., Werner, K., Chatterjee, D., Gande, S., Scholz, F., … Schwalbe, H. (2014). Characterization of the simultaneous decay kinetics of metarhodopsin states II and III in rhodopsin by solution-state NMR spectroscopy. *Angewandte Chemie - International Edition*, *53*(8), 2078–2084. https://doi.org/10.1002/anie.201309581

Stiles, M., Moiseyev, G. P., Budda, M. L., Linens, A., Brush, R. S., Qi, H., … Mandal, N. A. (2015). PBN (phenyl-N-tert-butylnitrone)-derivatives are effective in slowing the visual cycle and rhodopsin regeneration and in protecting the retina from light-induced damage. *PLoS ONE*, *10*(12), 1–17. https://doi.org/10.1371/journal.pone.0145305

Sugawara, T., Imai, H., Nikaido, M., Imamoto, Y., & Okada, N. (2010). Vertebrate Rhodopsin Adaptation to Dim Light via Rapid Meta-II Intermediate Formation. *Molecular Biology and Evolution*, *27*(3), 506–519. https://doi.org/10.1093/molbev/msp252

Sung, C. H., Schneider, B. G., Agarwal, N., Papermaster, D. S., & Nathans, J. (1991). Functional heterogeneity of mutant rhodopsins responsible for autosomal dominant retinitis pigmentosa. *Proceedings of the National Academy of Sciences*, *88*(19), 8840–4. https://doi.org/10.1073/pnas.88.19.8840

Szczepek, M., Beyrière, F., Hofmann, K. P., Elgeti, M., Kazmin, R., Rose, A., … Scheerer, P. (2014). Crystal structure of a common GPCR-binding interface for G protein and arrestin. *Nature Communications*, *5*(May), 4801. https://doi.org/10.1038/ncomms5801

Tam, B. M., & Moritz, O. L. (2009). The role of rhodopsin glycosylation in protein folding, trafficking, and light-sensitive retinal degeneration. *The Journal of Neuroscience: The Official Journal of the Society for*

Neuroscience, *29*(48), 15145–54. https://doi.org/10.1523/JNEUROSCI.4259-09.2009

Tam, B. M., Noorwez, S. M., Kaushal, S., Kono, M., & Moritz, O. L. (2014). Photoactivation-Induced Instability of Rhodopsin Mutants T4K and T17M in Rod Outer Segments Underlies Retinal Degeneration in X. laevis Transgenic Models of Retinitis Pigmentosa. *The Journal of Neuroscience: The Official Journal of the Society for Neuroscience*, *34*(40), 13336–13348. https://doi.org/10.1523/JNEUROSCI.1655-14.2014

Tan, Y., Yoder, A. D., Yamashita, N., & Li, W.-H. (2005). Evidence from opsin genes rejects nocturnality in ancestral primates. *Proceedings of the National Academy of Sciences*, *102*(41), 14712–6. https://doi.org/10.1073/pnas.0507042102

Terakita, A., Koyanagi, M., Tsukamoto, H., Yamashita, T., Miyata, T., & Shichida, Y. (2004). Counterion displacement in the molecular evolution of the rhodopsin family. *Nature Structural & Molecular Biology*, *11*(3), 284–289. https://doi.org/10.1038/nsmb731

Terakita, A., Yamashita, T., Nimbari, N., Kojima, D., & Shichida, Y. (2002). Functional interaction between bovine rhodopsin and G protein transducin. *Journal of Biological Chemistry*, *277*(1), 40–46. https://doi.org/10.1074/jbc.M104960200

Tesmer, J. J. G. (2010). The quest to understand heterotrimeric G protein signaling. *Nature Structural & Molecular Biology*, *17*(6), 650–652. https://doi.org/10.1038/nsmb0610-650

Tian, H., Sakmar, T. P., & Huber, T. (2017). Measurement of Slow Spontaneous Release of 11-cis-Retinal from Rhodopsin. *Biophysical*

Journal, *112*(1), 153–161. https://doi.org/10.1016/j.bpj.2016.12.005

Tobin, A. (2008). G-protein-coupled receptor phosphorylation: where, when and by whom. *British Journal of Pharmacology*, *153*(S1), S167–S176. https://doi.org/10.1038/sj.bjp.0707662

Toledo, D., Ramon, E., Aguila, M., Cordomi, A., Perez, J. J., Mendes, H. F., … Garriga, P. (2011). Molecular Mechanisms of Disease for Mutations at Gly-90 in Rhodopsin. *Journal of Biological Chemistry*, *286*(46), 39993–40001. https://doi.org/10.1074/jbc.M110.201517

Tritarelli, A., Oricchio, E., Ciciarello, M., Mangiacasale, R., Palena, A., Lavia, P., … Cundari, E. (2004). p53 Localization at Centrosomes during Mitosis and Postmitotic Checkpoint Are ATM-dependent and Require Serine 15 Phosphorylation. *Molecular Biology of the Cell*, *15*(April), 3751–3737. https://doi.org/10.1091/mbc.E03

Troilo, D., Rowland, H. C., & Judge, S. J. (1993). Visual optics and retinal cone topography in the common marmoset (Callithrix jacchus). *Vision Research*, *33*(10), 1301–1310. https://doi.org/10.1016/0042-6989(93)90038-X

Ueyama, H., Kuwayama, S., Imai, H., Tanabe, S., Oda, S., Nishida, Y., … Yamade, S. (2002). Novel missense mutations in red/green opsin genes in congenital color-vision deficiencies. *Biochemical and Biophysical Research Communications*, *294*(2), 205–209. https://doi.org/10.1016/S0006-291X(02)00458-8

Uhl, P. B., Amann, B., Hauck, S. M., & Deeg, C. A. (2015). Novel localization of peripherin 2, the photoreceptor-specific retinal degeneration slow protein, in retinal pigment epithelium. *International Journal of*

Molecular Sciences, *16*(2), 2678–2692. https://doi.org/10.3390/ijms16022678

van Hazel, I., Dungan, S. Z., Hauser, F. E., Morrow, J. M., Endler, J. A., & Chang, B. S. W. (2016). A comparative study of rhodopsin function in the great bowerbird (Ptilonorhynchus nuchalis): Spectral tuning and light-activated kinetics. *Protein Science*, (March), 1308–1318. https://doi.org/10.1002/pro.2902

Vega-Zuniga, T., Medina, F. S., Marín, G., Letelier, J. C., Palacios, A. G., Němec, P., … Mpodozis, J. (2017). Selective binocular vision loss in two subterranean caviomorph rodents: Spalacopus cyanus and Ctenomys talarum. *Scientific Reports*, *7*(February), 41704. https://doi.org/10.1038/srep41704

Veilleux, C. C., Louis, E. E., & Bolnick, D. A. (2013). Nocturnal light environments influence color vision and signatures of selection on the OPN1SW opsin gene in nocturnal lemurs. *Molecular Biology and Evolution*, *30*(6), 1420–1437. https://doi.org/10.1093/molbev/mst058

Venkatakrishnan, A. J., Deupi, X., Lebon, G., Tate, C. G., Schertler, G. F., & Babu, M. M. (2013). Molecular signatures of G-protein-coupled receptors. *Nature*, *494*(7436), 185–194. https://doi.org/10.1038/nature11896

Wang, H., Cui, X., Gu, Q., Chen, Y., Zhou, J., Kuang, Y., … Xu, X. (2012). Retinol dehydrogenase 13 protects the mouse retina from acute light damage. *Molecular Vision*, *18*(100), 1021–30. Retrieved from http://www.pubmedcentral.nih.gov/articlerender.fcgi?artid=3351414&tool=pmcentrez&rendertype=abstract

Wang, T., & Duan, Y. (2011). Retinal release from opsin in molecular dynamics simulations. *Journal of Molecular Recognition*, *24*(2), 350–358. https://doi.org/10.1002/jmr.1087

Warren, J. T., & Mysterud, I. (1978). Summer habitat use and activity patterns of domestic sheep on coniferous forest range in southern Norway. *Journal Of Range Management*, *44*(Lystad), 2–6.

Wikler, K. C., & Rakic, P. (1990). Distribution of photoreceptor subtypes in the retina of diurnal and nocturnal primates. *The Journal of Neuroscience: The Official Journal of the Society for Neuroscience*, *10*(10), 3390–401. Retrieved from http://www.ncbi.nlm.nih.gov/pubmed/2145402

Wiseman, R. L., Powers, E. T., Buxbaum, J. N., Kelly, J. W., & Balch, W. E. (2007). An Adaptable Standard for Protein Export from the Endoplasmic Reticulum. *Cell*, *131*(4), 809–821. https://doi.org/10.1016/j.cell.2007.10.025

Wong, W. S. W., Yang, Z., Goldman, N., & Nielsen, R. (2004). Accuracy and power of statistical methods for detecting adaptive evolution in protein coding sequences and for identifying positively selected sites. *Genetics*, *168*(2), 1041–1051. https://doi.org/10.1534/genetics.104.031153

Wu, Y., Wang, H., & Hadly, E. A. (2017). Invasion of Ancestral Mammals into Dim-light Environments Inferred from Adaptive Evolution of the Phototransduction Genes. *Scientific Reports*, *7*(April), 46542. https://doi.org/10.1038/srep46542

Xie, G., Gross, A. K., & Oprian, D. D. (2003). An Opsin Mutant with Increased Thermal Stability †. *Biochemistry*, *42*(7), 1995–2001.

https://doi.org/10.1021/bi02061lz

Yanagawa, M., Kojima, K., Yamashita, T., Imamoto, Y., Matsuyama, T., Nakanishi, K., … Shichida, Y. (2015). Origin of the low thermal isomerization rate of rhodopsin chromophore. *Scientific Reports*, *5*(1), 11081. https://doi.org/10.1038/srep11081

Yang, K., Farrens, D. L., Altenbach, C., Farahbakhsh, Z. T., Hubbell, W. L., & Gobind Khorana, H. (1996). Structure and function in rhodopsin. Cysteines 65 and 316 are in proximity in a rhodopsin mutant as indicated by disulfide formation and interactions between attached spin labels. *Biochemistry*, *35*(45), 14040–14046. https://doi.org/10.1021/bi962113u

Yang, K., Farrens, D. L., Hubbell, W. L., & Khorana, H. G. (1996). Structure and Function in Rhodopsin. Single Cysteine Substitution Mutants in the Cytoplasmic Interhelical E–F Loop Region Show Position-Specific Effects in Transducin Activation †. *Biochemistry*, *35*(38), 12464–12469. https://doi.org/10.1021/bi960848t

Yang, Z., Nielsen, R., Goldman, N., & Pedersen, A. M. (2000). Codon-substitution models for heterogeneous selection pressure at amino acid sites. *Genetics*, *155*(1), 431–49. https://doi.org/10.1093/oxfordjournals.molbev.a003981

Yang, Z., Wong, W. S. W., & Nielsen, R. (2005). Bayes empirical Bayes inference of amino acid sites under positive selection. *Molecular Biology and Evolution*, *22*(4), 1107–1118. https://doi.org/10.1093/molbev/msi097

Yokoyama, R., Knox, B. E., & Yokoyama, S. (1995). Rhodopsin From the Fish,

Astyanax: Role of Tyrosine 261 in the Red Shift. *Investigative Ophthalmology and Visual Science*, *36*(5), 939–945. Retrieved from http://iovs.arvojournals.org/pdfaccess.ashx?url=/data/Journals/IOVS/933185/

Yokoyama, S. (2000). Molecular evolution of vertebrate visual pigments. *Progress in Retinal and Eye Research*, *19*(4), 385–419. https://doi.org/10785616

Yokoyama, S., Tada, T., Zhang, H., & Britt, L. (2008). Elucidation of phenotypic adaptations: Molecular analyses of dim-light vision proteins in vertebrates. *Proceedings of the National Academy of Sciences*, *105*(36), 13480–13485. https://doi.org/10.1073/pnas.0802426105

Yokoyama, S., Xing, J., Liu, Y., Faggionato, D., Altun, A., & Starmer, W. T. (2014). Epistatic adaptive evolution of human color vision. *PLoS Genetics*, *10*(12), e1004884. https://doi.org/10.1371/journal.pgen.1004884

Zhang, J., Kiser, P. D., Badiee, M., Palczewska, G., Dong, Z., Golczak, M., … Palczewski, K. (2015). Molecular pharmacodynamics of emixustat in protection against retinal degeneration. *Journal of Clinical Investigation*, *125*(7), 2781–2794. https://doi.org/10.1172/JCI80950

Zhang, Z., Wu, J., Yu, J., & Xiao, J. (2012). A brief review on the evolution of GPCR: conservation and diversification. *Open Journal of Genetics*, *02*(04), 11–17. https://doi.org/10.4236/ojgen.2012.24B003

Zhao, H., Rossiter, S. J., Teeling, E. C., Li, C., Cotton, J. A., & Zhang, S. (2009). The evolution of color vision in nocturnal mammals. *Proceedings of the*

National Academy of Sciences, *106*(22), 8980–8985. https://doi.org/10.1073/pnas.0813201106

Zhao, H., Ru, B., Teeling, E. C., Faulkes, C. G., Zhang, S., & Rossiter, S. J. (2009). Rhodopsin Molecular Evolution in Mammals Inhabiting Low Light Environments. *PLoS ONE*, *4*(12), e8326. https://doi.org/10.1371/journal.pone.0008326

Zhu, L., Jang, G.-F., Jastrzebska, B., Filipek, S., Pearce-Kelling, S. E., Aguirre, G. D., … Palczewski, K. (2004). A Naturally Occurring Mutation of the Opsin Gene (T4R) in Dogs Affects Glycosylation and Stability of the G Protein-coupled Receptor. *Journal of Biological Chemistry*, *279*(51), 53828–53839. https://doi.org/10.1074/jbc.M408472200

Zhukovsky, E., Robinson, P., & Oprian, D. (1991). Transducin activation by rhodopsin without a covalent bond to the 11-cis-retinal chromophore. *Science*, *251*(4993), 558–560. https://doi.org/10.1126/science.1990431

Zuri, I., Su, W., & Halpern, M. (2003). Conspecific odor investigation by gray short-tailed opossums (Monodelphis domestica). *Physiology and Behavior*, *80*(2–3), 225–232. https://doi.org/10.1016/j.physbeh.2003.07.005

Acknowledgments

En primer lugar expresar mis más sinceros agradecimientos al Dr. Pere Garriga por acogerme en su laboratorio del GBMI y por ser mi director de tesis. Sus guía y enseñanzas a lo largo de estos años me han hecho crecer tanto profesional como personalmente tanto durante los buenos como en los momentos difíciles a lo largo del doctorado.

Quiero agradecer especialmente a la Dr. Eva Ramón por toda la ayuda y el apoyo prestados, por estar siempre dispuesta para comentar cualquier cuestión sobre ciencia y a la gran paciencia que siempre ha demostrado desde el primer día que llegué al laboratorio. También agradecer a la Dr. Margarita Morrillo por todos los ánimos mostrados.

Como no, agradecer al Dr. Brandon Invergo por su colaboración realizada en temas bioestadísticas y a la Dr. Gabriela Aguileta por la ayuda brindada con los arboles filogenéticos, también dar las gracias al Dr. Jaume Bertranpetit por sus consejos para publicaciones y a cuyo laboratorio han pertenecido Brandon y Gabriela.

Agradecer a todos los que pasaron por este laboratorio, en un gran ambiente de compañerismo, Mercé, Lupita, Sundar, Dong y en los últimos tiempos Neda; un pequeño grupo de personas de muy diversa procedencia y diferentes personalidades que me ha enseñado mucho y con el que me alegro de haber compartido tantas buenas experiencias tanto en el trabajo en el laboratorio como fuera de él. También agradecer al Dr. Tzanko Zanov y a quienes formaron o siguen formando parte de su laboratorio, en especial a Toni, Margarida, Elisabetta, Petya, Kristina y Diana, y a quienes fueron llegando después, Ivaylo, Silvia, Javier, Arnau, Aleksandra y Guillem, gracias

también por todas las conversaciones y las risas que amenizaron la tesis. No me quiero olvidar tampoco de los estudiantes que han ido pasando durante estos años por nuestro grupo, los cuales han ido dejando su granito de arena, como Luz, Tatiana, Jose, Marc, Francesca, Cristina y como no, Chiara.

A todos los grandes amigos que he hecho en Terrassa y en Barcelona, gracias por acompañarme en todos esos buenos tiempos pasados durante estos años. También agradecer a los amigos de Coruña y a los de la USC, ya que a pesar de la distancia siempre os he sentido cerca.

Agradecer infinitamente a mis padres por el apoyo incondicional que siempre me brindan y por todo lo que me han enseñado. También al resto de mi familia por todos los buenos momentos y por estar siempre que lo necesito. Sin ellos esta tesis no hubiera sido posible.

Por último no quiero terminar sin darle las gracias especiales a Susan, por haber estado a mi lado en los últimos años motivándome y aconsejándome en las dificultades de la tesis, pero sobre todo por todas las alegrías y sonrisas compartidas.

"Each friend represents a world in us, a world possibly not born until they arrive." - Anaïs Nin